
# 3D printing of medical device prototypes

Jenny Holländer

Student number 21061

Master´s thesis

Pharmaceutical Technology

Department of Biosciences

Åbo Akademi University

Finland

2014

# Table of contents

# Acknowledgements

I would like to thank my supervisors Professor Niklas Sandler at Åbo Akademi and Senior expert Harri Jukarainen at Bayer for giving me the opportunity to work with this innovative project. My sincerest thanks go to Dr. Natalja Genina for all help, support, comments and encouraging words during this project.

I would also like to thank all the staff in the Pharmaceutical Sciences laboratory for support and advices, especially PhD students Henrika Wickström and Mirja Palo. I would also like to thank Paul Vuorela for designing the prototype IUS 2 and for advises regarding the *Rhinoceros* software.

Special thanks go to Niko Palmroos at Bayer for teaching me the HME process, PhD students Mohammad Khajeheian at the Laboraroty of Polymer Technology ÅA, Ermei Mäkilä at the Laboratory of Industrial Physics TY and Lic.Sc. Tor Lauren at the Process Chemistry Center ÅA for helping me with the rheological, X-ray and SEM analysis, respectively.

I would also like to thank the staff at the MakerBot support for patiently answering all my questions regarding the printer.

Additionally I want to thank all the people that somehow have been part of this project and research group.

# Abstract

A decreased amount of new chemical entities (NCE) that are annually introduced on the market, the competition from generic drugs and life cycle management of products force the pharmaceutical companies to look for innovative ways in the manufacturing of drugs. 3D printing is a new innovative manufacturing method under investigation for pharmaceutical applications. In addition, the need for personalized medicine and customization potentially lead pharmaceutical companies to step toward more innovative manufacturing methods in the fabrication of their products.

The main aim of this work was to explore the potential of 3D printing in fabrication of polymer based delivery systems (PBDS) of two polymers, polycaprolactone (PCL) and ethylene vinyl acetate (EVA). The solid-state characteristics of the drug, the effect of drug loading on the printability and the drug release from the devices were studied.

This study showed that it was possible to print drug-loaded prototypes of PCL and certain grades of EVA with the 3D printing technique used in this study. The printing process, though, is a complex interplay between many variables and parameters, and the process needs optimization for each new feedstock. The drug release from the printed devices depended on the geometry of the devices, the matrix polymer and the degree of the crystallinity of the incorporated drug. Further investigations of the printed prototypes regarding mechanical strength, the stability of the drug in the polymer and the effect on different drug loadings and additives must be conducted in order to produce market-appropriate products. Moreover, the regulatory aspects of this new manufacturing technique of PBDS must be determined.

This study shows that 3D printing is an applicable method in the production of drug-containing pharmaceutical products that in the future could open new ways in the fabrication of long-lasting implantable devices.

# List of abbreviations

3D - Three- dimensional

3DP – Three-dimensional printing

ABS – Acrylonitrile butadiene styrene

AKF – Arburg Plastic Freeforming

API - Active pharmaceutical ingredient

ATR-IR – Attenuated total reflection infrared spectroscopy

CAD – Computer-aided design

CT – Computerized tomography

DDD – Drug delivery devices

DDS - Drug delivery systems

DEF – Diethylfumarate

DMLS – Direct Laser Metal Sintering

DMSO – Dimethyl sulfoxide

DSC – Differential scanning calorimetry

EBM – Electron Beam Melting

EVA – Poly(ethylene-co-vinyl acetate)

FDC – Fused deposition of ceramics

FDM – Fused Deposition Modelling

FDMet- Fused deposition of metals

FFF – Fused filament fabrication

FLEX – Fused Layer Extrusion

HA – Hydroxyapatite

HDPE – High-density polyethylene

HIPS – High-impact polystyrene

HIV – Human immunodeficiency virus

HME - Hot-met extrusion

IND – Indomethacin

IUD - Intrauterine device

IUS - Intrauterine system

IVR - Intra vaginal ring

LDPE – Low density polyethylene

MED – Mini Extruder Deposition

MI – Melt index

MRI – Magnetic resonance imaging

NCE - New chemical entity

NSAID – Non-steroidal anti-inflammatory drug

PBDS – Polymer based delivery systems

PC – Polycarbonate

PCL - Polycaprolactone

PCPP - Poly[1,3-bis(p-carboxy-phenoxy)propane]

PDMS – Polydimethylsiloxane

PDO – Polydioxanone

PDS – Polydioxanone

PED – Precision Extruding Deposition

PEEK – Polyether ether ketone

PEI – Polyetherimdie

PEKK – Polyether ketone ketone

PEVA - Poly(ethylene-co-vinyl acetate)

PGA – Poly(glycolic acid)

PLA – Polylactic acid

PLGA – Poly(lactic-co-glycolic acid

PLLA – Poly-DL-lactide

PMMA – Polymethylmethacrylate

PPF – Poly(propylene fumarate)

PPSF – Polyphenylsulfone

PSA – Poly(sebacic acid)

PTMC – Poly(trimethylene carbonate)

PU – Polyurethane

PVA – Polyvinyl alcohol

RCM – Rate controlling membrane

SD – Standard deviation

SEM – Scanning electron microscopy

SDM – Stick Deposition Moulding

SFF - Solid freeform fabrication

Si – Silicon

SLA – Stereolithography

SLS – Selective Laser Sintering

STL – Stereolithography

TCP – ß-tricalcium phosphate

USC – University of California

UV/VIS – Ultraviolet/Visible

VA- Vinyl acetate

XRD - X-ray diffraction

# 1. Introduction

A decreased amount of new chemical entities (NCE) that are annually introduced on the market and the competition from generic drugs force the pharmaceutical companies to look for innovative ways in the manufacturing of drugs. New formulations and delivery methods of existing drugs can extend the life-cycle of a product and improve the financial situation of the pharmaceutical companies (Valigra, 2012). In addition, the need for personalized medicine and customization potentially lead pharmaceutical companies to step toward more innovative manufacturing methods in the fabrication of their products.

Many technologies and manufacturing processes that have been used in other fields have been introduced into the biomedical and pharmaceutical field recently, such as hot-melt extrusion (HME) and different printing techniques, among them several three-dimensional printing (3D) techniques. In the HME process an active pharmaceutical ingredient (API) is blended with a thermoplastic polymer and then extruded as a rod or a film. Additive manufacturing techniques, e.g. the 3D printing technique called fused deposition modelling (FDM™) can manufacture 3D prototypes and models of a filament by melting and printing it. The FDM™ process includes the design of an item in a computer software, and the manufacturing of it with the printer. In 3D printing the product is built layer-by-layer (Beerman, 2012). The technique has been applied in the chemical, biomedical and the pharmaceutical field (Hutmacher et al., 2007, Espalin et al., 2010, Symes et al., 2012, Sandler et al., 2013, Goyanes et al. 2014).

Polymers have been used in drug delivery systems (DDS) for decades. Polymers used in DDS can be divided into two main groups, (i) biodegradable and (ii) non-degradable polymers. Biodegradable polymeric DDS are usually matrix systems, whereas non-degradable polymers can be as reservoir or matrix systems. The biodegradable polymers were developed for the biomedical and the pharmaceutical field with the aim that they would degrade in the body in a controlled rate into non-toxic products that could be eliminated through natural ways (Labarre et al., 2011).

One common biodegradable polymer used in DDS is polycaprolactone (PCL). PCL has high permeability to many drugs which makes it suitable for long-term DDS and has excellent biocompatibility (Sinha et al., 2004, Fialho et al., 2008, Woodruff et al., 2010). Capronor™

is a good example of a PCL based 1 year-contraceptive implant, which is totally eliminated from the body by bioerosion after 2-3 years (Merkli et al., 1998).

One of the most common non-degradable polymers that has been used for decades in the biomedical and pharmaceutical field is poly (ethylene-co-vinyl acetate) (EVA or PEVA). EVA is a chemically inert, biocompatible and an insoluble polymer. The first EVA based products on the market were the ophthalmic insert Ocusert® and the intrauterine device (IUD) Progestesert® (Hoffman et al., 2008).

Implantable PBDSs for contraceptives have been studied since the 1960s. The implantable PBDS for contraceptives has been manufactured as rods, intrauterine system (IUS) and intra vaginal ring (IVR). There are a limited number of polymers that can be used as IUSs or IVRs, since they have to be non-swellable and non-biodegradable or the degradation rate has to be very slow. The marketed IUSs and IVRs, consists of non-degradable polymers such as polydimethylsiloxane (PDMS) or EVA. The device backbone in the IUS that is currently on the market, Mirena®, is made of polyethene with a drug-delivery cylinder wrapped around it. The IVRs, Progering® and Nuvaring®, are made of silicone rubber/PDMS and EVA, respectively. The devices are manufactured by extrusion and injection molding.

Currently, there is a lot of research ongoing to combine additional drugs together with contraceptives into IVRs (Han et al., 2007, Malcolm et al., 2012, Thurman et al., 2013, Conrad, 2014). The purpose of the combinations is to gain a multiple effect by using a single product, such as to prevent sexually transmitted infections in additional with the contraceptive effect of a DDS. A non-hormonal copper IUS containing indomethacin is another example of DDS with a multipurpose application. The indomethacin is incorporated to decrease the adverse effects of the IUS (Liang et al., 2008).

The main goal of this work was to manufacture for the first time IUSs with the drug incorporated in the body of the device by using the 3D printing technique FDM™.

The manufacturing process of the filaments and the PBDS and the following characterization methods of the properties of the devices are presented in Figure 1.

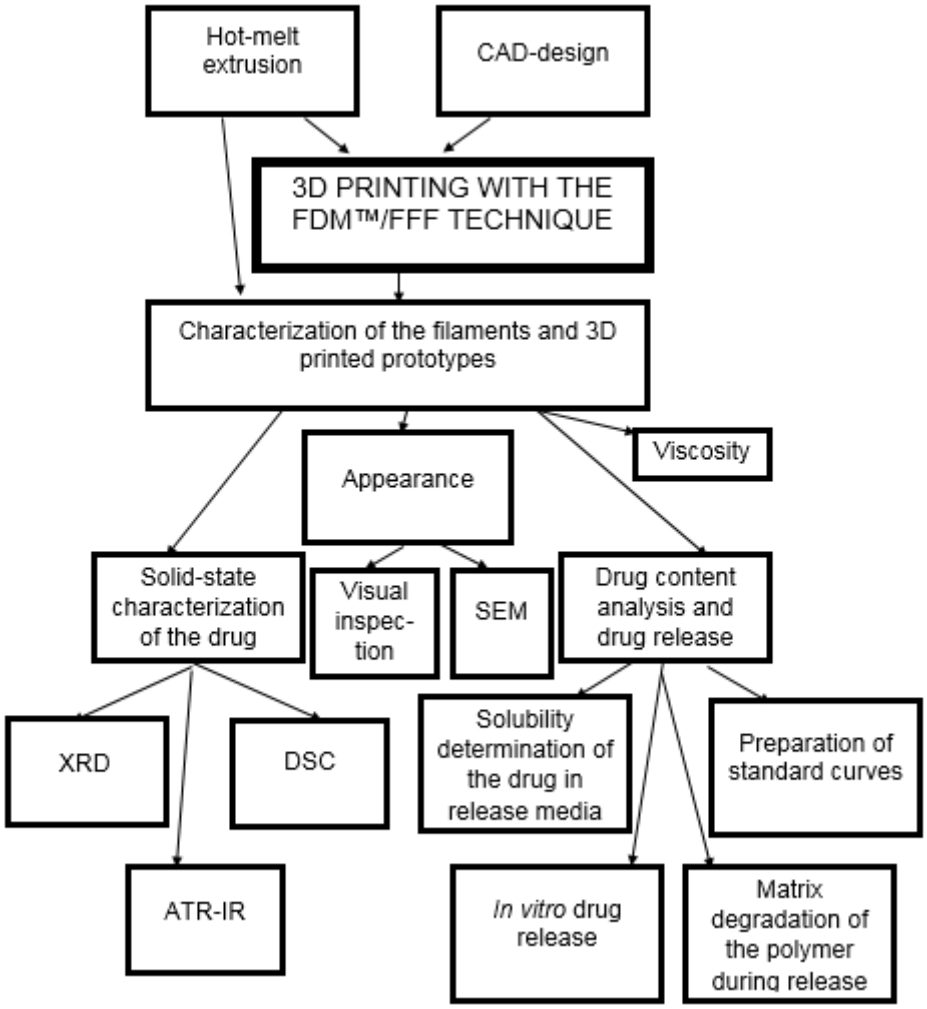


**Figure 1.** Manufacturing process of the filaments and the PBDS prototypes and the characterization methods used in this study are schematically presented. The drug content analysis and the viscosity measurements were done only for the filaments.

# 2. Literature review

## 2.1 3D printing

The introduction of the 3D printing technology as a new manufacturing process, among other new techniques, has been called the new industrial revolution or the third industrial revolution. The first industrial revolution, or the mechanization of the textile industry, began in the late 18$^{th}$ century. When Henry Ford introduced the mass production of cars, in the early of 20$^{th}$ century, it was called the second industrial revolution (The Economist, 2012). When the first and second industrial revolutions were based on the outcome of more products faster and with less costs, the third industrial revolution brings a new dimension to this with new technologies, manufacturing processes and materials.

The 3D printing, also called additive manufacturing, rapid prototyping, solid freeform fabrication and digital fabrication, has been expected to change the warehousing of spare parts and the geography of production sites, since the production can be done when there is a need of an item, by downloading the design and printing it with a 3D printer.

The 3D printing process includes the design of an item in a computer software and the manufacturing of it with a 3D printer. In 3D printing the product is built layer-by-layer. The layers are sliced by a 3D computer aided design (CAD) software, which determines how the layers will be constructed (Berman, 2012).

The 3D printing technology has been compared with mass customization processes and production techniques such as injection molding. The common feature between 3D printing and mass customization is that custom products can be economically built in small quantities, but the process and the logistic requirements are easier in the 3D printing technique. In comparison with the injection molding, it is a more cost-effective and faster technique, when the production quantities are small (Berman, 2012). In Table 1 the characteristics of the 3D manufacturing is presented.

**Table 1.** Characteristics of 3D manufacturing (modified from Berman, 2012).

| **Advantages of 3D Printing in Comparison to Other Technologies** |
|---|
| • Can economically build custom products in small quantities as if mass production were used. |
| Sources of cost effectiveness include: |
| ◦ No need for costly tools, molds, or punches |
| ◦ No scrap, milling, or sanding requirements |
| ◦ Automated manufacturing |
| ◦ Use of readily available supplies |
| ◦ Ability to recycle waste material |
| ◦ Minimal inventory risk as there is no unsold finished goods inventory |
| ◦ Improved working capital management as goods are paid for before being manufactured |
| • Ability to easily share designs and outsource manufacturing |
| • Speed and ease of designing and modifying products |
| **Current Limitations of 3D Printing** |
| • Higher costs for large production runs relative to injection molding and other technologies |
| • Reduced choice for materials, colors, and surface finishes |
| • Lower precision relative to other technologies |
| • Limited strength, resistance to heat and moisture, and color stability |

3D printing technique has been applied in small production volumes, such as prototyping, customization or when a product has a very complex design, which has been difficult to manufacture with traditional techniques (Berman, 2012). In media there are reported enormous amounts of applications using the 3D printing technique in different fields. For example on the 3D Printing Industry companies website, which is a global media company, are reports of 3D printed fashion, e.g. clothes, shoes, eyewear and jewelry, applications in aerospace, transport and agricultural, art and sculpture (3D Printing Industry, 2014). Business Industry reports of several 3D printing house projects. In China a company called Winsun has claimed that they have built 10 3D printed houses in just one day, and in Amsterdam a 3D printed canal house is under construction. The researches at the USC (University of Southern California) are trying to scale up the 3D house printing with a technique called contour crafting. The purpose is to develop a gigantic 3D printer that can build a house in one piece (Business Insider, 2014). In chemistry the 3D printing technique has been studied by Symes et al. (2012), a chemical reaction was initiated by printing the reagents directly into it, at the same time the reaction ware was printed.

### 2.1.1 3D printing techniques used in the biomedical and pharmaceutical area

Several 3D printing techniques has been made known since the first commercial system, stereolithography, was introduced in 1988 by 3D Systems Inc. The 3D printing techniques, or solid freeform fabrication (SFF) technologies as they also are called, have all in common: (i) they create the model from a three-dimensional model, obtained from a computer-aided design (CAD), computerized tomography (CT) or a magnetic resonance imaging (MRI) scan data (Rengier et al., 2010) and (ii) the model is sent to the printer´s software as a file and is then printed layer-by-layer. The 3D printing techniques that have been used in the medical field are presented in Figure 2. In this study the FDM™/FFF technique was used as the printing technique. The principles and the use of the other techniques in pharmaceutical and biomedical applications will only be briefly described. Besides of the presented techniques, there are other 3D printing techniques used in different applications reported in the literature. The website https://thre3d.com/how-it-works/3d-printing-process gives a good overview of the different techniques; many of them are not presented in this work.

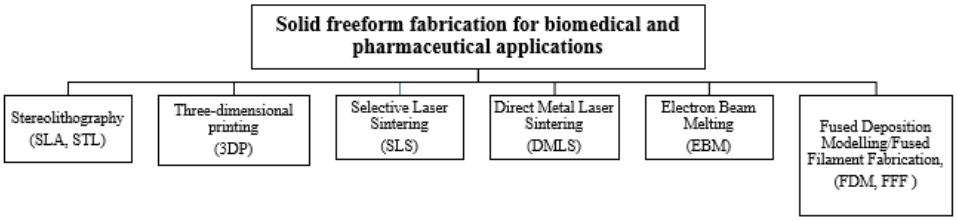


| **Principle** | **Photo-polymerisation** | **Powder+binder deposition** | **Powder sintering** | **Powder sintering** | **Powder sintering** | **Melt extrusion or plotting** |
|---|---|---|---|---|---|---|
| **Material** | Polymers<br>Ceramics<br>Composites<br>Pharmaceuticals?<br>Cells | Polymers<br>Ceramics<br>Metallic<br>Composite<br>Pharmaceuticals,<br>Cells | Polymers<br>Ceramics<br>Metallic<br>Composite<br>Pharmaceuticals? | Metallic<br>Pharmaceuticals? | Metallic<br>Pharmaceuticals? | Polymers<br>Pharmaceuticals |
| **Advantages** | Large part size | Low cost<br>Multiple materials | Good strength<br>Large part size<br>Variety of materials | Good strength | Good strength | Low cost,<br>Good strength |
| **Dis-advantages** | Moderate strength,<br>Limited materials | Moderate strength | High cost,<br>Powdery surface | Limited materials,<br>High temperatures | Limited materials,<br>High temperatures | Low speed |

**Figure 2.** Printing techniques used in the biomedical and pharmaceutical area.

### 2.1.1.1 Stereolithography (SLA, STL)

Stereolithography (SLA) was first introduced as a commercial system already 1988 by 3D Systems Inc. (Woodruff et al., 2010). The SLA uses the focused UV light to transform liquid photopolymer plastic into a solid form. The photopolymer reservoir is under the movable platform. When the first layer is built, the platform submerges into the reservoir just enough to create a thin layer and a UV laser beam passes back and forth over the liquid to transform it into a solid state. The layers are built by lowering the platform by one layer at a time (Hausman, 2014). The commercial SLA systems are using epoxy-based or acrylate-based resins (Woodruff et al., 2010). The process is presented in Figure 3.

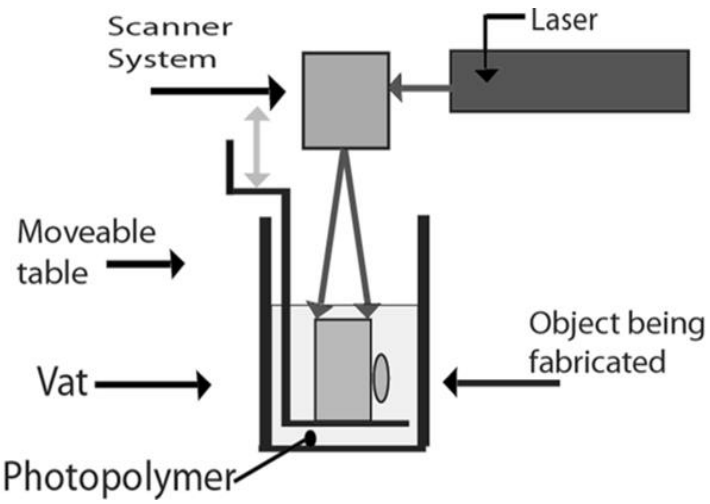


**Figure 3.** A schematic presentation of the SLA process (Martello, 2014a).

Since the original materials used in the SLA process are not biocompatible, and the system uses only photopolymerizable materials, the use in biomedical and pharmaceutical applications is limited. In biomedical engineering SLA has been used in fabrication of functional parts and patient-specific models, patient-specific implantable devices, tissue engineering and hydrogels containing cells (Melchles et al., 2010). Materials that has been used in the above mentioned applications are blends of poly(propylene fumarate)(PPF) and diethylfumarate (DEF), PPF and DEF with hydroxyapatite (HA), poly-DL-lactide (PLLA) and HA blends, ß-tricalcium phosphate (TCP), polycaprolactone (PCL), poly(trimethylene carbonate) (PTMC) (Melchels et al., 2009, Elomaa et al., 2011, Bose et al., 2013, Schüller-Ravoo et al., 2013). This technique has been studied in the use of ceramic particles, e.g. HA

and alumina. The printing process is possible with ceramics if the particle loading is under 53 wt% and the particle size is smaller than the layer thickness (Melchels et al., 2010).

Stratays has a variant of the SLA process that uses the ink-jet technique instead of a liquid reservoir system to deposit the liquid photopolymer. The material is liquid in cartridges from where small droplets are jetted and immediately cured by UV-light. The printer has capability to use several materials at the same time. It has been used to produce prosthetics and hearing aids. The benefit with this technique is that it can combine very different materials within the same object making it very versatile (Stratasys, 2014).

### 2.1.1.2 Three-dimensional printing (3DP)

The three-dimensional printing (3DP) was invented by Sachs et al. in 1992 and is widely studied in the fabricating of scaffolds and drug delivery devices (Sachs et al., 1992, Katstra et al., 1999, Yu et al., 2009, Rowe et al., 2000, Wu et al., 2014).

In the three-dimensional printing (3DP) the part is built up with powder as the built material, and liquid as a binding material. Briefly, a layer of powder is spread onto the build plate with a roller. An ink-jet print head is moving in the X-Y orientation to eject binding material onto the powder. The powder is bonded together only in the areas where the binding material is printed. The build plate is moved down in the Z-direction, when a layer is completed and the process is repeated (Yu et al., 2007, Zhou et al., 2011). The process is presented in Figure 4.

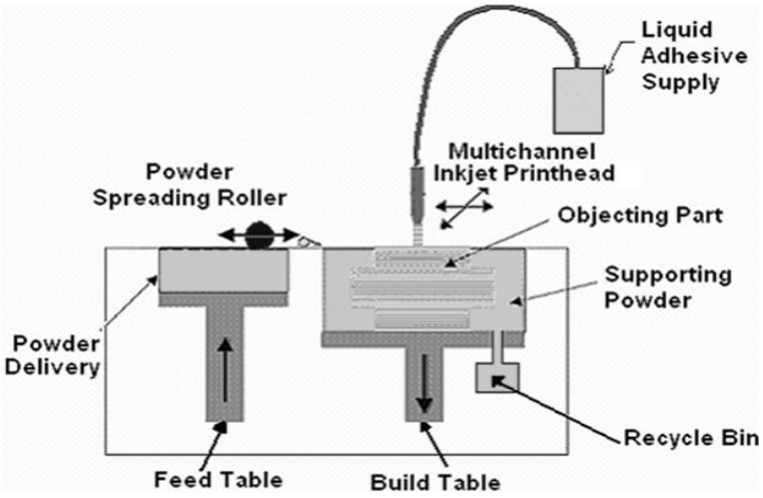


**Figure 4.** A schematic presentation of the 3DP process (Intechopen, 2014)

Materials that has been used in the fabrication of 3DP scaffolds includes ceramic, metallic, polymeric and composite materials, such as calcium phosphates, HA, PLA, PE (Bose et al., 2013) and PCL (Woodruff et al., 2010). 3D printed implantable dosage forms with ethinyl estradiol with different release rates has been investigated by Wu et al. (2014). Wu et al. (2014) studied also different drug release patterns of three different shapes of 3DP implants. 3DP has been studied in the manufacturing of oral dosage forms with complex release patterns (Rowe et al, 2000, Katstra et al., 2000, Yu, et al. 2009). The printers using the 3DP technique for manufacturing tablets, are commercially available (Yu et al., 2009).

#### 2.1.1.3 Selective laser sintering (SLS)

The SLS, like SLA, also uses focused UV light, but instead of liquid photopolymer as in the SLA technique, to sinter areas of loosely compacted powder. From the powder delivery system, a thin layer of powder is spread onto a flat platform with a roller. The powder is then raster-scanned with a high-power laser beam, and as a result of that the powder fuses. By moving the fabrication piston down, layers can be built on each other (Woodruff et al., 2010). The basic material for SLS is a polymeric powder with a mean diameter of 50 µm. Materials that are commercially available for SLS equipment are polyamide, polystyrene, polypropylene and thermoplastic elastomers as TPE (Mazzoli, 2013). The process is presented in Figure 5.

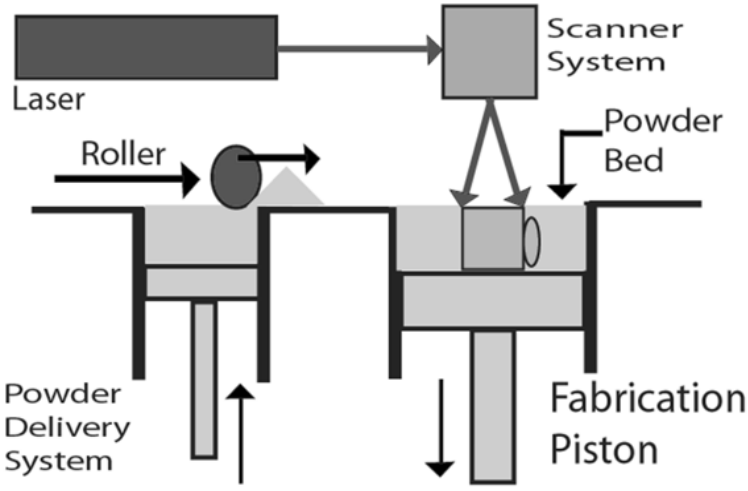


**Figure 5.** A schematic presentation of the SLS process (Martello, 2014b).

Like SLA, the application of SLS in the biomedical field has been studied in manufacturing of patient-specific models, e.g. oral, maxillofacial and orthopedics and in tissue engineering (Mazzoli, 2013). In tissue engineering materials, such as PCL, HA, calcium phosphate and PLLA, have been studied (Bose 2013, Mazzoli 2013). The first test of manufacturing implantable devices by SLS was made of polyether ether ketone (PEEK) (Mazzoli, 2013). An implantable device manufactured of polyether ketone ketone (PEKK) has got FDA approval, and has been implanted in a patient successfully (MDT, 2013).

### 2.1.1.4 Direct metal laser sintering (DMLS)

Direct metal laser sintering was the first method, which produces metal parts in a single process. It was developed in 1994 by EOS GmbH. The metal powder is melted by scanning with a high power laser beam to build the part in a layer-by-layer manner. The maximum diameter of the powdered metal used is 20 microns. The method can be performed by two different methods: powder deposition or powder bed deposition. In the former case, the powder is melted in a hopper and deposited on the build platform. In the latter case, the process is the same as in the SLS process. A laser then sinters the layer of powder metal, which is fused, and when the layer is finished the build plate is lowered. In the powder deposition method, several materials can be used at the same time, whereas in the bed method only one metal can be used at a time (Custompart, 2014a). The main difference between powder bed DMLS and SLS is the particle size. The maximum particle size in

DMLS is 20 µm, when in SLS bigger particles can be used. The process is presented in Figure 6.

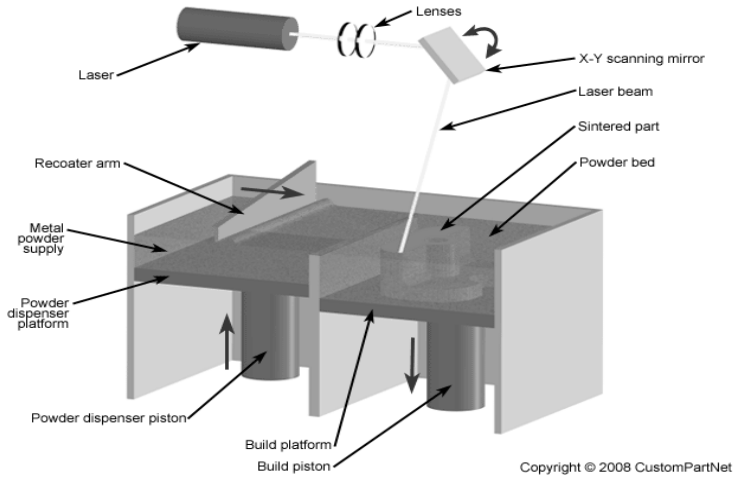


**Figure 6.** A schematic presentation of the DMLS process (Custompart, 2014b)**.**

This method has been used in the manufacturing of medical implants. Materials that can be used are stainless steel, alloy steel, aluminum, tool steel, bronze, cobalt chrome and titanium (Thre3D, 2014).

### 2.1.1.5 Electron beam melting (EBM)

Electron Beam Melting (EBM) is a process that uses an electron beam to melt the powdered metal inside a vacuum. When a layer is finished, the powder bed moves down, and an automated roller adds a new layer of material, which is melted to form the next section of the model. The model is built up layer-by-layer, when the process is repeated. EBM is used, when high strength or high temperatures are required. The process is developed in 1997 by Arcam (Thre3D, 2014). A schematic presentation of the process is presented in Figure 7.

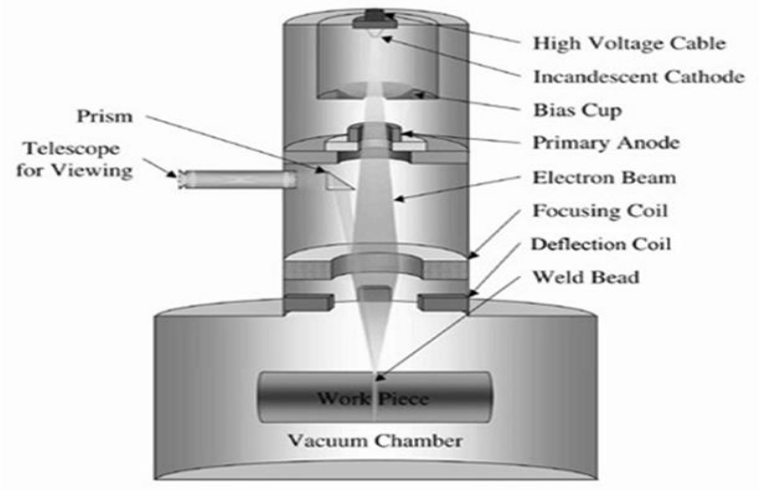


**Figure 7.** A schematic presentation of the EBM process (Popular3dprinters, 2014).

The EBM process is used in manufacturing of orthopedic implants. Many EBM manufactured implants with CE-certificate and FDA approval is on the market. The technique is used for both standard and custom-made implants. Materials used in this technique are titanium and cobalt chrome (Arcam, 2014).

### 2.1.1.6 Fused Deposition modeling (FDM™) or the Fused Filament Fabrication (FFF)

The fused deposition modeling process (FDM™) invented by Stratasys, is an extrusion-based process. Since the patent had already expired for the process, several similar extrusion-based constructions have entered the market, called fused filament fabrication (FFF) (Turner et al., 2014). The key elements in the FDM™ system include the material feedstock, loading system, liquefier, print head and the build plate. The printing process begins with loading of the filament by a motor, through a heating block. The melted polymer is extruded through a nozzle, and bonds to previous layers when it solidifies. When the layer is completed, the build plate is lowered and the process is repeated (Turner et al., 2014). An illustration of the process is presented in Figure 8. The FDM™ process uses material for two different purposes (i) to build the object and (ii) to support overhangs in the model. The printer can have a single extruder system or multi-extruder systems, but it prints only with one extruder at a time. The first feedstock material in a FDM™ process was acrylonitrile butadiene styrene, ABS (Stratasys, 2014). Other original feedstock materials are

polycarbonate (PC), polyetherimide (PEI) resin, polyphenylsulfone (PPSF), polyamides (Nylon), polylactic acid (PLA), high-impact polystyrene (HIPS), high-density polyethylene (HDPE) and polycaprolactone (PCL) (Stratasys, 2014, Hausman, 2014).

The original feedstock in the process has been polymers, but several studies have been done by using the polymers with incorporated metallic or ceramic particles. When using metallic or ceramic particles the technique have then been renamed as fused deposition of metals (FDMet) and fused deposition of ceramics (FDC) (Agarwala et al., 1996, Venkataraman et al., 2000). Printing with the FDM™ technique is a complex interplay of many process variables, which are summarized by Agarwala et al. (1996) in Table 2.

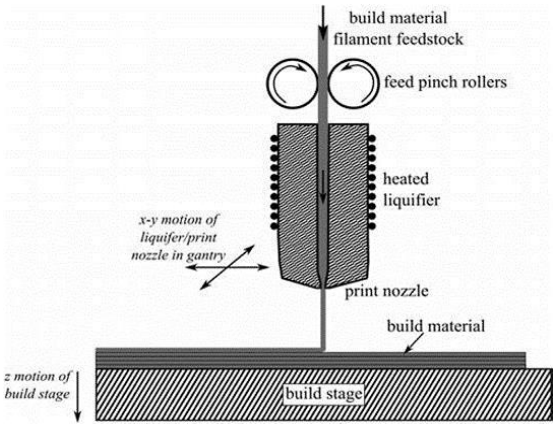


**Figure 8.** An illustration of a typical FDM™/FFF extruder (Turner et al., 2014).

**Table 2.** FDM™, FDMet and FDC process variables (modified from Agarwala et al. 1996).

| Operation specific | Machine specific | Materials specific | Geometry specific |
|---|---|---|---|
| Slice thickness | Nozzle diameter | Polymer characteristics | Fill vector length |
| Road width | Filament load rate | Viscosity | Support structure |
| Head speed | Roller speed | Stiffness (column strength) | |
| Extrusion temperature | Flow rate | Flexibility | |
| Envelope temperature | Filament diameter | Thermal conductivity | |
| Fill pattern | | | |

In the biomedical area several researchers has used FDM™ in the manufacturing of scaffolds with different porosity (Hutmacher et al., 2007, Espalin et al., 2010). In Goyanes et al. (2014) research the FDM™ technique was used in fabrication of tablets from a drug-loaded filament. The filament was loaded with the model drug by swelling of the polymer in a liquid containing the drug. Medical devices with anti-biofilm properties was fabricated with the FDM™ technique by Sandler et al. (2014) from drug-loaded filaments manufactured by HME. Biocompatible materials that have been used in this technique is PLA,

polymethylmethacrylate (PMMA) and the original FDM™ feedstock material PCL (Hutmacher et al., 2007, Espalin et al., 2010).

#### 2.1.1.6.1 New variants of the printing of polymers

The drawbacks of the FDM™ process are the limitations that the use of filaments causes. The material for the FDM™ technique has to be in form of the filament with a diameter of 1.75-3 mm. The raw polymers are usually in a form of a powder or pellets. In order to 3D print, the polymers have to be modified to the form of filaments by HME technique. It leads to an additional step in the manufacturing process of the 3D structures.

The properties of the rollers of the feeding system and the liquefier are optimized for each material. Therefore, the possibility to use other material than the original feedstock for the printer is limited. The rollers size and surface play an important role in the process of the filament loading. They have to create enough friction to load the material into the liquefier (Agarwala et al., 1996). The filament loading system is sensitive to variations in the filament diameter. The use of filament with the size outside the specified limits can affect the quality of the printed part, or even cause the complete stop of the extrusion process. Therefore, new variants of the 3D printing FDM™ process have been studied.

A variant of the FDM™ process called Stick Deposition Moulding (SDM) is utilized by a printer called "fabbster" manufactured by Sintermask GmbH. The feedstock is in a form of a 3x3mm toothed stick, instead of a round filament, which decreases the problems with slipping and uneven flow during loading and printing (CT, 2014).

Bellini et al. (2005) developed a system called mini extruder deposition (MED) with a mini-extruder mounted on a high-precision positioning system for extrusion of blends of polymers and ceramics. The mini-extruder uses granulated material as the feedstock. A research group at the Drexel University developed a variant called Precision Extruding Deposition (PED) for manufacturing of PCL/HA scaffolds (Shor et al., 2008). With the pressure from rotating screws the material is forced down the chamber and extruded through the nozzle. Khaled et al. (2014) used an extrusion printer to manufacture tablets from a drug-loaded paste, which was loaded into a syringe. Recently, Sculptify organized a kick-starter campaign to raise money for the manufacturing of the first commercially available melt extrusion printer, which uses pellets as feedstock instead of filaments (Sculptify, 2014). The printing technique

is called Fused Layer Extrusion (FLEX). The printer will be available in the spring 2015. The new techniques have their limitations and problems too, many of them the same as in the original FDM™ process, except for the filament specific ones. Bellini et al. (2005) reported that the size of the granulated material, and variations of it, had a strong influence on the melt flow. Even in the new techniques the liquefier length and nozzle angle has to be optimized for each material.

The use of polymer pellets as a feedstock material has been already utilized in a printer where the layers are built up from small droplets instead of roads that is the case in the FDM™ technique. This technique is commercially available by ARBURG GmbH. The printing technique, ARBURG Plastic Freeforming (AKF), is patented and the printer is called "freeformer" (Arburg, 2014). In this technique the pellets are melted and subsequently printed with a stationary nozzle by using the piezo technology. When the filament acts as a piston to extrude the melt in the FDM™ technique, this printer utilizes the piezo technology in the printing. This new technology may decrease some of the limitations that the filament and the liquefier properties entail, such as inappropriate column strength and melt flow behavior of the polymer. The building component can move along five axes, offering ability to print difficult geometries. There is no original feedstock material for this printer, the manufacturer states that all the plastics that can be used in injection molding, can be used in this printer (Arburg, 2014). However, the limitations, which the piezoelectric technique can induce, have to be taken into account by selecting the feedstock material for AKF technology.

.

## 2.2 Polymers in controlled drug-delivery systems

### 2.2.1 Definition of polymers and manufacturing of synthetic polymers

The definition of a polymer is*: a large macromolecule composed of many small molecules, monomers.* They can be built up with repeating units of one type, forming homopolymers, or repeating units of several types, forming copolymers (Nicholson, 1997, Labarre et al., 2011). The polymer backbone chains can be linked together in many ways, which affects the properties of the polymer. In biomedical and pharmaceutical applications it is important

to determine the molecular weight, composition and thermal properties of the polymer, because these properties may influence the properties of the final application (Labarre et al., 2011).

Both naturally occurring and synthetic polymers are used in the medical field. Cellulose and starch are examples of naturally occurring polymers used in pharmaceutical applications. The need for sustained controlled-release and targeted DDSs in the pharmaceutical field, and the lack of biomaterials in the biomedical field increased the interest in developing new polymers in the 1980s (Labarre et al., 2011). The synthetic polymers are synthesized by step or chain polymerization (Nicholson, 1997, Labarre et al., 2011). In step polymerization the polymerization process prolongs, when two active groups in the monomers react, and the polymer is formed, when the chains are slowly increasing in length. This can happen between unreacted monomers or between oligomers (short polymer chains formed by reaction between monomers). In the chain polymerization process the process is initiated by opening a bond or a cycle with an initiator in a monomer and the polymer is formed by additions of monomers to the monomer chain (Nicholson, 1997, Labarre et al., 2011). The monomers can contain of one or two double, triple bonds or cycles.

## 2.2.2 Biodegradable and non-degradable polymers

Polymers used in long-lasting drug delivery systems can be divided into two main groups, depending on the degradation mode, (i) biodegradable and (ii) non-degradable polymers.

### 2.2.3.1 Biodegradable polymers

The group of polymers that in the literature is called biodegradable polymers consists of polymers that degrades and eliminates from the body in different ways. The polymers can be divided into four groups based on the degradation mode and the elimination from the body. The definitions of the groups are presented in Table 3.

**Table 3.** Definitions of biodegradable, bioresorbable, bioabsorbable and bioerodable (Modified from Woodruff et al., 2010).

| |
|---|
| ***Biodegradables*** are solid polymeric materials and devices which **break down** due to macromolecular degradation with dispersion in vivo **but no proof for the elimination from the body** (this definition excludes environmental, fungi or bacterial degradation). Biodegradable polymeric systems or devices can be attacked by biological elements so that the integrity of the system, and in some cases but not necessarily, of the macromolecules themselves, is affected and gives fragments or other degradation by-products. Such fragments can move away from their site of action but not necessarily from the body. |
| ***Bioresorbables*** are solid polymeric materials and devices which show **bulk degradation** and further resorb in vivo; i.e. polymers which are eliminated through natural pathways either because of simple filtration of degradation by-products or after their metabolization. Bioresorption is thus a concept which reflects **total elimination** of the initial foreign material and of bulk degradation by-products (low molecular weight compounds) with no residual side effects. The use of the word 'bioresorbable' assumes that elimination is shown conclusively. |
| ***Bioerodibles*** are solid polymeric materials or devices, which show **surface degradation** and further, resorb in vivo. Bioerosion is thus a concept, too, which reflects **total elimination** of the initial foreign material and of surface degradation by-products (low molecular weight compounds) with no residual side effects. |
| ***Bioabsorbables*** are solid polymeric materials or devices, which can **dissolve** in body fluids without any polymer chain cleavage or molecular mass decrease. For example, it is the case of slow dissolution of water-soluble implants in body fluids. A bioabsorbable polymer **can be bioresorbable** if the dispersed macromolecules are excreted. |

Most commonly the degradation of biodegradable polymers in drug delivery devices begins via hydrolysis (Solorio et al, 2014). When the polymer begins to degrade the bonds between the monomers and oligomers are cleaved and the following reduction in the mass is known as erosion (Solorio et al., 2014). The erosion can proceed via surface or bulk degradation pathways (Woodruff et al., 2010). In surface degradation the hydrolytic cleavage of the polymer backbone occurs only on the surface, whilst bulk degradation causes hydrolysis through the entire polymer matrix (Woodruff et al., 2010). In Figure 9 the degradation modes are illustrated. Factors that affect the rate of degradation of polymers are crystallinity, the glass transition temperature, water uptake and the molecular weight (Fialho et al., 2008, Labarre et al., 2011).

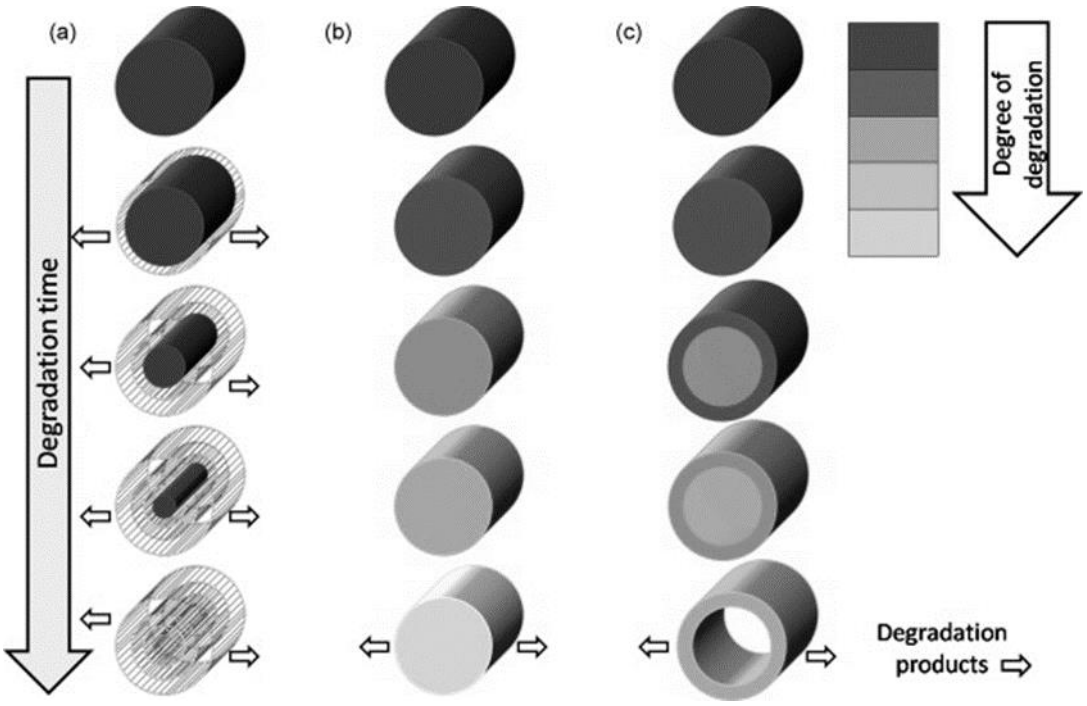


**Figure 9.** Degradation modes for degradable polymers: (a) surface erosion, (b) bulk degradation (and (c) bulk degradation with autocatalysis) (Woodruff et al., 2010).

The drug release from the biodegradable polymers is complex and involves many physical and chemical phenomena. Water intrusion into the device and the porosity of it, diffusion of the drug in the polymer matrix, the degree of crystallinity of the polymer and the drug and the degradation mode of the polymer are some examples that affect drug release from devices made from biodegradable polymers (Siepmann et al., 2001). In bulk-degrading systems the release occurs by diffusion and as a result of the degradation of the polymer. From the surface-eroding polymers the release only occurs as a result of the degradation of the polymer on the surface of the product.

Originally the biodegradable polymers were developed for the biomedical and the pharmaceutical field with the aim to degrade in the body with a controlled rate into non-toxic products that could be eliminated through natural ways (Labarre et al., 2011). The most common biodegradable polymers used in medical applications are PLA, poly (lactic-co-glycolic-acid) (PLGA) and PCL (Marin et al., 2013). The most common biodegradable polymers or copolymers that are found in FDA approved devices are besides of those above mentioned, polydioxanone (PDO or PDS), poly(glycolic acid) (PGA) and poly(PCPP-SA-anhydride) (Solorio et al., 2014). The most common polymeric controlled-release drug

delivery systems of biodegradable polymers on the market are based on PLGA, PLA, PCL or copolymers of PCPP(poly[1,3-bis(p-carboxy-phenoxy)propane]) and PSA (poly(sebacic acid). Some examples of implantable controlled-release drug delivery systems are presented in Table 4.

**Table 4.** Examples of implantable controlled-release DDD.

| Polymer | Drug | Indication | Product | Application |
|---|---|---|---|---|
| PLGA | goserelin acetate | prostate cancer<br>endometriosis | Zoladex | ISF implant system[1] |
| PLGA | leuprolide acetate | prostate cancer<br>breast cancer<br>endometriosis | Eligard | ISF implant system[1] |
| PCL | levonogestrol | contraceptive | Capronor | Rod |
| Poly(PCPP-SA anhydride) | carmustin | brain cancer | Gliadel | Implant, wafer |

**1**ISF implant system= *In situ* forming implant system

### 2.2.3.1.1 Polycaprolactone (PCL), a biodegradable polymer used in this study

PCL is a slowly biodegradable homopolymer, with a total elimination from the body after 3-4 years. PCL is prepared by ring-opening polymerization of Ɛ-caprolactone or of 2-methylene-1-3-dioxepane.

In literature it has been reported that the PCL degradation occurs via bulk degradation (Li et al., 2010, Bosworth et al., 2010, Sinha et al., 2004). The degradation products of PCL are 6-hydrohexanoic acid and acetyl coenzyme A, which are eliminated from the body via the citric acid cycle (Woodruff et al., 2010, Li et al., 2014).

PCL have high permeability to many drugs, which makes it suitable for long-term DDSs (Sinha et al., 2004, Fialho et al., 2008, Woodruff et al., 2010). PCL has excellent biocompatibility, and therefore, it is widely used as a biomaterial and as DDS. Many PCL based DDS and scaffolds have FDA approval and CE mark registration (Sinha et al., Fialho et al., 2008, Cheng et al., 2010). Capronor™ is a PCL based 1 year-contraceptive implant, which is totally eliminated from the body by bioerosion after 2-3 years (Merkli et al., 1998). PCL-based DDDs have been prepared by melt molding, compression molding, injection molding, solvent evaporation, spray drying, or extrusion (Bodmeier et al., 1989, Fialho et al., 2008, Cheng et al., 2010, Li et al., 2010, Rong et al., 2012). PCL scaffolds have been prepared by solvent casting, electrospinning and different solid freeform fabrication techniques (Zein et al., 2002, Bosworth et al., 2010, Woodruff et al., 2010, Aghdam et al.,

2011). PCL has the ability to form compatible blends with many other polymers facilitating tailoring of drug-delivery systems with desirable rates for drug release (Sinha et al., 2004, Woodruff et al., 2010, Perstorp, 2014). In this study PCL was used in the manufacturing of an implantable device.

#### 2.2.3.2 Non-degradable polymers

Non-degradable polymers has been used in drug delivery systems for decades. The drug release from a non-degradable polymer is not as complex as from a biodegradable polymer, the drug is released by diffusion. The drug release rate from non-degradable implants can be modulated, and depends on factors, such as pore size in the matrix or polymer membrane, pore interconnectivity and tortuosity within the matrix, the distribution of the drug throughout the implant and the affinity for the drug to the polymer (Solorio et al., 2014). Even the drug concentration outside the implant affects. Most of the implantable non-degradable DDSs can be divided into two categories: reservoir or matrix systems (Solorio et al., 2014). In Figure 10 the schematic representation of a reservoir- and a matrix or monolithic system is presented. In both systems the limiting step on the drug release rate is the drug diffusion through the polymer. The drug release from a reservoir system can be modeled by the Fick´s second law and, if certain criteria are filled, it presents a zero-order release up to 60% cumulative release (Fu et al., 2010, Solorio et al., 2014). From a matrix system the release profile follows a first-order kinetics, but only if the polymer is a non-swellable polymer (Solorio et al., 2014). First, there is an initial burst release of the drug followed by a slower release until equilibrium is reached. The burst release can happen both from reservoir and matrix systems (Huang et al., 2001). In the reservoir systems it is due to the fact that the polymer membrane has been saturated under storage. In matrix systems it is due to that drug particles have been trapped on the surface during the manufacturing process.

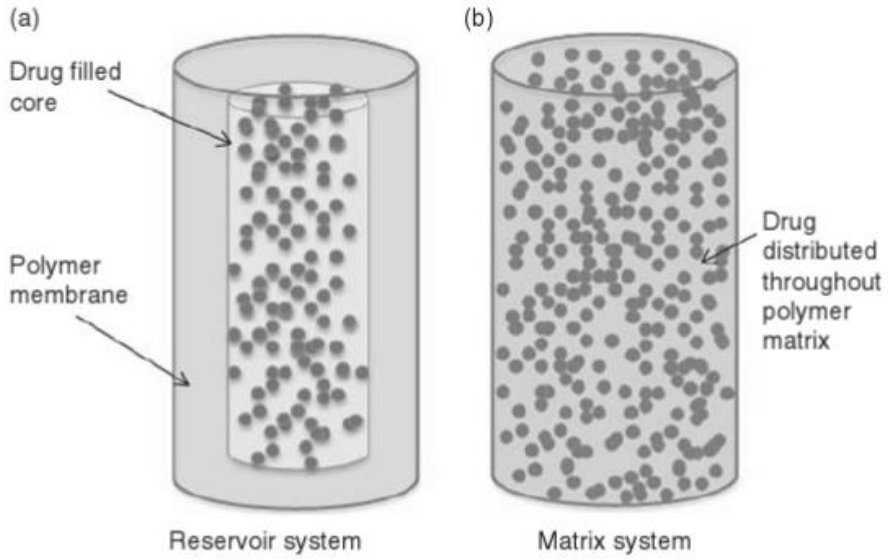


**Figure 10.** Schematic representation of a (a) reservoir- and (b) a matrix or monolithic drug delivery system (Solorio et al., 2014).

The most common non-degradable polymers used in the biomedical and pharmaceutical field are PDMS, EVA and polyurethane (PU). The chemical structures are presented in Figure 11.

One of the most common non-degradable polymer used in drug delivery systems is silicone elastomer, PDMS. The PDMS differ from other biomedical polymers in the way that its backbone consists of inorganic Si-O-Si units, instead of the hydrocarbon chains present in the other polymers. PDMS is liquid at room temperature. To achieve desirable mechanical properties, necessary for implantable material, modifications of the polymer structure are done to change the degree of cross-linking (Solorio et al., 2014). PDMS is a hydrophobic polymer, and drugs with a hydrophobic nature are usually incorporated in the polymer for sustained release (Fu et al., 2010). Controlled release from PDMS of several drugs, e.g. hormones, digitoxin, histamine and atropine from DDDs with different shapes has been reported (Chien et al., 1987, Hoffman et al., 2008, Solorio et al., 2014). PDMS has been used in both matrix and reservoir systems. There the drug has been incorporated in the PDMS matrix or as a PDMS rate-limiting membrane from a reservoir system (Chien et al., 1987).

Another polymer used in biomedical and pharmaceutical applications is PU. PU is used as a coating in breast implants and as an antibacterial coating for implants (Schierholz et al., 1997, Simmons et al., 2008, Basak et al., 2009, Pompci et al., 2012).

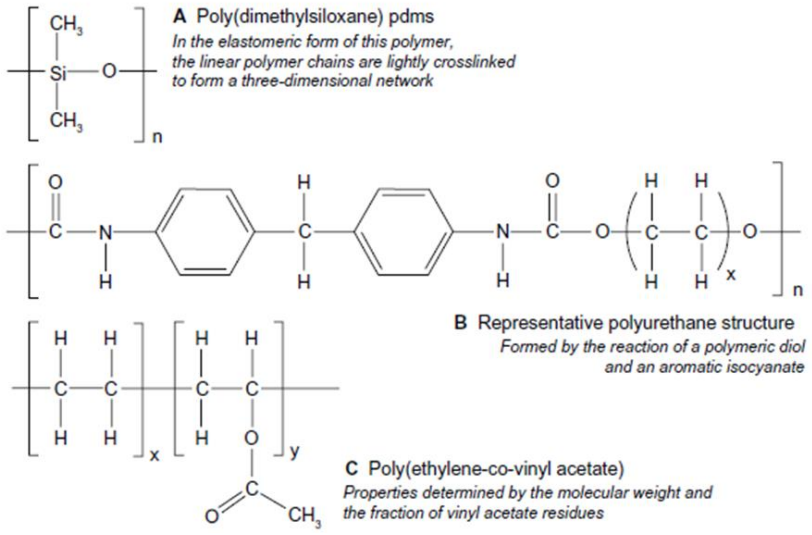


**Figure 11.** Chemical structures of non-degradable polymers used in DDS, (A) PDMS, (B) PU and (C) EVA copolymer (Malcolm et al., 2012).

#### 2.2.3.2.1 Ethylene vinyl acetate (EVA), a non-degradable polymer used in this study

EVA is one of the most commonly used non-degradable polymer, together with PDMS in implantable controlled-released applications. EVA is a biocompatible and non-toxic copolymer of ethylene and vinyl acetate which have FDA approval (Celanese, 2014a). The copolymer EVA is created via a chain polymerization, e.g. free-radical addition polymerization through the double bonds of the two monomers (Reyes, 2014b). The polymerization process is presented in Figure 12.

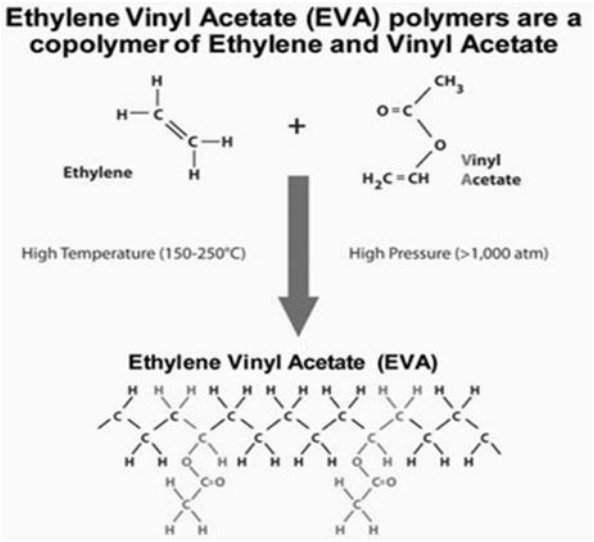


**Figure 12.** The copolymerization of ethylene and vinyl acetate (Vitaldose, 2014).

The vinyl acetate (VA) content in an EVA copolymer can range between 0 - 40% (Celanese, 2014). Depending on the content of VA in the copolymer the properties of the copolymers are different. In Table 5 the EVA properties, which are affected by the VA content, are presented.

**Table 5.** Polymer properties that change with increased VA content (modified from Celanese, 2014a).

| **Higher VA content results in:** | |
|---|---|
| **Increased** | **Decreased** |
| Polarity, affect the compatibility with different APIs | Stiffness |
| Adhesion | Softening point |
| Impact resistance | Melting point, compatible with heat sensitive APIs |
| Flexibility | Crystallinity, have an impact on the release rate |
| Optical properties | |
| Compatibility, more compatible with other polymers | |

The first EVA-based DDSs for controlled release was introduced in 1964 by Alza, Ocusert® and Progestesert® (Hoffman, 2008). The drug release was controlled with a rate-controlling membrane based on the EVA copolymer. Since then, EVA copolymers have been used in varying routes of administration: transdermal, subcutaneous, intra vaginal, ocular, buccal, sublingual and rectal (Celanese, 2014a). The products based on EVA can deliver a wide range of drugs from low molecular weight drugs to proteins, such as levodopa, 5-fluorouracil, tetracycline, bovine serum albumin, heparin as some examples (Celanese, 2014a, Solorio et al., 2014). The EVA copolymer has also been used as coatings of drug eluting stents and has been studied for the use in an esophageal stent (Mani, 2007, Guo et al

2007). Research has been done to apply EVA copolymer in delivery of stem cells, growth factors and biological agents (Reyes et al., 2014b). EVA copolymers can be treated using common pharmaceutical processes and can be sterilized (Celanese, 2014a). In Table 6 some of the applications of the EVA copolymer is presented.

**Table 6.** Some pharmaceutical applications of the EVA copolymer (Celanese, 2014a).

| Trade Name | Manufacturer | Active Ingredient | Indication/Application |
|---|---|---|---|
| Ocusert | Alza | Pilocarpine | Glaucoma |
| Progestesert | Alza | Progesterone | Intrauterine device |
| Implanon | Organon | Etonogestrel | Contraceptive implant |
| NuvaRing | Organon | Etonogestrel/Ethinylestradiol | Contraceptive intravaginal ring |
| Actisite | Alza/J & J | Tetracycline | Periodontitis |
| Cypher | Cordis/J&J | Sirolimus | Vascular restenosis |
| Vitrasert | Bausch & Lomb | Gancyclovir | CMV retinitis |
| Bravo Matrix | Surmodics | Varies | Stent coatings; intravitreal implants |

EVA copolymers have also been used in medical applications in combinations with other polymers. Vitrasert is an implant, containing an antiviral medicine for ophthalmic insert, which is based on the mixture of EVA copolymer with polyvinyl alcohol (PVA) (Soloris et al., 2014). Almeida et al. (2012) investigated the drug release from EVA matrixes containing polyethylene oxide.

Although both PDMS and EVA have been used in pharmaceutical applications for decades, they are still the most used polymers in implantable DDS.

### 2.2.3 Essential polymer properties in pharmaceutical implantable controlled-release applications

In the early stage of the development of PBDSs the polymers ability to be processed and sterilized must be taken into account. Additives can be used to modify the properties of polymers during the processing (Labarre et al., 2011). The available sterilization methods, e.g. autoclaving, ethylene oxide or γ-radiation, are not suitable for all polymers nor all drugs (Woodruff et al., 2010, Labarre et al., 2011). The problems during or after the sterilization process can occur with regard to the used high temperatures that can be the reason for the inducing reactions in chemical groups of the polymer or modifications of the polymer

structure under sterilization. When selecting the sterilization method, the structure of the device, the properties of the polymer and the final application must be taken into account.

In order to use polymers in the medical field they have to be biocompatible and non-toxic. One definition of biocompatible from 1986 is, according to Labarre et al.; *"The ability of a material to perform with an appropriate host response in a specific application"*. Nowadays the definition is wider and more complex, and includes both tissue and blood compatibility. A schematic representation of the processes involved in the term biocompatibility is presented in Figure 13.

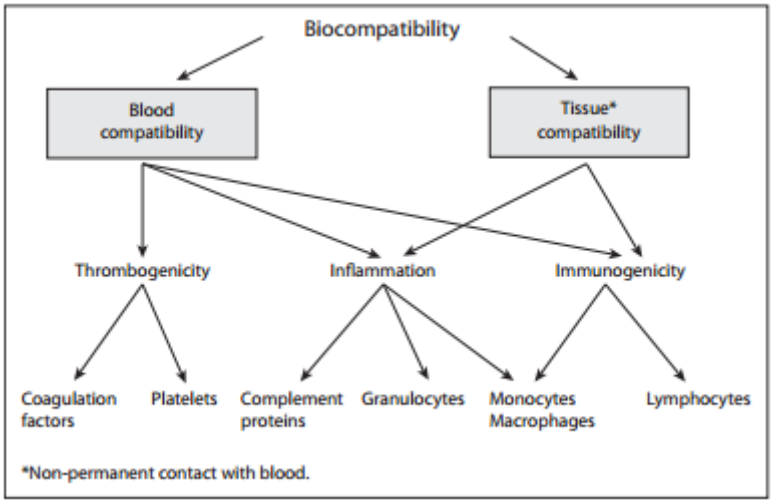


**Figure 13.** Schematic representation of the possible reactions that polymeric materials of the implantable devices can cause during administration *in vivo*. For the sake of simplicity, water and ions are not included (Labarre et al., 2011).

The toxicity of a material is related to the cell death generally induced by soluble products from the polymer. The toxicity can either be local or systemic (Labarre et al., 2011). The toxicity of polymers is caused by products that leach out of the polymer. The leachants can be unreacted or residual monomers or residual catalyst from the polymerization process, degradation products of the polymer, fillers or sterilization agents (Shastri et al., 2002, Woodruff et al., 2010). The polymers used in DDSs have to be non-toxic. The toxicity of them has to be evaluated also after the manufacturing and sterilization processes, since the additives or the sterilization agents can produce toxic byproducts that can leach from the PBDS.

## 2.3 Contraceptive polymer drug delivery devices

Implantable drug delivery systems for contraceptives have been studied since the 1960s. Controlled drug delivery of contraceptives has many advantages over tablets and injections. Some examples of the advantages are (i) reduced dosing, (ii) improved bioavailability and (ii) improved patient compliance (Shastri, 2002). Polymeric contraceptive DDSs have been manufactured as rods, IUSs and IVRs. There is a limited number of polymers that can be used as IUSs or IVRs since they have to be non-swellable and non-biodegradable or the degradation rate has to be very slow. The marketed IUSs and IVRs consist of non-degradable polymers such as PDMS or EVA. The non-degradable devices need to be removed from the site when the drug has released. Nor IUS neither IVR of biodegradable polymers have been marketed. The disadvantages with the potential use of biodegradable IUSs or IVRs are that (i) they cannot be removed from the site and (ii) there can be inter-variance between patients. Even a sufficient mechanical strength of the device for insertion can be a problem with biodegradable IUSs or IVRs.

A summary of the contraceptive IUSs and IVRs that have been previously or are currently on the market and their manufacturing methods are presented in Table 7.

**Table 7.** Contraceptive IUSs and IVRs previous or currently on the market.

| Trademark | Drug | Polymer | Device | Manufacturing method | Reference |
|---|---|---|---|---|---|
| Progestasert® | progesterone | EVA (rcm)[1] | IUS | Extrusion/Injection molding | Chien et al., 1987, Hoffman, 2008 |
| Vaginal ring® | medroxy-progesterone | Silicone rubber, PDMS (matrix and rcm) | IVR | NA | Hoffman, 2008 |
| Nuvaring® | etonogestrol, ethinylestradiol | EVA (matrix and rcm) | IVR | Extrusion/Injection molding | Baum et al., 2012 https://www.merck.com/product/usa/pi_circulars/n/nuvaring/nuvaring_ppi.pdf |
| Mirena® | levonorgestrel | PDMS (matrix and rcm) | IUS | Extrusion/Injection molding | http://www.mirena-us.com/ |
| Progering® | progesterone | Silicone elastomer (matrix) | IVR | NA | http://www.path.org/publications/files/RHSC_progesterone_br.pdf Thurman et al., 2013 |

[1] rcm= Rate-controlling membrane

In the IUS that is currently on the market, Mirena®, the device backbone is made of polyethene with a drug-delivery cylinder wrapped around it. The IVRs, Progering® and Nuvaring®, are made of the silicone rubber/PDMS and EVA, respectively. The devices are manufactured by extrusion and injection molding.

There is currently a lot of research ongoing of incorporating anti-viral agents together with contraceptives into the IVR (Han et al., 2007, Malcolm et al., 2012, Thurman et al., 2013, Conrad, 2014). The technology is called multipurpose prevention technologies (MPT) and are consisting of IVRs, gels and films containing a contraceptive, anti-viral and/or anti-sexually transmitted infections properties (Conrad, 2014). Combinations with non-hormonal contraceptives levonogestrol/3-Azido-3-deoxythamidine, levonogestrol/ tenovir, levonogestrol/dapivirine and levonogestrol/medivir-150/zinc acetate are currently under development (Han et al., 2007, Thurman et al., 2013, Conrad, 2014). The aim of the combination is the prevention of both pregnancy and infection caused by human immunodeficiency virus (HIV). Most of the MPT currently under research are based on PDMS, PU or EVA.

A non-polymeric indomethacin-containing copper IUS is commercially available in China. The drug is incorporated in the device in a separate compartment to decrease the bleeding and pain that is related to the presence of the IUS in the body (Liang et al., 2008).

The Population Council (2014) has developed a one-year contraceptive IVR with an entirely NCE, Nestorone®. It is a combination of Nestorone® with estrogen, and it is developed as an alternative with decreased risk for venous thrombosis. The product is designed for 3 months of continuous use (Brache et al., 2013). It is currently under clinical Phase 2 trial (Clinical trials, 2014). Another NCE under research is estetrol for use in combination with levonogestrol or etonogestrol (Sitruk-Ware et al., 2013).

Progesterone receptor modulator IVRs with ulipristal actetate in a silicone rubber matrix is under development for women with contraindications to estrogens (Jensen, 2013).

To sum up, the contraceptive IUSs and IVRs have been used for decades. The polymeric IUSs and IVRs have usually employed PDMS or EVA as the reservoir or matrix for the incorporated drug(s). In the IUS the drug has been released from a cylinder wrapped around the IUS backbone, whereas in the IVRs the drug has been released from the IVR interior through a polymeric rate-controlling membrane. The implantable IUSs and IVRs are manufactured by extrusion and injection molding. A major part of the ongoing research is focusing on MPT, where an additional drug(s) are incorporated into the device. NCEs are studied in the development of alternatives with less adverse effects, e.g. lower risk for venous thrombosis. Up to date, there has not been reported any research in the field of new manufacturing methods for IUS and IVR devices.

# 3. Aims of the study

The main aim of this work was to explore the potential of 3D printing in fabrication of PBDS prototypes. Furthermore, the goal was to investigate the suitability of a new feedstock material for the printer used. The solid-state characteristics of the drug, the effect on drug loading on the printability and the drug release from the devices were studied.

The specific aims were:

- study the printability of PBDS prototypes with a 3D printer using the FDM™ technique
- study the printability of a new feedstock material for the printer
- perform solid-state characterization of the drug substance in the printed PBDS
- study the appearance and the drug release properties of the printed PBDS

# 4. Materials

Materials used in this work were two polymers, PCL (CAPA™6500, Perstorp) and different grades of the EVA copolymer containing different amounts of vinyl acetate, and as a model drug the poorly soluble micronized indomethacin was used (Esteve Quimica S.A, Spain, 99.9%). As dissolution media, three different media were tested, milli-Q-water, sodium chloride (Sigma-Aldrich, China) and (2-Hydroxypropyl)-β-cyclodextrin (Sigma-Aldrich, China). To prepare a metastable α-form of indomethacin, absolute ethanol (Etax Aa, 99.5 m/m%, Altia, Finland) was used. Chloroform (Merck KGaA, Germany) and dimethyl sulfoxide, DMSO (≥99,5%, Sigma-Aldrich, France), was used in the drug content analysis.

## 4.1 Indomethacin

Indomethacin is a white, crystalline powder. It is practically insoluble in water, sparingly soluble in alcohol (Martindale). Indomethacin is a non-steroidal anti-inflammatory drug (NSAID) with a molecular weight of 357.57 g/mol and melting point of 158 ºC. In Figure 14 the structure of indomethacin is presented. Indomethacin can exist in many polymorphic forms, stable γ-form, metastable α-form and amorphous form are the most known solid-state forms, but recently additional polymorphic forms has been discovered. Surwase et al. (2013) reported of four new polymorphic forms, δ, ζ, η and Ɛ-forms of indomethacin. Indomethacin has an anti-inflammatory, analgesic and antipyretic effect. It inhibits the synthesis of prostaglandins involved in pain, fever and inflammation. Its pharmacological effect is mediated through inhibition of the enzyme cyclooxygenase (Martindale).

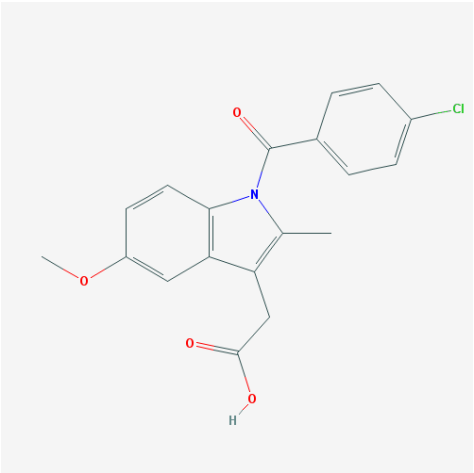


**Figure 14.** The molecular structure of indomethacin (Pubmed, 2014).

## 4.2 Polymers

### 4.2.1 Polycaprolactone

Polycaprolactone (PCL) is a biodegradable hydrophobic semi-crystalline polymer. The PCL used in this study, CAPA™6500 is a high molecular weight linear polyester. Mean molecular weight is 47500 ± 2000, melting point 60-62 ºC, glass transition temperature -60 ºC and heat of fusion 76.9 J/g. The degree of crystallinity is 56% and crystallization temperature is 25.2 ºC (CAPA™6500, 2014). The density of PCL is 1.1g/cm$^3$. The empirical formula of PCL is $[-O(CH_2)_5CO-]_n$. The molecular structure is presented in Figure 15. PCL is soluble in many solvents at room temperature, e.g. chloroform, dichloromethane and toluene. It is insoluble in water, alcohol, petroleum ether and diethyl ether (Woodruff, et al. 2010).

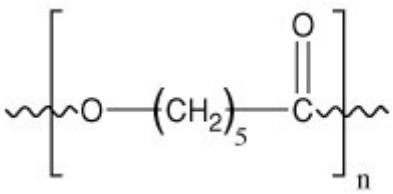


**Figure 15.** The molecular structure of PCL (Polysciences, 2014).

### 4.2.2 Ethylene vinyl acetate

EVA is a semi-crystalline non-degradable copolymer of ethylene and vinyl acetate monomers. The VA content of the EVA copolymers used in this study varied between 9-33 %. Melting points of the polymers was between 60-102 ºC, the linear relationship between melting point and VA-content is presented in Figure 16. The melt index varied between 1.1-500 g/10min. The densities of the EVA copolymers varied between 0.924-0.952 g/cm$^3$. The decomposition temperature of all grades is 210 ºC. The molecular structure is presented in Figure 17.

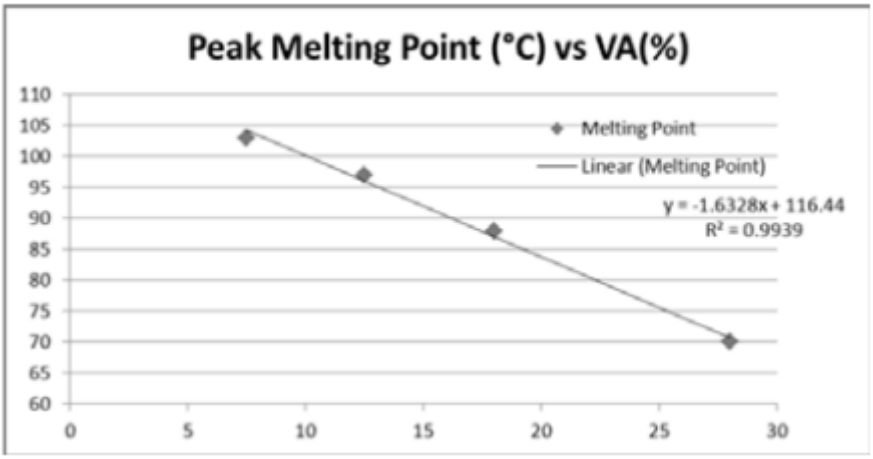


**Figure 16.** The linear relationship between melting point and VA-content in EVA copolymers (Celanese, 2014).

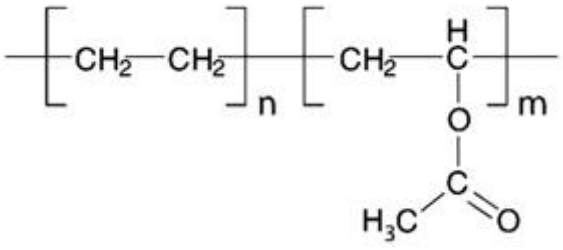


**Figure 17.** The molecular structure of the EVA copolymer (Vitaldose, 2014).

## 4.3 Formulations

The formulations used in this study are presented in Table 8. The formulation of EVA 3 with 15 % indomethacin was used only as a filament in the drug release media evaluations, and therefore, no additional investigations of the filaments were performed.

**Table 8.** The formulations used in the release study.

| Polymer | Drug content |
|---|---|
| PCL | 5 |
| PCL | 15 |
| PCL | 30 |
| EVA 3[1] | 15 |
| EVA 5 | 5 |
| EVA 5 | 15 |

[1] Used only in the preliminary release tests

# 5. Methods

## 5.1 Fabrication of the prototypes

The fabrication process of the prototypes consisted of the following steps: (i) filament manufacturing by hot melt extrusion, (ii) CAD designing of the prototypes and (iii) printing of the samples with a desktop 3D printer.

### 5.1.1 Hot melt extrusion (HME)

The hot melt extrusion was done with a HAAKE miniCTW micro-conical twin-screw extruder (Thermo Fisher Scientific, Karlsruhe, Germany). The extruder is a small-scale conical twin-screw extruder with co- and counter-rotating screws. The maximum load of the extruder is 7 $cm^3$.

To begin the hot melt extrusion process, the extruder temperature has to be adjusted first. The applied extrusion temperature was about 15 - 40 ºC above the melting point of the polymer, depending on the rheological properties of the polymer (Table 9). All selected extrusion temperatures were below the melting point of indomethacin. After the extruder had reached the target temperature the screw rotation was turned on. The rotation speed for the melting and blending process was set to 30 rpm. The API and the polymer were separately weighed into small plastic bags. First, about 1/5 of the polymer were fed into the extruder and when it had melted, subsequently, micronized indomethacin and the polymer were added into the extruder hopper. When feeding and blending, the extruder was run in a circulation mode, and therefore it was possible to feed the materials separately. The extruder had a manual feed mechanism. The materials were fed into the barrel, when a piston was manually pressed down in the hopper. The torques in the extrusions varied from 0.20-1.45 Nm.

The residence time in this study was 10 minutes. Residence time in the barrel, was defined as the time from which all material was fed into the barrel and the torque had stabilized, until the die at the end of the barrel was opened. After blending for 10 minutes the rotation

speed was set to 10 rpm and the drug-polymer mixture was extruded as filament through a die that was located at the end of the barrel. The used dies were 1.5-2.5 mm in diameter, depending on the swelling properties of the polymers. According to the manufacturer of the printer the filament diameter for the printing should be 1.75 mm ± 0.05 mm. The diameter of the extruded filament was controlled on-line with a laser diameter measurement device (HAAKE, Karlsruhe, Germany) equipped with a data display (Zumbach USYS, Orpund, Switzerland). The equipment was placed right after the extruder to directly monitor the diameter of the extruded filament. A conveyer belt (Thermo Scientific, Karlsruhe, Germany) was placed after the diameter monitoring equipment to slowly cool down the coming filament as well as to adjust the filament diameter to the desired range by changing the speed of the belt. When the extruded filaments had cooled down, their diameter was measured again. Only filaments with acceptable size limits were used for 3D printing. In Figure 18 the hot melt extrusion set-up is presented.

**Table 9.** Polymer properties and the applied process parameters in the hot melt extrusion process.

| **Polymer** | **VA (vinylactetate) content(%)[1]** | **MI (g/10min) 2.16kg/190ºC[1]** | **Flexural modulus (MPa)[1] ASTM D790** | **Melting point (ºC) [1]** | **Extrusion temp (ºC)** | **Die (mm)** | **Drug content (%)** |
|---|---|---|---|---|---|---|---|
| PCL | | 28 | 411 | 60 | 100 | 1.5 | 0, 5, 15, 30 |
| EVA 1 | 9 | 2.8 | 101 | 101 | 120 | 1.5 | NA |
| EVA 2 | 9 | 8 | 115 | 98 | 120 | 1.5 | NA |
| EVA 3 | 9 | 1.1 | 123 | 102 | 120 | 1.5 | 0,15 |
| EVA 4 | 12 | 10 | NA | 95 | 120 | 1.5 | NA |
| EVA 5 | 16 | 28 | 60 | 89 | 105-110 | 1.5 | 0, 5, 15 |
| EVA 6 | 18 | 3 | 45 | 87 | 120 | 1.5 | NA |
| EVA 7 | 18 | 150 | 42 | 84 | 100 | 2.0 | NA |
| EVA 8 | 18 | 500[2] | 31 | 78 | 110 | 2.5 | NA |
| EVA 9 | 28 | 28 | NA | 70 | 100 | 1.5 | NA |
| EVA 10 | 33 | 33 | 7 | 60 | 100 | 1.5 | NA |
| EVA 11[3] | NA | NA | NA | NA | 120 | 2.5 | NA |
| EVA 12[4] | NA | NA | NA | NA | 120 | 2.0 | NA |

[1] Polymer properties from the manufacturer data sheets
[2] At 125ºC/0.325kg
[3] A blend of EVA 3 and EVA 8 (50:50)
[4] A blend of EVA 3 and EVA 8 (75:25)

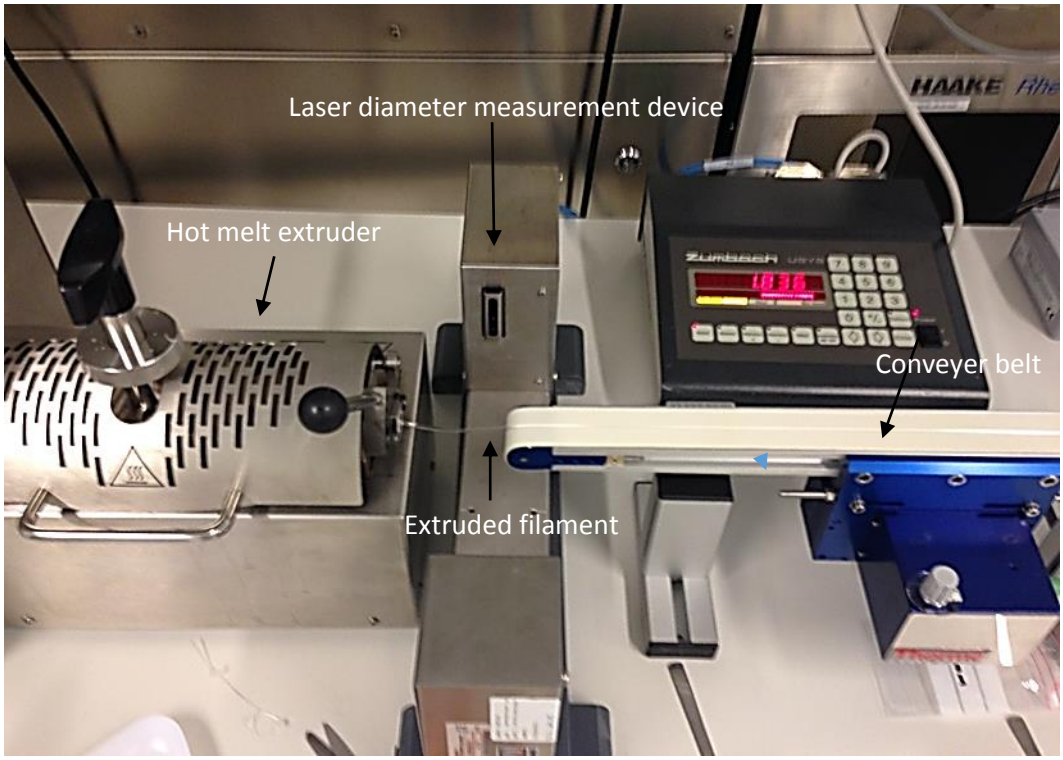


**Figure 18.** The photography of the hot melt extrusion set-up.

### 5.1.2 Design of the prototypes

Different prototypes, called IUS2, Sleeve, Rod and Ring, were designed for this study with a three-dimensional computer-aided design (3D CAD) program, *Rhinoceros 5.0*. One prototype design was kindly provided by an external company, called IUS1. After designing the prototypes in the software, the files were saved as stereolithography files (.stl) and then uploaded in the MakerWare software of the printer. In Figure 19 screenshots of the prototypes from *Rhinoceros 5.0*. software are shown.

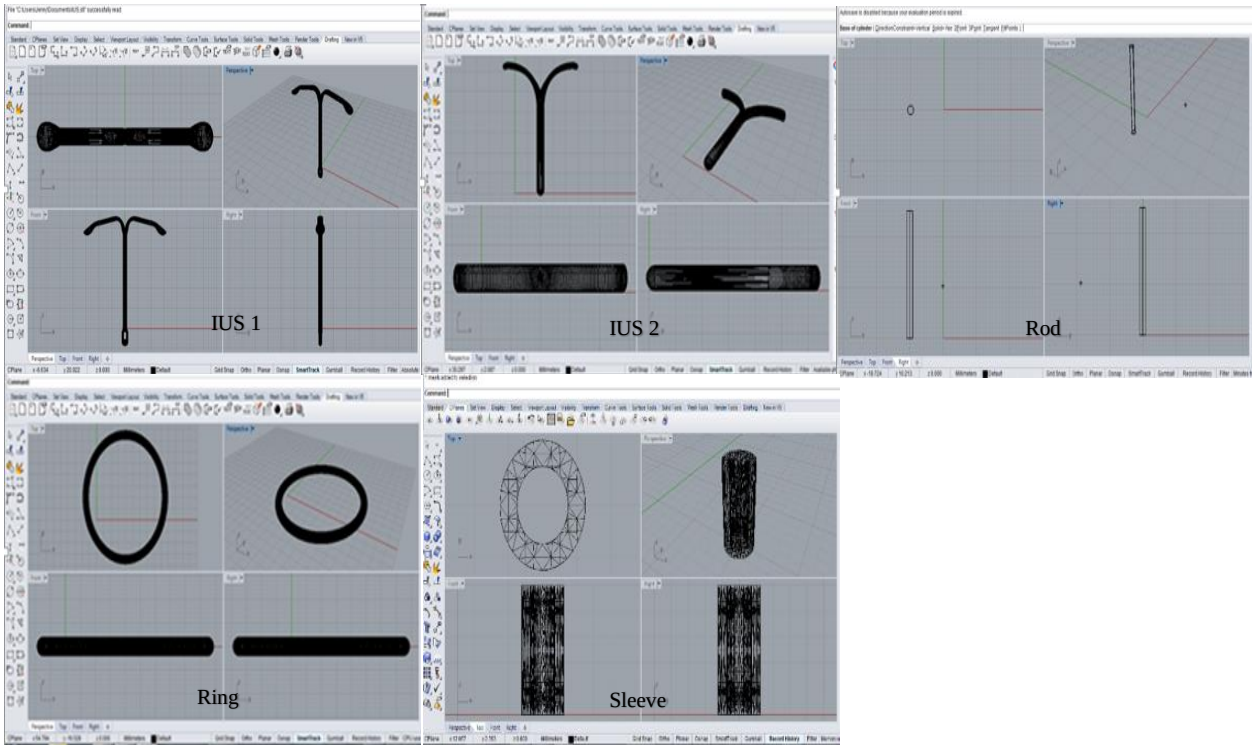


**Figure 19.** Screenshots of the prototypes in *Rhinoceros 5.0* software.

### 5.1.3 3D printing with the fused filament fabrication technique (FFF)

3D printing was performed with a MakerBot Replicator 2 (USA) desktop printer, which uses the fused filament fabrication technique (FFF) for 3D printing. FFF is a solid freeform fabrication technique based on the fused deposition modelling, FDM$^{TM}$, patented by Stratasys. The printer original feedstock materials are PLA and PCL. The printing process starts usually with loading the filament into the printer and importing the 3D CAD model into the printer software. When the filament is loaded and the file imported the printing process begins. In Figure 20 a picture of the printer and a schematic representation of the MakerBot replicator 2 extruder is presented.

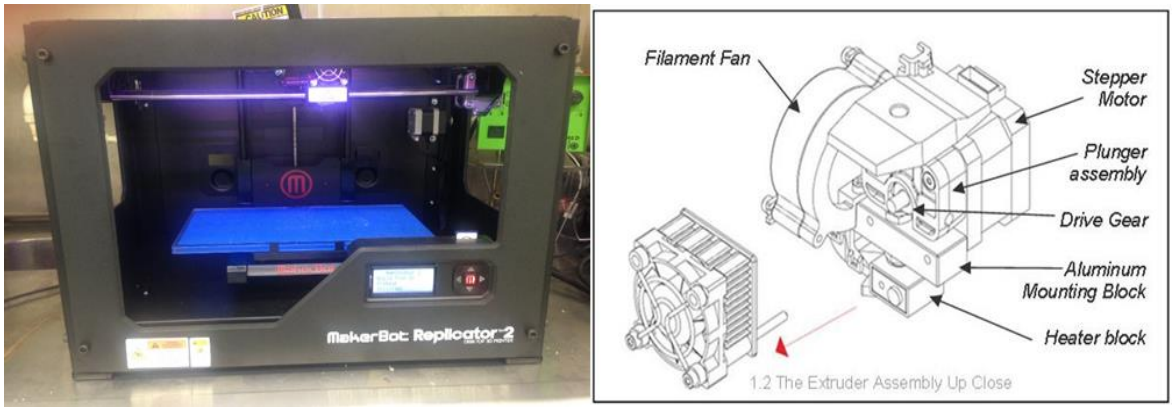


**Figure 20.** The photography of MakerBot Replicator 2 desktop 3D printer (left), and the schematic representation of The MakerBot Replicator 2 extruder (right) (Bilby3D, 2014).

In this study the filament loading process started with heating of the liquefier and nozzle to temperatures well above the melting point of the polymer, about 60 ºC – 115 ºC above melting point, depending on the properties of the polymer. The loading temperatures are presented in Table 11. When the set temperature for the loading was reached, the filament was fed into the liquefier via pinch rollers until melted polymer got extruded from the nozzle. The purpose of the extrusion was to empty the liquefier and nozzle from previous filament residues and to check that the flow of the extruded material was good enough for printing. The default nozzle size in MakerBot Replicator 2 was 0.4 mm.

When the filament was successfully loaded and the flow was appropriate, the printing process continued by importing the 3D CAD model as a .stl file into the MakerWare software. Other files that the MakerWare software supports are .obj or .thing. The software has a slicing tool, called MakerBot slicer, which translates the 3D CAD model into a code for the printer by slicing it into thin horizontal layers. In Figure 21 screenshots of the printer software is presented.

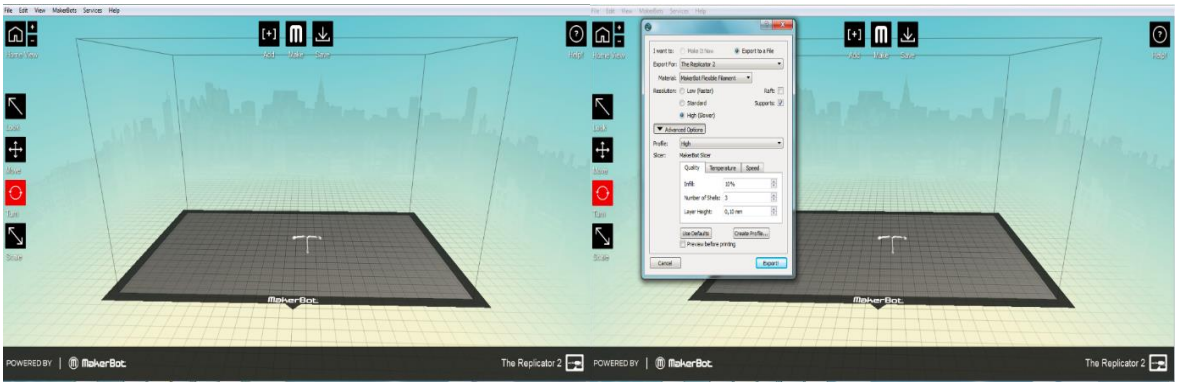

**Figure 21.** Screenshots from the printer software, on the left IUS 1 prototype, on the right the process parameter window included.

In the printer software, quality parameters, temperature and speeds, traveling speed of the nozzle and printing speed, was set prior printing. The possible quality parameters were percentage infill, layer height and number of shells. The infill is the internal structure of the object. A higher percentage gives a more solid object: 100 % infill is completely solid and 0 % infill completely hollow. The number of shells is the amount of outlines printed on each layer of the object. More shells give a stronger object. Available settings were between 1 and 100. The layer height gives the thickness of each layer. The smaller is the layer height, the finer is the vertical resolution. The possible layer heights were in the range of 0.01-0.40 mm. The achievable maximum printing temperature was 250 ºC. The extruding and traveling speed span was from 10 mm/s to 200 mm/s. The traveling speed means the speed, which the extruder travels between objects on the platform. Besides these parameters, it was possible to create an own custom slicing profile with the MakerBot slicer, where several parameters could be changed, for example, filament diameter, infill patterns, minimum layer duration and filament cooling. In this work only changeable parameters within the default profiles were used. The quality parameters, number of shells and layer height, were set to be the same for printing of all prototypes. The infill parameter varied between prototypes. In Table 10 the printing parameters for different prototypes are presented. The prototype, *sleeve*, was not successfully printed and, therefore, not presented.

**Table 10.** The printing parameters set for different prototypes.

| Prototype | Infill (%) | Layer height (mm) | Number of shells |
|---|---|---|---|
| IUS1 | 10 | 0.1 | 3 |
| IUS2 | 100 | 0.1 | 3 |
| Ring | 100 | 0.1 | 3 |
| Rod (EVA) | 100 | 0.1 | 3 |

After the filament was loaded, the file imported to the printer software and the printing settings were set, the printing began. The filament melted in the liquefier and nozzle before it was extruded layer by layer on the build plate, starting from the bottom of the prototype. When the filament was extruded from the nozzle, more filament was automatically fed into the liquefier. The needed filament loading speed was calculated by the software, based on the pre-set printing speed, road width and layer height. The extruder of the printer moved in X- and Y- directions to complete one layer at a time and when the layer was finished, the build plate moved down, in Z-direction by a pre-set layer height (0.1mm). Kapton® polyimide tape as a surface of built plate was used for PCL, whereas low density

polyethylene (LDPE) film was chosen for printing of EVA polymers. When the printed prototypes had cooled down, they were removed from the build plate. MakerBot Replicator 2 has only a single extruder, therefore, the necessary support structures and rafts, were built with the same drug-free polymer material as the prototypes and were then cut off from the medical devices. The melting points, the tested loading and printing temperatures and the tested printing speeds of the polymers are presented in Table 11. Different grades of EVA (Table 9) was tested in this study, but only those which were successfully loaded and printed are presented in Table 11.

**Table 11.** The melting points, loading and printing temperatures, printing speeds and melt index for the different polymers.

| Polymer | Melting point (ºC)[1] | Loading temp (ºC) | Printing temp (ºC) | Printing speed (mm/s) | Melt index (g/10min), 190ºC, 2.16kg)[1] | Drug content (%) |
|---|---|---|---|---|---|---|
| PCL | 60 | 120 | 100 | 45 | 28 | 0, 5, 15, 30 |
| EVA 1 | 101 | 215 | 210-215 | 10-35 | 2.8 | |
| EVA 2 | 98 | 170-190 | 160-190 | 10 | 8.0 | |
| EVA 4 | 95 | 190 | 170-190 | 10 | 10 | |
| EVA 5 | 89 | 160-165 | 150-170 | 10-30 | 28 | 0, 5, 15 |
| EVA 7 | 84 | 160 | 145-155 | 10-20 | 150 | |
| EVA 12[2] | NA | 215 | 205-215 | 40 | NA | |

[1] Melting points and melt index from the manufacturer product data sheets

[2] A blend of EVA 3 and EVA 8 (75:25), melting point and melt index not detected

## 5.2 Rheology measurements

Rheology measurements were carried out to determine the viscosity of the polymers at the printing temperatures. The measurements were done on the drug-free and the drug-loaded filaments. The measurements were conducted with a rotational AR 2000 rheometer (TA instruments, USA) using a parallel-plate geometry. The gap and the geometry of the plates were 1 and 15 mm, respectively. Shear rate range was 0.005 to 200 $s^{-1}$. Sample size was 0.6 g. The polymers were measured at printing temperatures, 100 ºC and 165 ºC for PCL and EVA, respectively. The filaments with the highest drug loading were also measured at 165 ºC (PCL) and 135 ºC (EVA), since additional printing experiments were done at those temperatures. The viscosity was calculated as the ratio between the applied stress and the rotation speed.

## 5.3 Drug content analysis

Drug content analysis were done with the extruded PCL filaments containing indomethacin to determine the exact amount of indomethacin in the sample as well as the homogeneity of the drug distribution in the samples. The drug content analysis were first done with chloroform as a solvent for both PCL and indomethacin and diluted with DMSO and the second experiment was done with only chloroform.

First, the exact amount of the extruded filaments with and without the drug in the range of 130.0 mg ± 1 mg was dissolved in 2 ml chloroform. After the polymer had dissolved, 3 ml DMSO was added to the solution. The DMSO is an excellent solvent for indomethacin. But it is not a solvent for PCL (Bordes et al., 2010), and it can cause precipitation of the polymer. However, it will take time for PCL to crystallize in the presence of DMSO. Therefore, the drug content analysis was done quickly to avoid a prominent precipitation of PCL and by that prevent entrapping of the drug into the formed PCL particles. The solutions were then diluted with DMSO, the dilution factors are presented in Table 12. The dilutions were filtered with a 0.45µm polypropylene filter and the absorbance was measured with an UV/VIS spectrophotometer (Lambda35, PerkinElmer, USA) at 265 nm. Before content analysis a standard curve was built up for indomethacin in DMSO as the solvent, from a stock solution of 1mg/ml, to be able to calculate the exact amount of drug in the filaments. The wavelength, at which the absorbance maximum of indomethacin in DMSO occurs, was found out by scanning 0.01mg/ml dilution from 400 to 190 nm, using UV/VIS spectrophotometer. The obtained standard curve is presented in Figure 22. Linearity was proven with the $R^2$ value of 0.9988.

Because of the risk for precipitation and entrapping of the drug in the PCL particles a second drug content analyze was done with only chloroform as a solvent and dilution agent. First, the exact amount of the extruded filaments with and without the drug in the range of 130.0 ± 1mg was dissolved in 5 ml chloroform. After the filament had completely dissolved (about 1 hour) the solutions were further diluted with chloroform before the UV/VIS measurements to get detectable absorbance. The dilution factors and the theoretical amount of indomethacin for each sample is presented in Table 12. The samples were measured without filtering, because there were no risk for precipitation of any component as chloroform is a good solvent for the amount of both ingredients used in this study. A standard curve was

done for indomethacin in chloroform (Figure 12), the same way as for DMSO. Linearity was proven with the $R^2$ value of 0.9996.

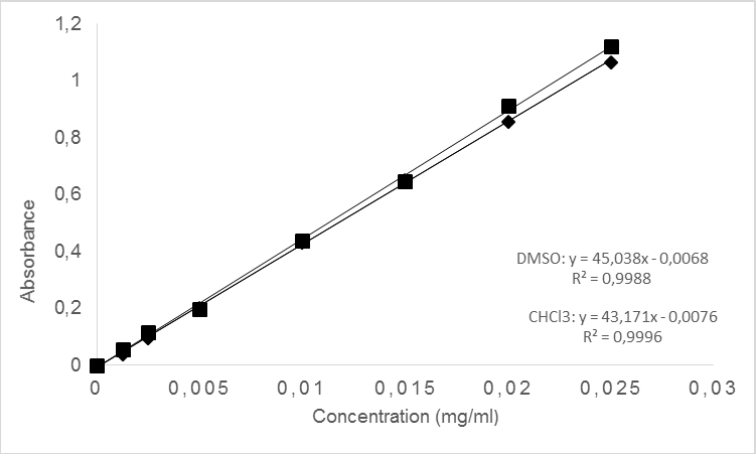


**Figure 22.** The standard curves for (■) DMSO and (♦) chloroform.

**Table 12.** Drug content analysis dilutions factors and theoretical drug amount (the experiment with only chloroform), n=3.

| IND:PCL ratio | Dilution factor | Theoretical IND amount (mg) |
|---|---|---|
| 5:95 | 400 | 6.5 ± 0.014 |
| 15:85 | 1000 | 19.6 ± 0.038 |
| 30:70 | 2000 | 39.3 ± 0.014 |

## 5.4 Scanning electron microscope and energy-dispersive X-ray analysis (SEM-EDX)

The morphological appearance of the extruded filaments, printed prototypes and samples (surface and cross-section) after drug release tests were analyzed by scanning electron miscroscopy (SEM). A LEO Gemini 1530 with a Thermo Scientific UltraDry Silicon Drift Detector (Oberkochen, Germany) equipped with secondary electron and backscattered electron detectors was used. The working voltage of 8 kV was used. A thin carbon coating was evaporated onto the samples surfaces to make them electrically conductive. In addition, the presence and the location of the remaining drug in the filaments and 3D prototypes after 30 days of the release studies was detected by performing the elemental analysis by means of EDX (Thermo Scientific, Madison, Wisconsin, USA) as an extension of SEM. The quantitative and qualitative analysis of chlorine element (present in the molecular structure of indomethacin) was performed at magnification of 50x, using an accelerated voltage of 15 kV, an image resolution of 512 x 384 and an image pixel size of 4.71 µm.

## 5.5 Preparation of physical mixture

The physical mixtures of the drug and polymers were prepared to compare the XRD, DSC and ATR-IR data with the extruded filaments and printed prototypes. The physical mixture was obtained by mixing the polymer and the micronized drug with a mortar and pestle. Before mixing the extruded polymer filaments were sliced into small pieces to obtain a homogenous mixture.

## 5.6 Preparation of polymorphic and amorphous forms of indomethacin

Indomethacin can appear in different polymorphic forms (Kaneniwa et al., 1985). To characterize in what solid-state form indomethacin was in the extruded and printed samples, amorphous and α-polymorphic form of indomethacin was made for comparison. The indomethacin used in the study was the stable γ-form, from which amorphous and α-indomethacin was made. The amorphous indomethacin was prepared by quench-cooling (Savolainen et al., 2007). Briefly, γ-indomethacin was melted on an aluminum pan at 165 ºC. When the sample was completely melted and had turned yellow, liquid nitrogen was poured over the pan.

The α-form of indomethacin was prepared by dissolving a small amount of γ-indomethacin in absolute ethanol (EtaxAA, 99,5m/m%) under stirring and heating to the maximum 60 ºC (Kaneniwa et al., 1985, Savolainen et al., 2007). The solution turned yellow, indicating that the drug was dissolved. After that milli-Q-water as the anti-solvent was added to precipitate the drug as solubility of indomethacin in water is poor. Within 30 minutes the drug was recrystallized, forming a white suspension in ethanol-water mixture. The suspension was filtered under vacuum to collect the precipitated drug. The drug was dried in the desiccator over silica under vacuum at room temperature overnight.

## 5.7 X-ray diffraction (XRD)

XRD patterns were determined on 3D printed samples, hot melt extruded filaments, γ-, α- and amorphous indomethacin and physical mixtures of drug and polymer with the help of X-ray diffractometer (Philips, X-Pert PRO MPD, Holland). The 3D printed samples were analyzed as 12 mm x 15 mm x 1 mm pieces and the filaments were analyzed as filaments with a diameter of about 1.75 mm. Indomethacin samples were analyzed as powders and the physical mixture of indomethacin and polymer was done by mixing indomethacin with small pieces of pure polymer cut from a filament with a diameter of about 1.75 mm. The samples were placed in a steel holder and scanned over $7^o < 2\theta < 40^o$ with time per step of 10.2 s. XRD scans were performed in θ/2θ Bragg-Bretano geometry using CuKα radiation (λ = 1.54 Å) with a voltage of 40 kV and a current of 50 mA using a PIXcel$^{1D}$ detector (Panalytical, Holland)

## 5.8 Differential scanning calorimetry (DSC)

To determine the thermal behavior of the raw materials, their physical mixture, filaments and printed samples, differential scanning calorimetry (DSC) were performed with the DSC Q 2000 instrument (TA instruments, USA), with a refrigerated cooling accessory, RCS 40 cooling system, that allows the temperature going down up to -40ºC. A DSC run measures the heat flow into or out of a sample in relation to the reference as a function of time. Heat into a sample, or endothermic events, are melting, Tg and evaporation and heat out of a sample, or exothermic events, are crystallization and oxidation.

The samples were run as a conventional DSC in a heat/cool/heat cycle at a temperature range of -40 ºC to 180 ºC with a heating and cooling rate of 10 ºC/min in a closed Tzero aluminum pan. As a purge gas nitrogen was used with a flow rate of 50 ml/min. The data sampling interval was 0.20 s/pt. Samples of 2±1 mg for different solid-state forms of the pure API and 10±1 mg for polymer-containing materials were used. The thermograms were analyzed with the TA Instruments universal software. The DSC system was calibrated using sapphire crystals (cell resistance & capacitance) and indium (cell constant & temperature).

## 5.9 Attenuated total reflectance infrared spectroscope (ATR-IR)

Mid-Infrared (IR) spectroscopy is a method that gives information of the molecular structure of a material. Every material has a unique spectrum, which arises from absorption of radiation into the molecular vibrational modes of the sample. The IR region is 4000 - 400 $cm^{-1}$. In this study the IR absorption spectra were obtained with an attenuated total reflectance (ATR) accessory. In ATR-IR the infrared beam passes through a crystal of a high reflective index material at such an angle that the beam is contained within the crystal, but a part of the energy extends outside the crystal and a sample in close contact with the crystal can absorb some of the radiation. ATR-IR needs minimal sample preparation, and is therefore a fast and robust technique. The used ATR-IR spectrometer was a Spectrum two IR Spectrometer (Perkin-Elmer, UK) and the spectrums were analyzed with the Spectrum10™ software. The powdered samples were analyzed as such, whereas cross-sections of polymer-containing samples were prepared for analysis. In addition, spectra from the surface of the polymer-based samples were obtained. A spectral resolution of 4 $cm^{-1}$ with 4 co-added scans over spectral range of 4000 to 400 $cm^{-1}$ was used in this study. Each sample was placed on a sampling window and 110-120 N, 140-150 N and 75 N force was applied for pure API, PCL-containing samples and EVA-containing samples, respectively. The obtained spectra were pretreated with baseline correction, normalization and data-tune up processing according to the manufacturers recommendations.

## 5.10 *In vitro* drug release

### 5.10.1 Standard curves

The release experiments were started by selecting the media in which the release testing will be done and by making standard curves of indomethacin in those media. The release test was done on the EVA 3 filaments containing 15 % indomethacin. The possible release media were purified water, 0.9% NaCl and 1 % (2-Hydroxypropyl)-β-cyclodextrin. A 0.1 mg/ml stock solution of indomethacin in ethanol (EtaxA) was prepared as the solubility of

indomethacin in the abovementioned solvents was known to be very poor. Briefly, 10 mg indomethacin was weighed into 100 ml ethanol (EtaxA) and placed on a magnetic stirrer overnight at room temperature. For all three media the wavelengths at which the absorbance maximum of indomethacin occurs were found out by scanning 0.01 mg/ml dilution from 400 to 190 nm, using an UV/VIS spectrophotometer. As the absorbance maximum was obtained at wavelength 265 nm, the standard curves were built up at that wavelength. The obtained standard curves are presented in Figure 23. Linearity was proven with a $R^2$ value of 0.9998 for water and 0.9% NaCl, and 1 for 1% (2-Hydroxypropyl)-β-cyclodextrin.

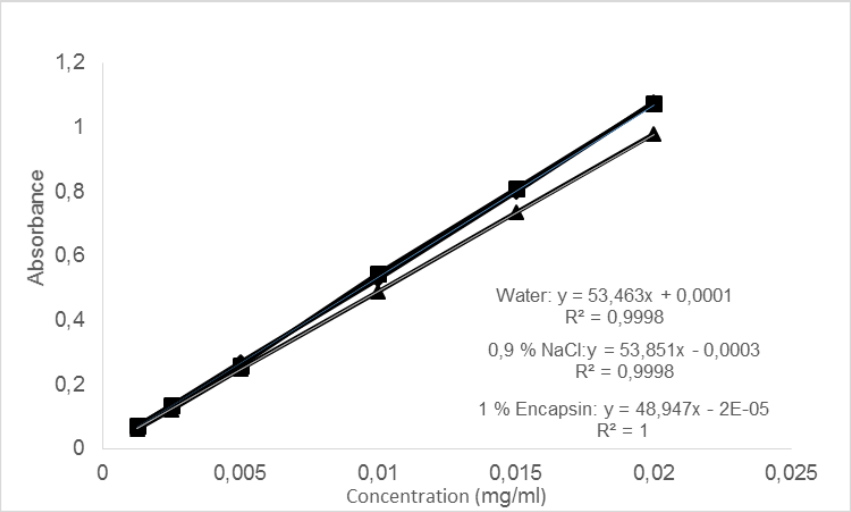


**Figure 23.** The standard curves of (♦) Water, (■) 0,9% NaCl and (▲)1% (2-Hydroxypropyl)-β-cyclodextrin (Encapsin).

## 5.10.2 Determination of solubility of indomethacin in the release media

The solubility determination of indomethacin in the release media was done to identify how often the release media had to be changed to maintain sink conditions during the release experiments. When the concentration of dissolved drug is less than 20% of the saturation condition, the system is under sink condition (Sinko, 2011). Sink condition was defined as a volume of dissolution media that was five times higher than the saturation point of indomethacin in the media.

Indomethacin is a poorly soluble drug in the chosen release media and undissolved drug particles in the sample during solubility experiments could affect the measurements. Two methods are commonly used to remove undissolved particles from the samples: filtration

and centrifugation (Liu et al., 2011). Both methods can affect the concentration of the sample. In filtration small particles can pass through the filter, giving too high concentrations. In addition, hydrophobic drug molecules can interact with the filter membrane, giving too low concentrations (Liu et al., 2011). A long separation time and possible high temperatures for a high-speed centrifugation can dissolve undissolved particles in the release media (Liu et al., 2011). The methods were compared by using indomethacin in water to determine, which method was suitable in the determination of drug solubility in the media in this study. An excess amount of indomethacin in water was stirred with a magnetic stirrer at room temperature for 15 hours. The samples (n=5) were either centrifuged (Heraeus, PICO17, Thermo Electron) at 13 000 rpm for 10 minutes or filtered through a 0.45 µm polypropylene filter using the same filter for all samples. The samples for centrifugation and filtration, were taken from the same supernatant. The results from the test is presented in Figure 24. The results shows that the drug concentrations in the three first filtered samples were lower than in the centrifuged samples, because the filter absorbed the drug. When the filter was saturated, the concentration was near the same. Based on those findings, centrifugation was chosen as an intermediate step in the determination of the solubility of indomethacin.

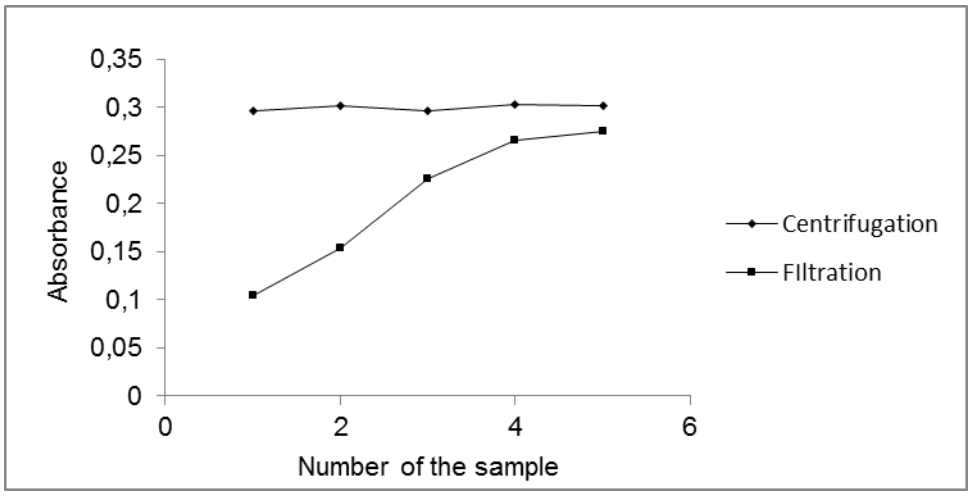


**Figure 24.** Drug concentrations in the centrifuged and filtered samples.

To determine the solubility of indomethacin in the release media an excess amount of IND was mixed with all three release media, both at 37 ºC and at room temperature. The samples were shaken for 21 hours at 37 ºC on a thermoshaker (BioSan Thermoshaker PST-100) at 700 rpm and at room temperature on a multishaker (BioSan Multishaker PSU-20) at 110

rpm. They were then centrifuged at 13 000 rpm for 10 minutes before UV/VIS spectrophotometer measurements of supernatants at 265 nm.

### 5.10.3 *In vitro* drug release tests

The drug release for both the 3D printed prototypes and the extruded filaments was studied to determine the release profiles of them and to find out possible differences between the formulations. The samples were placed within a stainless steel compression spring, which was attached to a 4 mm stainless steel threaded rod with a stainless steel wire. The steel rod was then attached to the cap to keep it straight and above the bottom of the 250 ml brown bottle. This assembly was needed to avoid the prototypes lying on the bottom of the bottle (PCL, density 1.1 g/cm$^3$, (Perstorp, 2014)) or prevent them from floating on the surface of the release media (EVA, density 0.93-0.96 g/cm$^3$, (Celanese, 2014)). A photography of the assembly is presented in Figure 25. The bottles were placed on a shaking bath (Julabo SW22, Seelbach, Germany) at 37.0 ± 0.2 ºC with shaking speed 100 rpm for 30 days. The *in vitro* release tests were carried out in triplicate, except for the PCL IUS 2 (n=1). The release media was exchanged when needed to maintain sink conditions. Samples were taken at defined time points and the concentration of indomethacin in the release media was measured spectrophotometrically at 265 nm.


**Figure 25.** The design of the set-up for the release tests.

## 5.10.4 Matrix degradation during *in vitro* release tests

Before and after *in vitro* release tests the filaments and the prototypes of the biodegradable polymer PCL were weighed to determine the drug release percentage and polymer weight loss during release experiments. After the dissolution tests the samples were dried in room temperature overnight and then weighed. The weights of the samples before the release tests are presented in Table 13. The mass loss calculations were based on the drug content analysis results and the actual drug polymer ratio was used. The percentage of released indomethacin and polymer mass loss were calculated as follows:

**Drug release percent** (%)

$$= \frac{Weight\ of\ drug\ released}{Total\ actual\ weight\ of\ drug} * 100\ \%$$

**Mass loss of the polymer** (%)

$$= \frac{(The\ initial\ weight\ of\ sample - the\ final\ weight\ of\ sample - the\ weight\ drug\ released)}{Total\ actual\ weight\ of\ the\ polymer} * 100\%$$

**Table 13.** The weights before dissolution for the PCL samples are presented.

| Sample | Theoretical drug content | Weight before dissolution test | n |
|---|---|---|---|
| Filament | 5 | 129.4 ±1.85 | 3 |
| Filament | 15 | 138.9±0.20 | 3 |
| Filament | 30 | 120.3±1.78 | 3 |
| IUS 1 | 5 | 131.7 ±1.15 | 3 |
| IUS 1 | 15 | 142.8±1.35 | 3 |
| IUS 1 | 30 | 123.3±0.35 | 3 |
| IU2 2 | 5 | 304.6 | 1 |

# 6. Results and discussion

## 6.1. Solid-state characterization of indomethacin

From the raw indomethacin amorphous and α-indomethacin was prepared to be able to characterize in which form the indomethacin was in the HME filaments and in the 3D printed prototypes. XRD, DSC and ATR-IR analyses were performed on the raw indomethacin and the prepared polymorphic forms.

### 6.1.1. X-ray diffraction

According to the literature the stable and crystalline γ-indomethacin have distinguish peaks in the X-ray diffractogram at 2θ at 10.2, 11.7, 12.7 and 17.0º (Kaneniwa et al., 1985). From Figure 26 can be seen that the raw indomethacin used in this study had peaks at 10.2, 11.7, 12.7 and 17.0º. According to Karmwar et al. (2011) the amorphous indomethacin has a complete absence of diffraction peaks in the X-ray diffractograms. The diffractograms of the amorphous form of indomethacin prepared by quench-cooling, shows a halo pattern that is in accordance with the results by Karmwar et al. (2011). The α-indomethacin form have diffractogram peaks at 7.0, 8.5, 11.5, 12.0 and 14.0 (Kaneniwa et al., 1985). The α-indomethacin diffractogram in this study was different from those reported in literature, partially due to the fact that there was not enough precipitated drug to get a good XRD pattern.

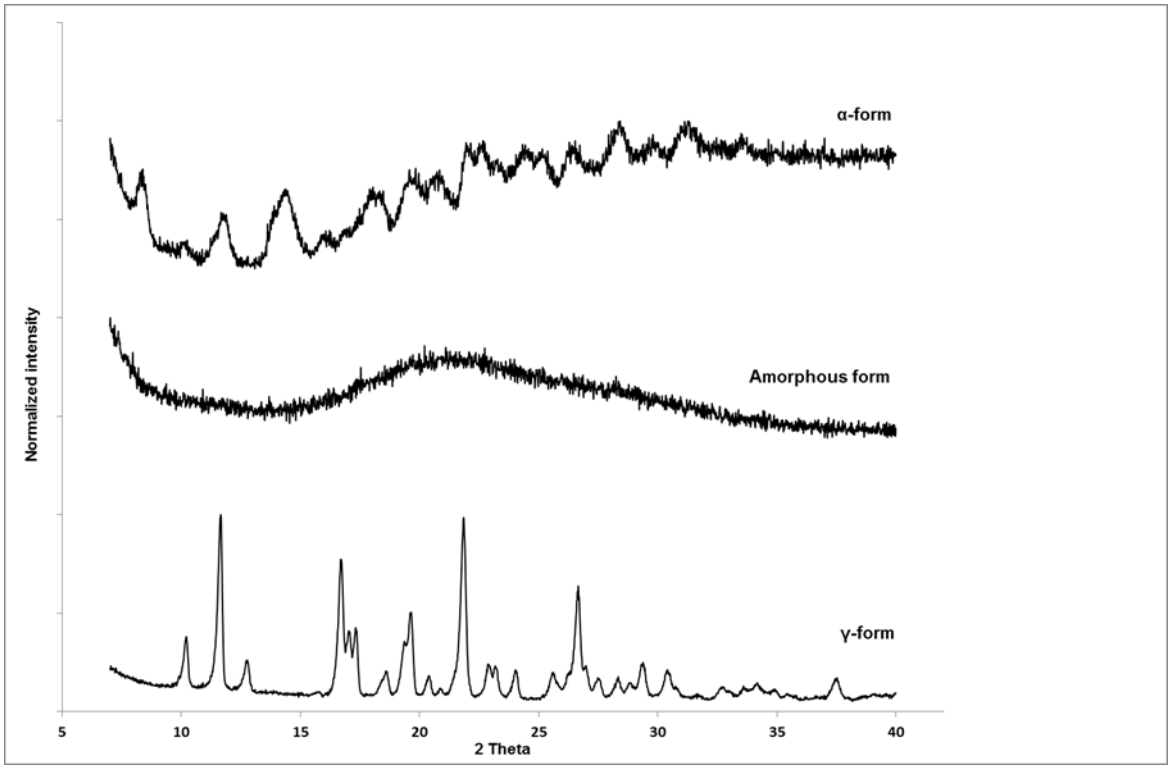


**Figure 26.** XRD diffractograms of different solid-state forms of indomethacin, γ-indomethacin, amorphous form and α-form (*there was not enough powder for measuring XRD of alpha-form*).

## 6.1.2. Thermal analysis

Further identification of the prepared forms of indomethacin was performed with a DSC. A conventional DSC was done with a heat/cool/heat cycle. For γ-indomethacin and α-indomethacin an endothermic event with onset at 160 ºC and 148-155 ºC, respectively, have been reported due to melting of the indomethacin (Kaneniwa et al., 1985, Karmwar et al. 2011). The raw indomethacin showed an endothermic event with onset at 160 ºC due to melting of the γ-form and the prepared α-indomethacin showed an endothermic event with onset at about 152 ºC (Figure 27) . The amorphous form of indomethacin has been reported to have a melting endotherm with onset temperature at 155 ºC, an exothermic event in the temperature range of 60-100 ºC due to recrystallization of the drug and a change in heat capacity due to glass transition (Tg) at 45 ºC (Savolainen et al., 2007). The prepared amorphous indomethacin had an endothermic event at onset 154 ± 1 ºC, an exothermic event onset at 99 ± 1 ºC and a change in heat capacity at about 46 ± 1 ºC.

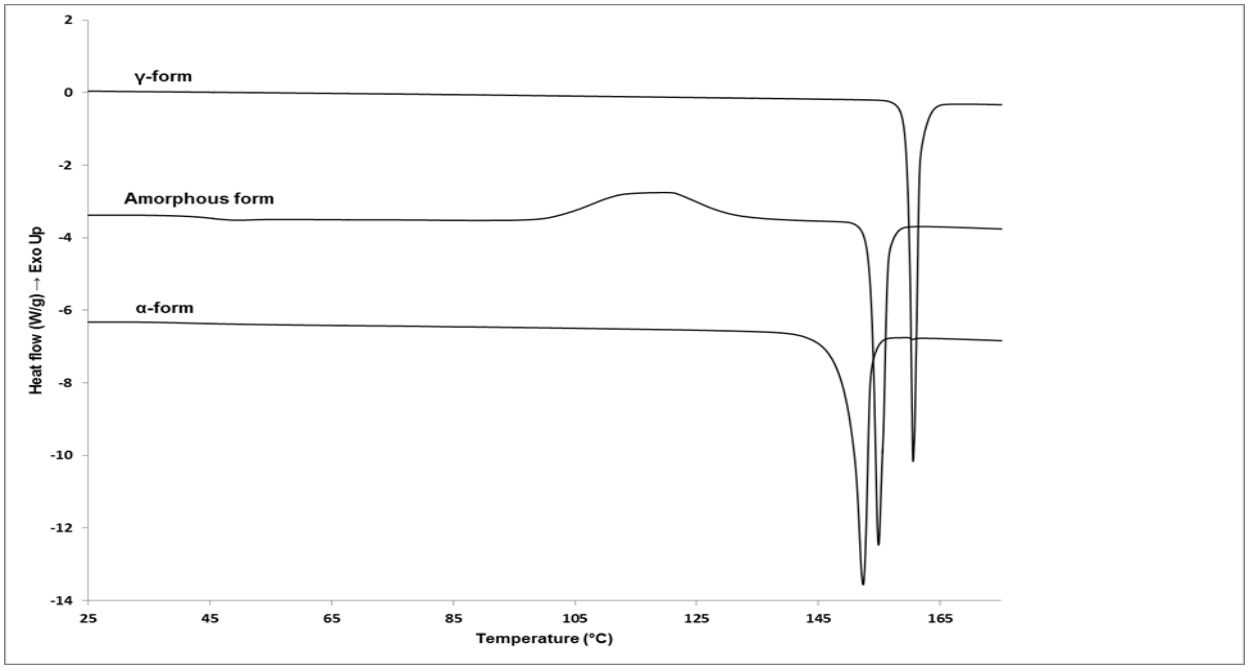


**Figure 27.** DSC thermograms of different solid-state forms of indomethacin, α-form, amorphous form and γ-form.

## 6.1.3. ATR-IR

ATR-IR analysis was conducted to confirm the results obtained from the abovementioned analysis. Indomethacin contains two different C=O groups, respectively from the carboxylic acid and benzoyl functional groups (Ewing et al., 2014). The characteristic spectral region for the stretching of carbonyl bands are in the region between 1800 and 1500 $cm^{-1}$ (Ewing et al., 2014). The characteristic band positions for the respective polymorphic forms are: at 1712 and 1690 $cm^{-1}$ for γ-form, 1735, 1688, 1680, 1649 $cm^{-1}$ for α-form and 1735, 1706 and 1680 $cm^{-1}$ for the amorphous form (Ewing et al., 2014). Karnwar et al. (2011) reports characteristic peaks for the γ-form at 1715, 1690 and 1590 $cm^{-1}$, and for the α-form at 1735, 1690 and 1650 $cm^{-1}$. As can be seen in Figure 28 the raw material for preparation of the polymorphic forms of indomethacin has the characteristic peaks for γ-indomethacin. The bands appeared in the prepared α-indomethacin (1734, 1690 and 1648 $cm^{-1}$) and the amorphous form (1735, 1705 and 1678 $cm^{-1}$) of indomethacin are in accordance to those found in the literature.

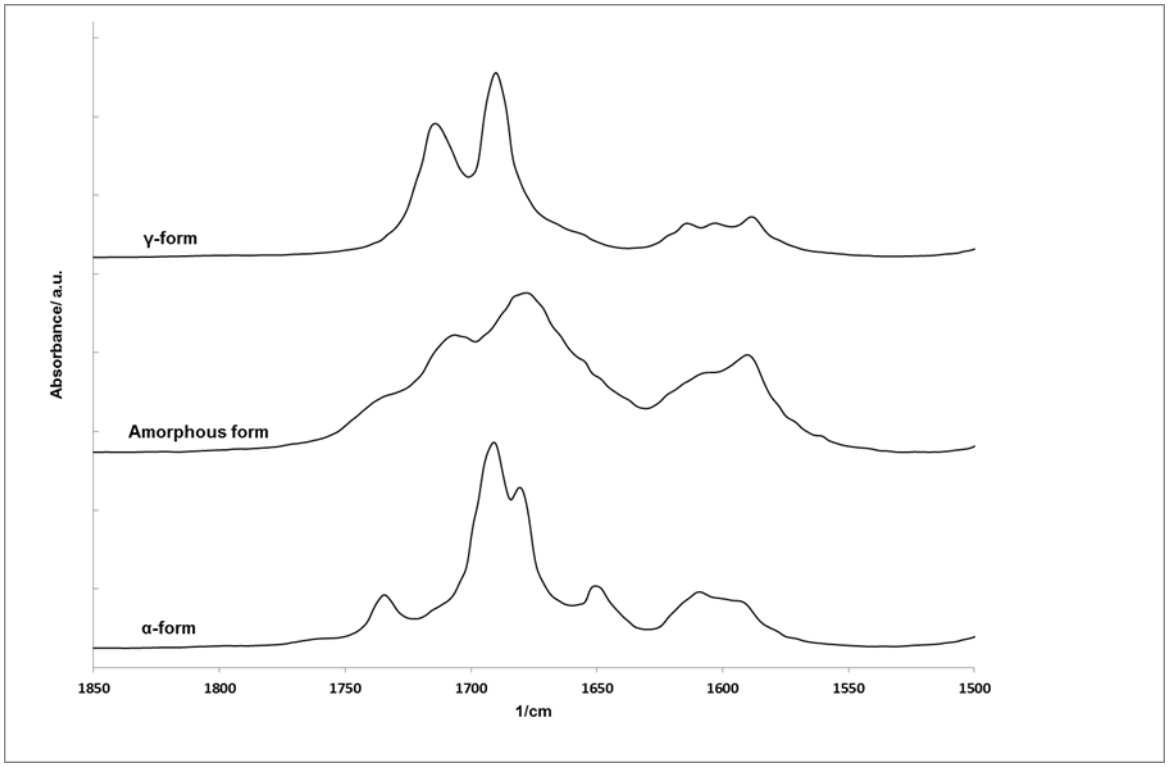


**Figure 28.** ATR-FTIR spectra of different solid-state forms of indomethacin over spectral region of 1850-1500 $cm^{-1}$.

## 6.2 3D printing of the prototypes

### 6.2.1 Filament manufacturing by HME

The FDM™ printing process uses a filament as the feedstock. The raw materials used in this study were received as powder (drug), filament (PCL) or pellets (EVA). HME was performed to produce filaments and to incorporate the drug into the matrix of the polymers. The appropriate filament diameter for the printing process was known to be 1.75 ± 0.05 mm. Therefore a laser diameter measurement device was placed after the extruder to measure the filament diameter on-line. The diameter of the filament was usually a bit bigger than 1.75 ± 0.05 mm, when extruded from the die, and, therefore, a conveyer belt was placed after the diameter measurement device to adjust the diameter. By changing the speed of the belt, the diameter was adjusted.

The factors that affected the manufacturing process of the filament, e.g. the filament diameter were i) screw speed, ii) viscosity of the melt, which affected the die diameter, iii) filling level of the extruder and iv) thermal conductivity of the polymer.

The screw speed was set to 10 rpm prior to opening the extruder die at the end of the barrel. If the screw speed was higher it was difficult to get uniform filaments with the correct dimensions in the beginning of the extrusion process. The screw speed was gradually increased at the end of the extrusion process to be able to obtain more filaments with the right diameter.

To find out the right die diameter, different dies were tested before the final extrusion of the filaments. The expansion of the extruded filament depended on the melt viscosity, e.g. melt index and temperature. When extruding polymers with a lower melt index, polymer swelling was bigger. As a result smaller dies should be used. For most of the extruded formulations (polymers with melt indexes from 1.1 to 43 g/10 min) a 1.5 mm die was applied. When the melt index for the polymer was higher than 150 g/10 min a 2.0 mm die was selected. For polymers with a melt index of 500 g/10 min a 2.5 mm die was used. The temperature at which the extrusion was performed affected the viscosity of the melt. When the extrusion temperatures were closer to the melting point of the polymer, the extrusion was easier because the viscosity was higher. The extrusion temperatures varied between 15 - 40 ºC above the melting point of the polymers.

Although the used die was the same for the whole extrusion process, the diameter of the extruded filament varied a lot. This was due to the fact that the filling level of the extruder got smaller when materials were extruded, and as a result of that the pressure in the barrel decreased, that in turn affected the amount of material to be supplied to the die. This was especially an issue, when extruding PCL-containing filaments as the total volume of the extruding mass was smaller due to higher density of the polymer. PCL has a density of 1.1 $g/cm^3$ whereas the densities of different EVA grades varied between 0.93-0.95 $g/cm^3$.

The thermal conductivity of the polymer affects the time for the filament to cool down. When the polymer cools down fast, there is less time to adjust the diameter; therefore, the speed of the conveyer belt needs to be higher in order to get the right diameter of the filaments. EVA-based filaments cooled down faster than PCL, as a result higher speed of the conveyer belt was used.

### 6.2.2 3D printing with the FDM™ technique

The selection of the appropriate printing material plays an important role in order to proceed with the successful printing. The suitable material for the FDM™ process has to be in the form of filament with the right diameter, flexural modulus and strength and flow properties (Comb et al., 1994, Mostafa et al., 2009). Besides the material properties, the printers hard- and software process parameters as well as the prototype geometry are crucial for a successful printing and a good quality of the printed prototypes (Agarwala et al., 1996). In this study the main focus has been pointed at the material properties, such as filament stiffness, viscosity and drug-loading. In addition, some hardware properties, such as build plate and loading system and software properties, such as printing temperatures and speeds, are discussed.

With both PCL and EVA and both the drug-free and the drug-loaded filaments, the challenges with the loading and printing process were, (i) the filament diameter, (ii) build plate adhesion and (iii) prototype geometry.

The diameter of the extruded filaments varied due to manufacturing challenges of the HME process. It led to the loading problems of the filament during 3D printing. Briefly, the filament is fed into the liquefier of the 3D printer via pinch rollers, and a stepper motor is connected to one of the rollers providing energy to move the filament down the system (Turner et al., 2014). The printer used in this study had counter-rotating steel rollers with diameters of about 5 and 10 mm. The smaller roller had a smooth surface and the bigger roller which is connected to the motor, had a surface with a grooved texture. Too thick filaments could not be fed, because the liquefier diameter was only a little bigger than the desired dimensions of the filaments (1.75+0.05 mm). Filaments thinner than 1.70 mm could not be fed, because of unsufficient friction between the rollers, leading to too low pressure on the filament with slipping as a result. By changing the properties of the rollers (their dimensions and materials), the limits of the desired diameters of the filaments could be wider. Comb et al. (1993) has studied the required drive traction of feeding systems, with different roller sizes and surface materials, to load the filament into the liquefier without slipping. Drive traction is the force provided by the feeding system to load the filament into the liquefier. It was reported that smaller (1/2'') elastomeric wheels increases the traction force, due to their higher coefficient of friction, and are therefore better able to conform to

variations of the filament, than the bigger wheels (Comb et al., 1993). In Figure 29 (left) is illustrated the effect of the rollers size and surface, and the filament diameter on the traction force. It is important that the filament is of uniform size, as a non-uniform filament gives rise to fluctuations in the flow rate of the extruding material, causing defects and poor bonding between layers in the printed prototypes (Agarwala et al., 1996).

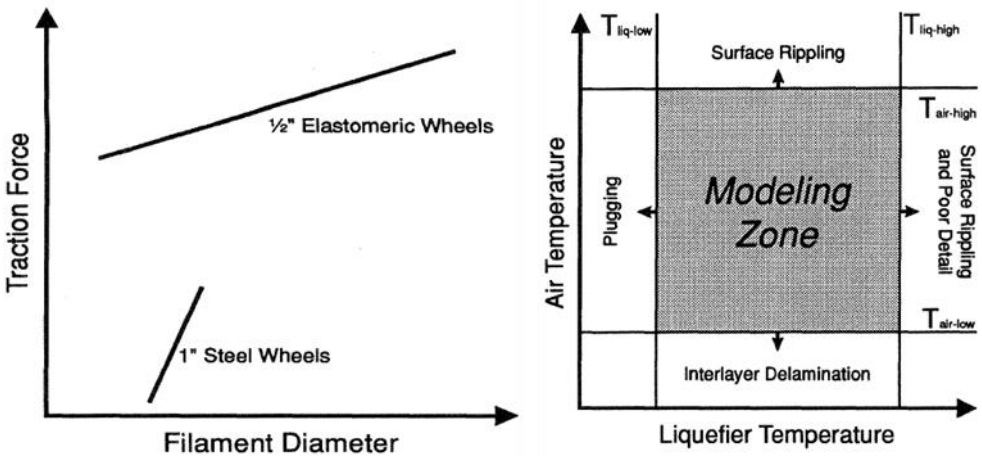


**Figures 29.** Drive traction versus filament diameter for two different pinch roller drives (left) and the modelling zone temperature parameters for a material (right) (Comb et al. 1993).

The printer has an acrylic build plate in the default setup, but neither PCL nor EVA did adhere to it properly. Therefore, PCL prototypes were built on Kapton® polyimide tape, which was recommended from the printer manufacturer. EVA did not adhere to the polyimide tape and after testing different materials, e.g. glass, painter tape, different plastics, aluminum, the EVA prototypes were printed on LDPE films, because it had the best attaching properties of all tested surfaces. All IUS 1 prototypes were printed with rafts, because unsupported prototypes wrapped during printing on the build plate. The rafts adhered better to the build plate as they were of larger attaching-to-the plate area than prototypes alone. In addition, the adhesion problem of the printed prototypes was partly due to the geometry of the prototype and partly due to surface characteristics of the build plate as well as ambient conditions such as the environment temperature. The heat capacity and the thermal conductivity of the material determines the viable process temperatures (Turner et al. 2014). Agarwala et al. (1996) has reported that a material to be successfully printed has a threshold in the environment temperature. During printing below the desired temperature range, bonding or adhesion to the build plate, adjacent roads and layers are poor (Agarwala et al. 1996). A printer with an adjustable envelope temperature and a heated or a vacuum build platform could have decreased the adhesion problems to the build plate.

According to Comb et al. (1993) there is not only a lower limit, when printing above a threshold temperature the quality of the surface of the prototype suffers (Figure 29, right).

The printed prototype IUS 1 needed a support structure to be built on, due to the geometry of the prototype. As the printer had only a single extruder, the support structure was printed with the same pure polymer, without any drug inside. The support structure was then manually cut off from the prototype after cooling down. The removing of the supports structure affects the prototype surface (Agarwala et al. 1996). The prototypes that can be built without a need for any support structures have better surface finish than those built with additional supportive elements. Some of the impact of the support structure on the final prototypes surface, can be decreased by using a dual-extruder printer. With such a printer, the support structure can be built from an alternate build material, which forms weaker interfaces with the actual build material, and can, therefore, be more easily removed.

The prototype *Sleeve* could not be printed with any of the tested drug-free or drug-loaded polymers. The geometry of this tube was: OD 2.9 mm, ID 1.5 mm and length 5 mm. This geometry was apparently too difficult for the printer to print. The prototype collapsed under printing, due to the fact that the wall was only 1.4 mm thick. Several experiments were tested with different amount of sleeves printed at the same time, giving longer time for the layers to cool down, which could have prevented the collapsing of the structure. However, when the time between subsequent layers was longer, the binding of the new layer to the previous layer was weaker. Printers with better resolution parameters that are able to print structures with thin details can be tried to overcome this problem.

#### 6.2.3.1 Printing with drug-loaded PCL filaments

PCL is one of the original feedstock material for the printer. The default printing speed for PCL is 45 mm/s. The maximum printing speed for a material depends on the process parameters such as the printed road width and height, printing temperature and nozzle size as well as on the geometry of the nozzle and polymer melt viscosity (Comb et al., 1993). Higher printing speeds results in the underflow of the polymer melt from the nozzle with poor printing quality as a result. In this study the process parameters and the geometry of the nozzle were kept the same for the drug-free and the drug-loaded filaments. The viscosity of the pure PCL filament and the drug-loaded filaments were almost the same at the printing

temperature of 100 ºC (Figure 30). All drug-loaded PCL filaments could be successfully fed into the liquefier and printed without problems at the applied printing temperature.

The XRD, DSC and ATR-IR analyses indicated that there was undissolved indomethacin after the extrusion process in the filaments containing 15% and 30% indomethacin as the extrusion temperature was far below the melting point of the raw indomethacin. A printing experiment at printing temperature of 165 ºC, that is above the melting point of raw indomethacin was performed, by using the filament containing 30% indomethacin. It was possible to print at 165 ºC, but quality of the product was poorer than at 100 ºC. Obviously, it was due to a poor adhesion of the polymer melt between the printed layers. When printing is done at higher temperatures, it takes longer time for the printed polymer to cool down. Sun et al. (2008) has reported that the thermal history of a material has an impact on the bonding strength between adjacent layers and roads achieved under printing. In addition, Comb et al. (1993) has reported that every material has upper and lower limits for the liquefier and air temperatures, Figure 29 (right). The viscosity of the 30% drug-loaded PCL at 165 ºC was much lower than the viscosity of the material at 100 ºC, for the shear rate range up to 100 $s^{-1}$. Above the shear rate of 100 $s^{-1}$ the viscosity of the polymer melt at 165 º C was higher than at 100 ºC. Venkataraman et al. (2000) reported that the shear rate region is 100-200 $s^{-1}$ for a 0.508 mm nozzle in a FDC process. The nozzle used in this study was 0.4 mm, and therefore, the shear rate region can be different from the abovementioned. Even the nozzle length and angle affect the shear rate. Since the shear rate region for the nozzle used in this study is not determined, it is not possible to say what viscosity the polymer has to have to be printable with the used printer. To sum up, the differences in the viscosity profiles between printing materials at two different printing temperatures were most likely responsible for the unacceptably poor quality of the prototypes printed at 165 ºC. In addition, the problems in adhesion between the subsequent layers and roads of the materials during printing at higher temperature add to that matter. This is in accordance with the results Comb et al. (1993) reported about the modelling zone, whereas printing above a threshold temperature the printing quality is poorer than printing at lower temperatures (Figure 29, right). The further analysis was continued only with the prototypes printed at 100 ºC.

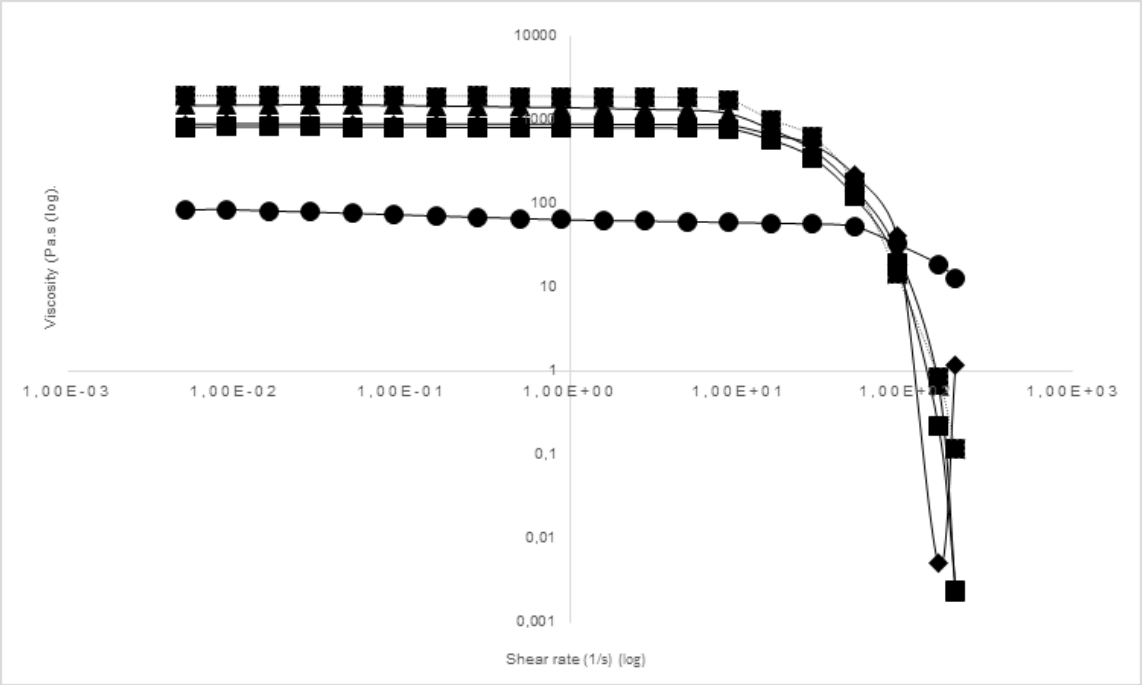


**Figure 30.** The viscosity versus shear rate of PCL filaments, (‥■‥) pure PCL filament, (♦) PCL 5% IND, (■) PCL15% IND, (▲) PCL 30% IND at 100 ºC and (●) PCL 30% IND at 165ºC.

The mean weight and the weight variation (SD) of the printed drug-loaded IUS 1 prototypes is presented in Table 14. The smallest variation can be seen in the prototypes containing 5% indomethacin. The 30% drug-containing prototype had the highest weight variation and the lowest weight. This was due to the fact that there was a higher amount of drug particles present in the polymer melt, which made the printing more difficult, leading to the poorer quality of the printed prototypes with highest drug loading.

**Table 14.** Weight variation of the printed PCL prototypes, n=3.

| **Prototype** | **Mean weight + SD (mg)** |
|---|---|
| IUS 1 5% | 131.73±1.38 |
| IUS 1 15% | 142.77±1.66 |
| IUS 1 30% | 120.25±2.18 |

### 6.2.3.2 Printing with drug-free and drug-loaded EVA 5 filaments

The loading of the EVA filaments inside the printer extruder was a problem with both the drug-free and drug-loaded filaments. Despite the fact that the filaments were of the right diameter, the loading process did not always succeed. Most of the elastic EVA grades could

not act as a piston to push the melted polymer through the nozzle, and therefore, they were bended or buckled above the liquefier during the loading stage. This was due to too low column strength of the filament. The column strength is a function of the filament diameter, flexural modulus and strength of the filament (Comb et al., 1994). The diameter of all filaments was the same, and equal to 1.75 ± 0.05 mm. The filaments' flexural or tensile strength could not be an issue, since none of the filaments were deformed or broke under the loading procedure. The flexural modulus shows the tendency for a material to bend. The flexural modulus of the EVA grades and PCL was 7-123 Mpa and 411 MPa, respectively (Celanese 2014, Perstorp 2014). The flexural modulus for all the different EVA grades are presented in Table 9 (under methods). The flexural modulus of the EVA filaments was much lower than for the original feedstock PCL. The value decreased with increased VA content of the EVA polymer. It was found that most of the EVA grades with flexural modulus values between 42 MPa and 123 MPa could be fed into the liquefier. However, EVA 6 with the flexural modulus value of 45 was not fed successfully, which was due to high viscosity.

Besides the column strength, the viscosity of the melt was critical for the loading and printing process to succeed. The force needed to press the melt through the nozzle depends on the pressure drop in the nozzle. The pressure drop depends on the geometry of the print head and the viscosity of the melt (Turner et al., 2014). Since the geometry of the print head was the same for all printing experiments, the pressure drop variation depended on the viscosity of the melt. A material with higher viscosity needs more power from the piston acting filament to be extruded through the nozzle. The used EVA grades had melt indexes (MI) varying between 1.1-150 g/10min and 500 g/10min (Celanese 2014). The MI is a measure of the ease for a melt to flow under pressure, at a defined temperature. The MI increases with increased VA content and decreased molecular weight of the EVA polymer. If the MI was too low, the drop pressure was too high for the filament to push the melt through the nozzle. EVA grades that were successfully loaded had MI between 2.8 and 500, but not all of them in that range could be fed because of low flexural modulus value. To add, the MI values reported in the manufacturer material sheets were measured at 190 ºC, which differ from the applied printing temperatures. Rheological tests were not performed to determine the MI at the printing temperature, and therefore, the exact MI values at the printing temperature are not revealed. Not only low MI was a problem in the FDM™ process with EVA. If the MI was too high, which was the case with the EVA 8 with MI 500 g/10min, the polymer was easily fed (in spite of low value of flexural modulus) but it was extruded

as droplets, not as a continuous line, and as a result the printing failed. That was also the case with EVA 11, but the exact MI value was not revealed because it was a blend with 50% of EVA 8.

It can be concluded that both the column strength and the MI plays a pivotal role in the successful loading and printing process. Any boundary values for the materials flexural modulus or MI cannot be specified for a successful loading and printing process, because the process depends on the ratio between them. To determine the boundary ratio, further experiments must be done. The successfully loaded and printed EVA grades are presented in Table 15.

**Table 15.** Successfully loaded and printed EVA grades.

| EVA grade | VA content (%) | Flexural modulus (MPa) | MI (g/10min, 2.16kg/190°C) | API content |
|---|---|---|---|---|
| **EVA 1** | 9 | 101 | 2.8 | |
| **EVA 2** | 9 | 115 | 8 | |
| **EVA 4** | 12 | NA | 10 | |
| **EVA 5** | 16 | 60 | 28 | |
| **EVA 7** | 18 | 42 | 150 | 0, 5, 15 |
| **EVA 12**[1] | NA | NA | NA | |

[1] Blend between EVA 3 and EVA 8 (75:25)

Besides the material properties, hardware properties, such as the pinch rollers surface and groove depth affect the loading process. Some of the problems with the filament loading process of EVA, was due to slipping between the pinch rollers. The rollers surface and the groove depth have to match with the printing material to prevent slipping (Agarwala et al., 1996). An optimized surface material and groove depth on the rollers, could have prevented some of the filament loading problems with EVA.

The printing speeds for EVA varied between 10-40 mm/s. As discussed under the printing of PCL, the parameters that affect the printing speed are the printer extruded roads width and height, printing temperature and nozzle size, but also the geometry of the nozzle and polymer melt viscosity. In the literature it has been reported that the thermal behavior of PCL in the liquefier differ from other commonly used FDM™ feedstock, e.g. ABS (Ramanath et al. 2008). The liquefier length required for PCL to fully melt is much shorter than for ABS. The thermal behavior in the liquefier of the EVA polymer was not determined. The melt behavior of the EVA polymer can differ from PCL, and the required length of the liquefier can be longer than for the original liquefier optimized for PCL. It is possible that EVA needs longer time in the liquefier before it melts and that in turn affect the printing

speed. Printing experiments was done at higher temperatures with higher speeds, but the printing result was poorer, due to weaker bonding between layers.

The drug loaded filaments was printed at 165 ºC at a speed of 10 mm/s. The viscosity of the drug-free and drug-loaded EVA 5 filaments compared to the viscosity of drug-free PCL is presented in Figure 31. The values are obtained at the printing temperature of each polymer, 165 ºC as well as 135 ºC for EVA 5 and 100 ºC for PCL. The viscosity of the polymers was near the same at the shear rates up to 10 $s^{-1}$. The viscosity of the drug-free and the 5% drug-loaded filament was close to each other. The viscosity of the 15% drug-loaded filament was lower, that is due to the higher amount of melted drug in the filament. The viscosity for PCL decreased more rapidly than for the others and especially at the shear rate from 1 $s^{-1}$, which is the shear rate region that Venkataraman et al. (2000) reported for a FDC process. But as discussed above the nozzle and polymer blend was different in that study, and therefore the exact shear rate region for the printing process for this printer and the following boundary viscosity values cannot be determined.

Out of both polymers and with and without drug-loadings, the 15 % drug-loaded EVA 5 filament was the easiest to print and the printing result was best for both the IUS 1 and IUS 2 prototype.

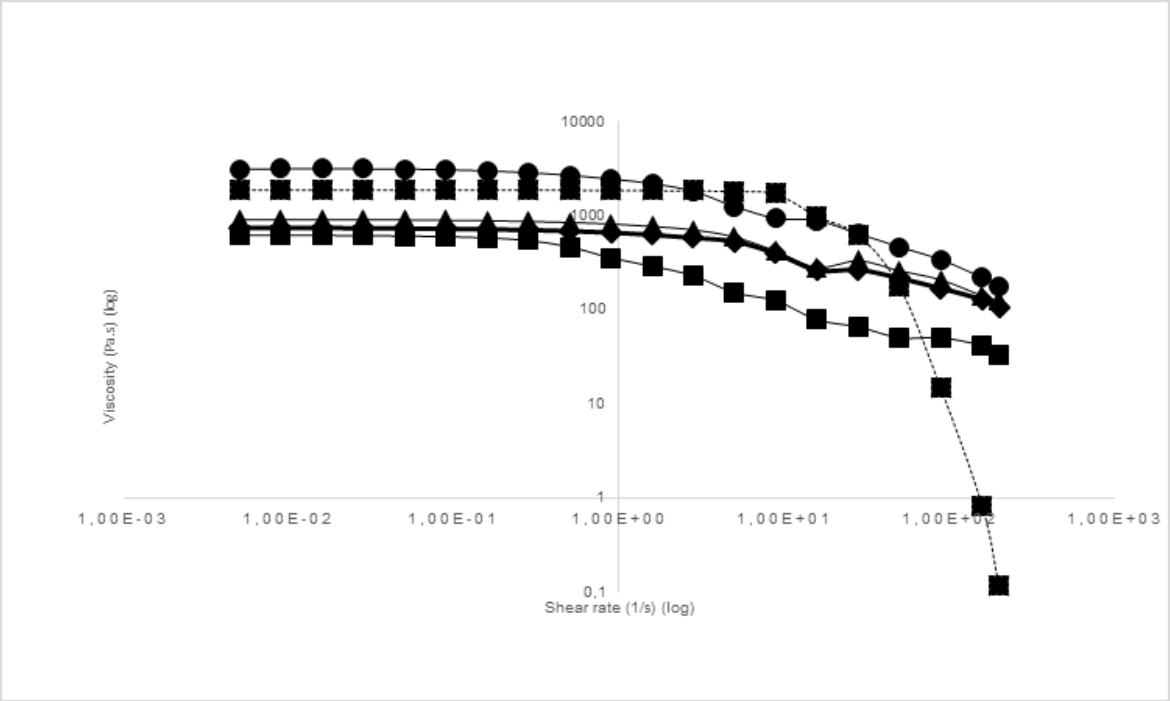


**Figure 31.** The viscosity versus shear rate of EVA 5 filaments, (▲) drug-free EVA filament, (♦) EVA 5 %IND, (■) EVA 15% IND at 165ºC and (●)EVA 15% IND at 135ºC and ( ··■··) drug-free PCL at 100 ºC.

Since the printing temperature was above the melting point of the drug, a printing experiment was done at 135 ºC for the 15%-indomethacin loaded filament, to be able to compare between the dissolution profiles of prototypes containing melted (165 ºC) or crystalline (135 ºC) drug. The 15%-indomethacin had a higher viscosity at 135 ºC, than for 165 ºC due to crystalline indomethacin present in the polymer. The higher viscosity made it impossible to print or even load the filament at 135 ºC due to buckling of the filament. The higher viscosity at 135 ºC increased the liquefier pressure (e.g. pressure drop), and the column strength of the filament was exceeded with buckling as a result.

The weights of the printed prototypes with the standard deviations are presented in Table 16. The filament containing 15 % indomethacin hade better printability than the filament with 5 % indomethacin, because of lower viscosity of the former material.

**Table 16.** Weight variation of 3D printed EVA 5 prototypes and rods, n=3.

| **Prototype** | **Mean weight ± SD (mg)** |
|---|---|
| IUS 2 5% | 245.90±5.92 |
| IUS 2 15% | 245.87±1.37 |
| 3D Rod 5% | 57.07±0.45 |
| 3D Rod 15% | 66.50±0.44 |

## 6.3 Characterization of the filaments and the 3D printed prototypes

### 6.3.1 The appearance of the filaments and the printed prototypes

#### 6.3.1.1 PCL filaments and prototypes

The unloaded PCL filament was white and opaque after extrusion. The fabricated filaments containing IND turned to be of yellow color. The filament with 5% indomethacin was yellow and translucent. The filament with 15% indomethacin was slightly brighter yellow and opaque. The filament with 30% indomethacin was opaque, but lighter yellow than the 15% filament. The extruded PCL filaments are shown in Figure 32. It is known that dissolved and amorphous indomethacin has a yellow color. Further investigations, e.g. XRD, DSC and ATR-IR confirmed that the drug had dissolved in the polymer melt to some extent. The different shades of yellow color were due to the fact that there were different amounts of undissolved drug in the filaments.

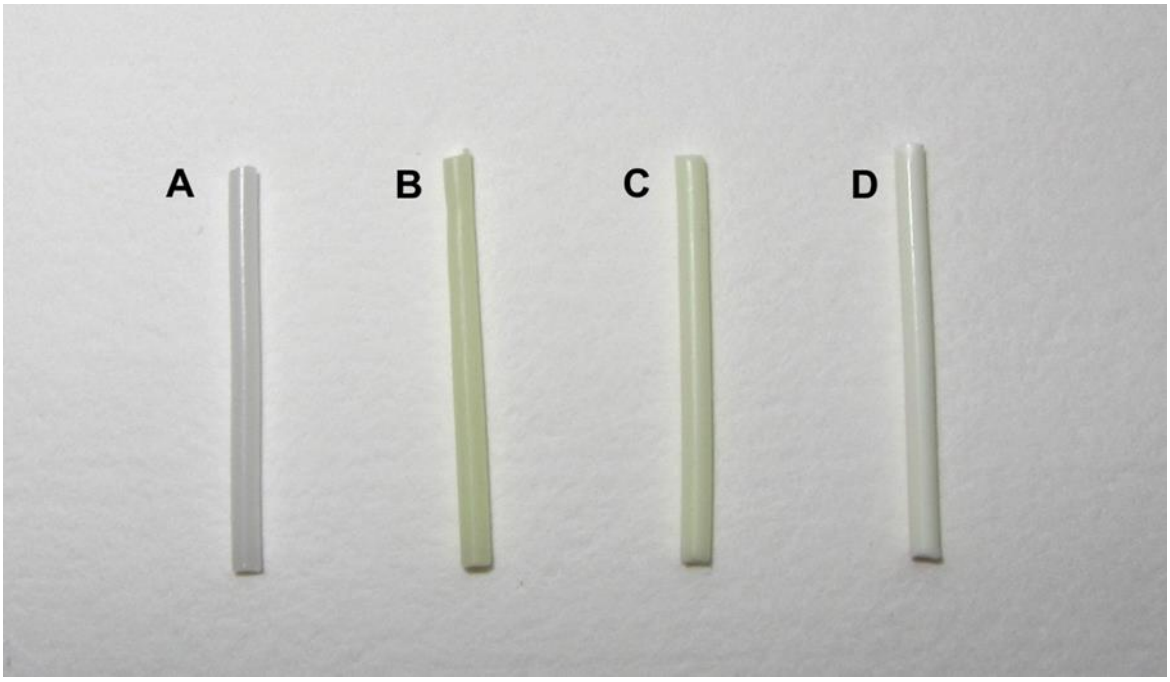


**Figure 32.** PCL filaments: (A) drug-free PCL filament, (B) 5% indomethacin-containing filament, (C) 15% indomethacin-containing filament and (D) 30% indomethacin-containing filament.

The HME process for fabrication of the PCL filaments was performed at 100 ºC, which is above the melting point of PCL, but under the melting point of indomethacin (160 ºC). In a HME process where the temperature is below the melting point of the drug, the solid drug acts as a solute and the polymer as a viscous solvent (Gogos et al., 2012). The drug gradually dissolves into the polymer melt, resulting in a polymer-drug solid dispersion. The drug particles size decreases until the particles disappear and a homogenous solution is formed. The particles diminish completely or until the limit of drug solubility in the polymer at the processing temperature is reached. The solubility parameter of PCL is 19.1-19.3 $MPa^{1/2}$ (Perstorp, 2014) and the solubility parameter of IND is 22.1 $MPa^{1/2}$ (Forster et al., 2001). The difference is 2.8-3.0 $MPA^{1/2}$. According to Greenhalgh et al. (1999) if the difference is less than 7 $MPa^{1/2}$, the compounds show at least some miscibility. The closer the values, the higher should the degree of miscibility be and a glass solution can be formed if both ingredients are in the amorphous state upon cooling (Forster et al., 2001). Since the processing temperature was below the melting point of the drug and the PCL recrystallizes upon cooling, a glass solution could not be obtained, but it can be concluded that indomethacin dissolves in the melted PCL during HME at least at some extent. Further investigations, e.g. X-ray diffraction, DSC and ATR-IR, confirmed that in the formulation with lowest drug polymer load (5%), the indomethacin had completely dissolved, whereas some of the indomethacin was undissolved in both of the other formulations (15 % and 30 %).

SEM analysis was performed on approx. 3 months old filaments to get further insight into the morphology of the samples. The surface of the drug-free and up to 15% drug-loaded filaments were smooth, but on the surface of the 30% drug-loaded filaments some cracks could be seen. The cross-sections of the drug-loaded filaments the surface was not as smooth as of the drug-free filament, which was due to small drug particles. The cross-section of the extruded 30% drug-loaded filament showed a more uneven surface than the others. In Figure 33 SEM images of the filaments surfaces and cross-sections are presented.

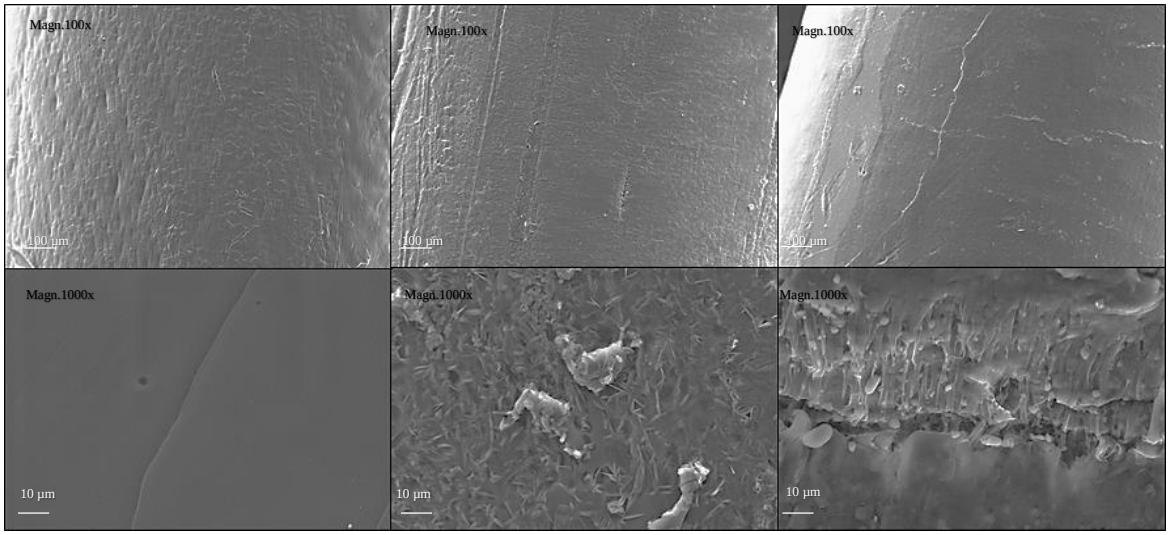


**Figure 33.** SEM images of filaments surfaces (upper) and filaments cross-sections, drug-free PCL (left), 5% drug-loaded PCL and 30 % drug loaded (right) filaments.

The color of the printed prototypes containing 5% indomethacin was the same color as the filament containing 5 % indomethacin. The prototypes printed with the 15 % drug loaded filament were slightly brighter yellow than the filament (Figure 34). The prototypes containing 30% indomethacin were slightly more yellow than the filament, but not as bright yellow as the prototype containing 15% indomethacin. The change in the color indicates that under the printing process more indomethacin had dissolved or melted in the polymer, as a result of the heating during printing.

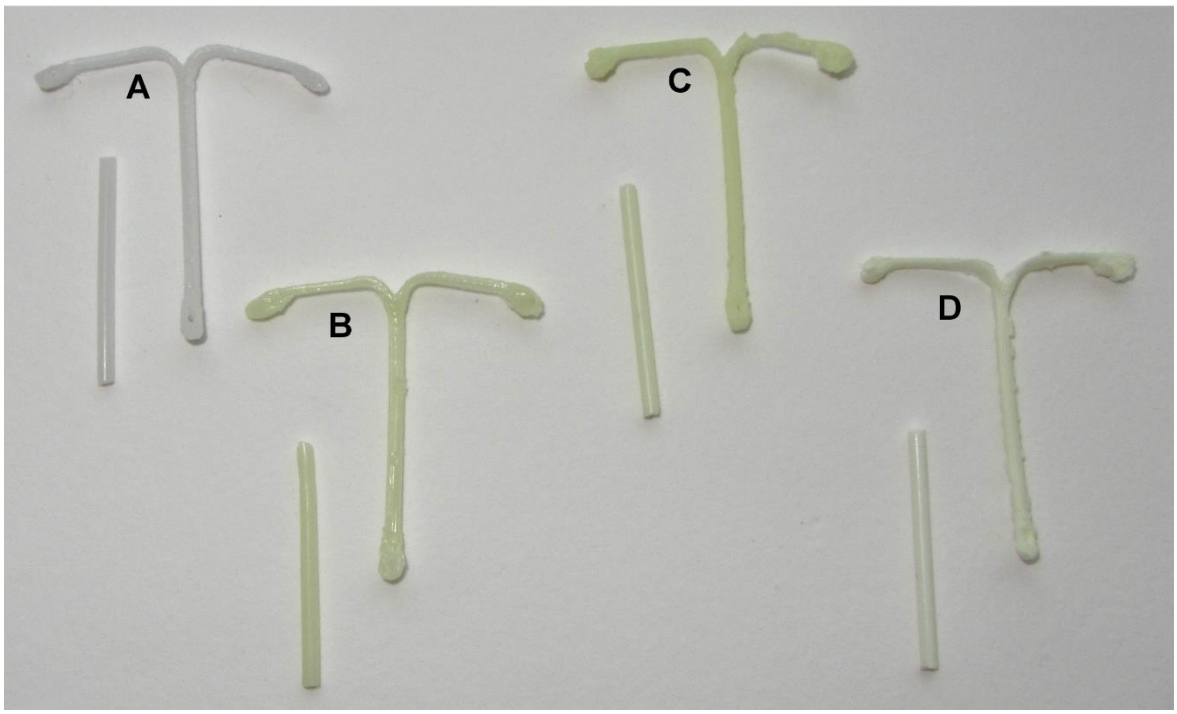


**Figure 34.** Printed prototypes and filaments of PCL: (A) Pure PCL, (B) 5 % indomethacin, (C) 15% indomethacin and (D) 30% indomethacin.

SEM images of the printed prototypes surfaces and cross-sections are presented in Figure 35. All prototypes showed a layered structure on the surface of the prototypes. The cross-section of the drug-free prototype and the 5% drug-loaded prototype is smooth, in the cross-section of the 5% drug-loaded prototype some drug particles can be seen. The observed drug nucleus (size is below 1 µm) can be an indication of an undissolved part of the drug during extrusion and printing as well as a result of recrystallization of the drug upon storage as SEM analysis was not done immediately after preparation of the prototypes. The cross-section of the 30% drug-loaded prototype is uneven and has small voids.

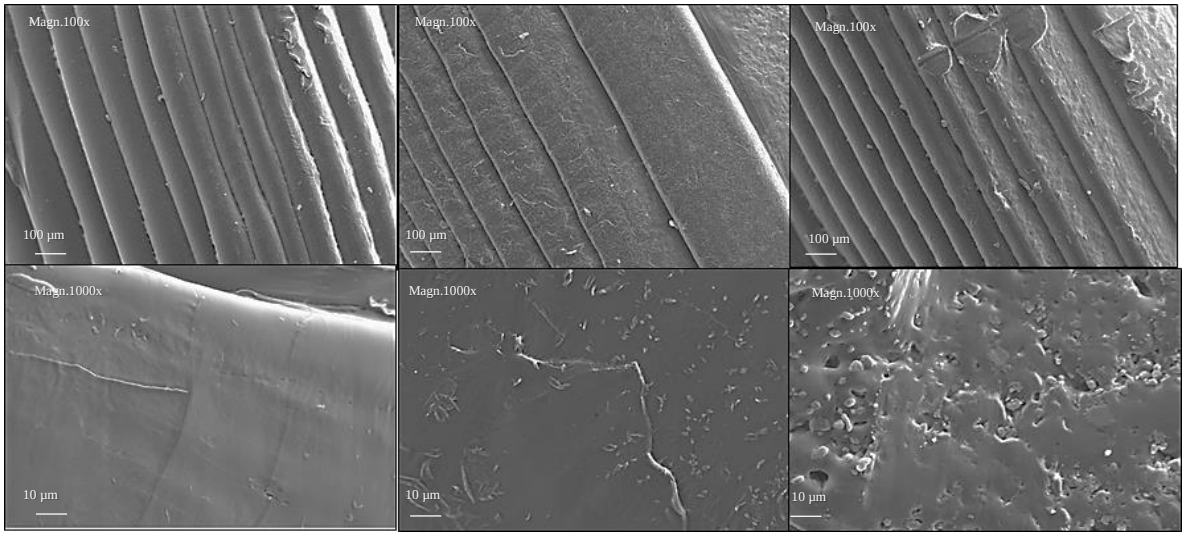


**Figure 35.** SEM images of the printed prototypes surface (upper) and cross-sections, drug free PCL prototype (left), 5 % containing prototype, and 30 % containing prototype (right).

### 6.3.1.2 EVA filaments and prototypes

The HME extrusion process of the EVA grades was carried out at 105-120 ºC, depending on the melting point and the viscosity of different grades. EVA grades with a lower VA content has a higher molecular weight, which increases the polymer melt viscosity (Almeida et al., 2011). The filaments of all the extruded drug-free EVA grades were translucent. When the EVA grades (EVA 3 and EVA 5) were extruded with indomethacin, the extruded drug loaded filaments were opaque and white. The filament containing 15% was a bit whiter than the filament containing 5% indomethacin (Figure 36, left). Since the extrusion temperature was below the melting point of the drug, the drug had not melted. The color indicates also that the indomethacin had not dissolved in the melted polymer, since the filaments had not turned yellow. From literature it can be concluded that EVA 5 with a VA content of 16% has a solubility parameter between 16.33-17.4 $MPa^{1/2}$. The solubility parameter for other grades of EVA is between 16.33-18.38 $MPa^{1/2}$, depending on the vinyl acetate content (Coleman et al., 1990). According to Díez et al. (2014) the solubility parameter for EVA with 18% was 17.4 $MPa^{1/2}$. As a conclusion of this the difference between the solubility parameters of drug and polymer is likely to be in the range of 4.7-5.77 $MPa^{1/2}$. Forster et al. (2001) suggested that if the difference between the solubility parameters of drug and excipient is smaller than 2 $MPa^{1/2}$, they are likely to be miscible and form glass solutions when melt extruded if both drug and polymer are in the amorphous state. Since the difference

is >2 MPa $^{1/2}$ and the extruded filaments are white, the drug and the polymer were not miscible and a glass solution could not be obtained. In Figure 37 the SEM images of the EVA 5 extruded filaments are shown. From the SEM images can be seen that the surface of the extruded EVA filaments has cracks and that small drug particles are present on the surface. The cross-section of the drug-free filament is smooth but have some cracks. The cross-sections of the drug-loaded filaments are more uneven, due to drug particles incorporated in the polymer.

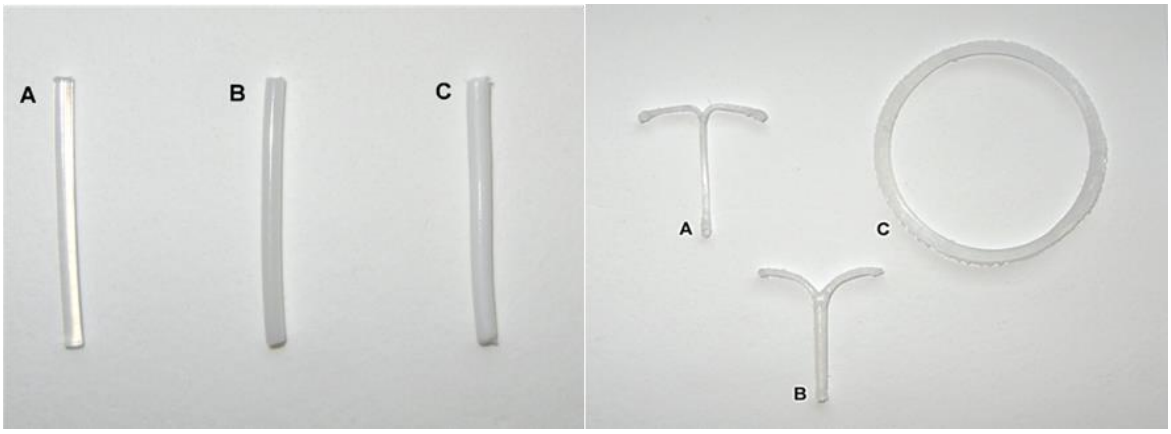


**Figures 36.** Extruded filaments of EVA 5 (left), (A). drug-free filament, (B). 5% indomethacin-containing filament and (C). 15% indomethacin-containing filament and printed drug-free EVA 5 prototypes (right), (A). IUS 1, (B). IUS 2 and (C). Ring.

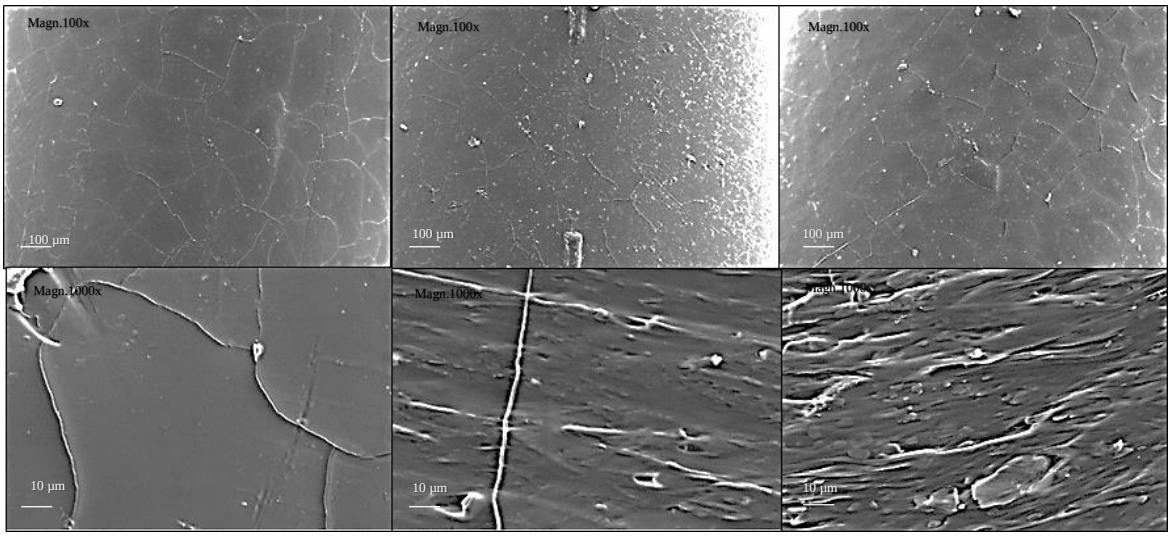


**Figure 37.** SEM images of the extruded EVA 5 filaments surface (upper) and cross-sections, drug-free (left), 5% drug-loaded and 15% drug-loaded (right) filaments.

The printing of the prototypes, based on EVA5, was carried out above the melting point of indomethacin at 165 ºC. In figure 36 (right) the drug-free printed prototypes are presented. The obtained prototypes containing 5% indomethacin was translucent and yellow, indicating

that all indomethacin had melted and possibly dissolved at some extent under the printing process. The prototypes containing 15% indomethacin had turned yellow, but they were opaque. It can be concluded that crystalline drug was still present in the 3D printed prototype containing 15% indomethacin. This can be due to the fact that the printing process was too fast for the whole drug amount to melt and/or partly dissolve in the polymer. In addition the exceedance of the saturation point of the drug in the molten polymer can be taken into consideration as the drug shows some degree of miscibility in the molten polymer at elevated temperatures (cf. DSC analysis). In Figures 38 and 39 the printed prototypes and SEM images of the surfaces and cross-sections of the prototypes are presented.

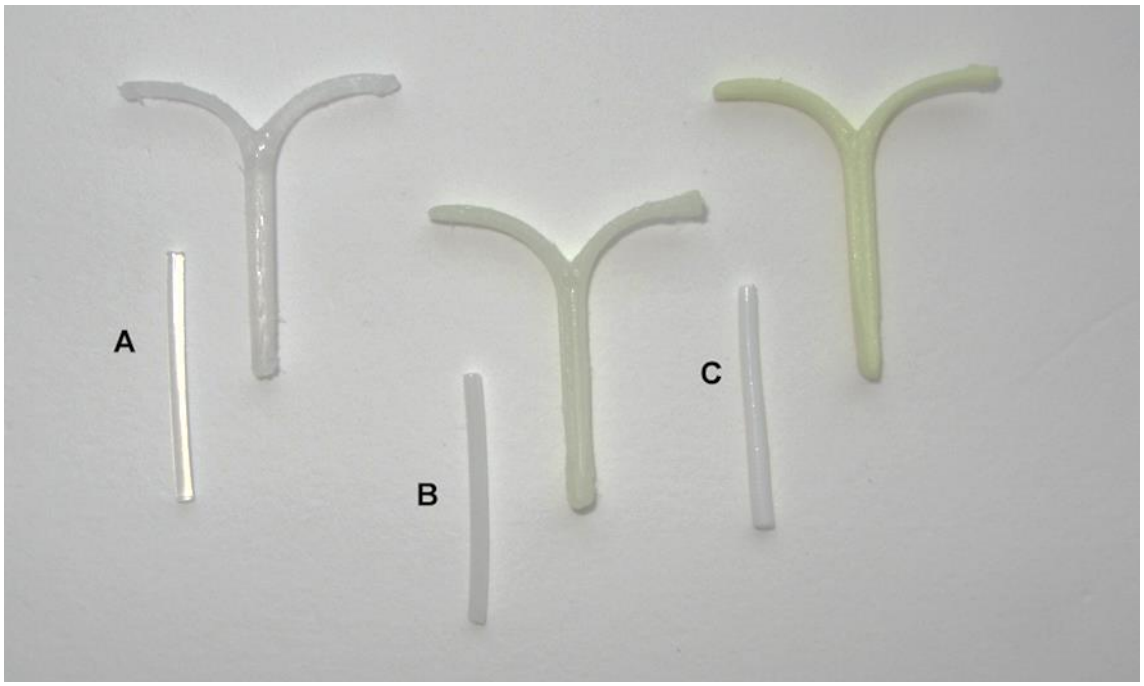


**Figure 38.** Filaments and printed prototypes of EVA 5: (A) drug-free, (B) 5% indomethacin-containing and (C) 15% indomethacin-containing filaments and IUS 2 prototypes.

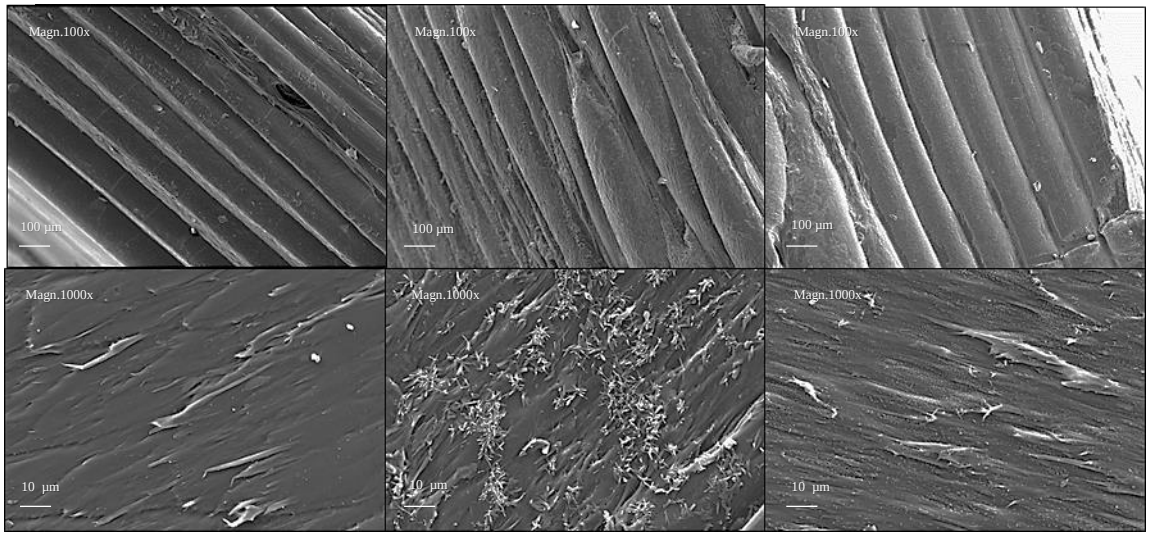


**Figure 39.** SEM images of the printed prototypes surface (upper) and cross-sections, drug-free EVA prototype (left), 5 % containing prototype, and 15 % containing prototype (right).

The SEM analysis showed that all prototypes had a layered structure on the surface of the prototypes. The cross-sections of the drug-free prototype is not as smooth as the cross-section of the filament. The cross-sections of the drug-loaded filaments are uneven, and especially in the filament containing 5% indomethacin some drug particles can be observed. The observed drug nucleus can be an indication of undissolved part of the drug during extrusion and printing as well as a result of recrystallization of the drug under storage as SEM analysis was not done immediately after preparation of the prototypes.

## 6.3.2 XRD analysis

To verify the degree of crystallinity of the drug in the HME filaments, printed prototypes and physical mixtures of the drug and the polymer, XRD analysis was performed.

### 6.3.2.1 XRD analysis of PCL filaments and printed prototypes

The printed samples and physical mixtures were 1 day old, whereas the filaments were over 1 month old at the time of the XRD experiments. The semi-crystalline PCL has two characteristic Braggs peaks between 20º and 25º reported in literature (Cheng et al., 2010, Li et al., 2010). The XRD diffractograms of the filaments and the printed prototypes showed

two Bragg´s peaks at approximately 21-22º and 23-24º, indicating that PCL remained in the semi-crystalline state after extrusion and printing (Figure 40). All the prepared filaments contained the crystalline drug at some extent, shown in Figure 40, left d-f. The XRD diffractogram of the filament containing 5% of the drug showed a single indomethacin-relevant peak at 12º, whereas the filament with 15% of the drug revealed already extra characteristic peaks (the more distinguished at approximately 12º and 17º). The degree of crystallinity increased further for the filament containing 30% of the drug. There near all characteristic peaks of indomethacin appeared to be on the diffractogram. Even the intensity of the drug crystalline peaks increased with higher drug loading. It can be concluded that not all the drug used in each of three formulations dissolved completely in the melted polymer during hot-melt extrusion. XRD diffractograms of 3D printed samples revealed a presence of crystalline indomethacin only in the formulation containing the highest percentage of the drug (Figure 40, right). It brings us to the conclusion that 3D printing process, conducted at the temperature of 100 ºC caused further dissolution of API in the melted polymer. Liu et al. have reported that longer processing time at elevated temperature decreases the amount of solid indomethacin particles in the molten polymer (Liu et al., 2010). In addition, it is possible that crystalline API could undergo solid-state transformation during hot-melt extrusion and 3D printing process. However, it was impossible to distinguish between different forms of indomethacin by using XRD, because the X-ray diffraction peaks of α- and γ-forms overlap (Kaneniwa et al., 1985). In addition, a difference in the height of the probes during XRD analysis could induce a slight shift in the position of the characteristic peaks as the filaments and 3D printing prototypes were used as they are. The mechanical grinding of the filaments and prototypes could be performed to adjust the height of the probe. However, the mechanical stress could induce some other changes in the solid-state properties of the used materials that are not related to HME and 3D printing process (Jenkins et al., 1996).

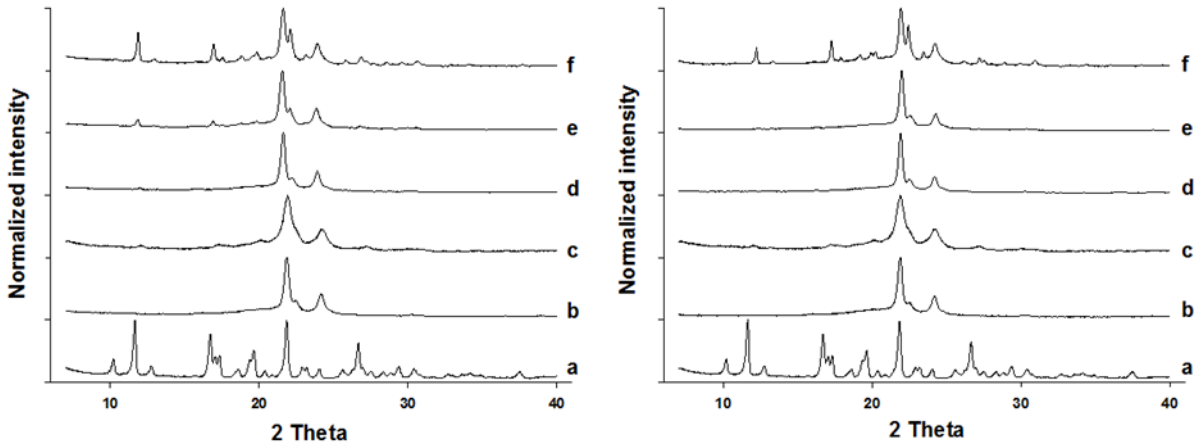


**Figure 40.** XRD pattern of: filaments (left, b, d-f) and 3D printed samples (right, b, d-f): (a) raw γ-indomethacin; (b) drug-free PCL; (c) physical mixture of PCL filament with 15% (left) and 30 % (right) indomethacin; (d) formulation with 5% indomethacin; (e) 15% indomethacin and (f) 30% indomethacin.

To check the solid state stability of the drug in the filaments and printed samples over time, the second XRD analysis was performed in one month (Figure 41). The XRD diffractograms of the filaments after extra month of storage was identical to the previous ones (Figure 40), indicating that the solid state of the drug in the filaments remained the same. However, the drug has recrystallized in the printed samples during storage as the indomethacin-related peaks appeared on the diffractograms of the prototypes containing 5% and 15% drug. The degree of recrystallization in 30% drug containing samples is impossible to reveal as both diffractograms before and after storage look similar. It brings us to the conclusion that the just printed samples contained the drug in the supersaturated state that started slowly recrystallize towards the saturation state during storage. This phenomenon has previously been observed by other researchers (van Laarhoven et al., 2002).

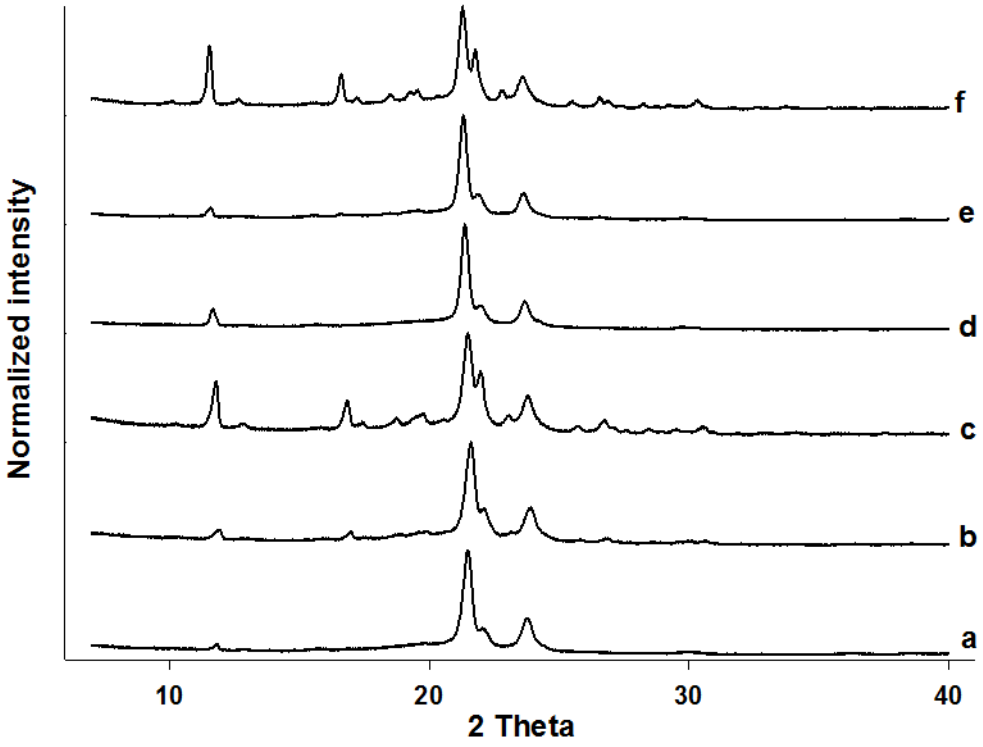


**Figure 41.** XRD diffractograms of (a) 5% drug containing filament; (b) 15% drug containing filament; (c) 30% drug containing filament; (d) 5% drug containing prototype; (e) 15% drug containing prototype and (f) 30% drug containing prototype. The filaments and 3D printed samples were analyzed after storage for over 2 months and over 1 months, respectively, in ambient conditions (22±1 ºC).

### 6.3.2.2 XRD analysis of EVA 5 extruded filaments and printed prototypes

The EVA 5 has a characteristic Bragg´s peak at about 21º reported in literature (Almeida 2011). The XRD diffractograms of all the filaments and the printed prototypes showed the characteristic peak at 21º (Figure 42). The prepared drug-loaded filaments contained the crystalline drug at some extent. Their XRD diffractogram showed two indomethacin-relevant peaks at 12º and 17º. The intensity of the drug-related peaks increased with an increase in the amount of incorporated drug. The diffractograms of the 3D printed prototypes had only the EVA characteristic peak. The printing was performed at 165 ºC, which is above the melting point of the indomethacin. Evidently, such a high printing temperature was the

reason for at least partial amorphisation of the drug in the 3D printed prototypes. Further investigations, e.g. DSC and ATR-IR were undertaken to reveal the solid state of the drug.

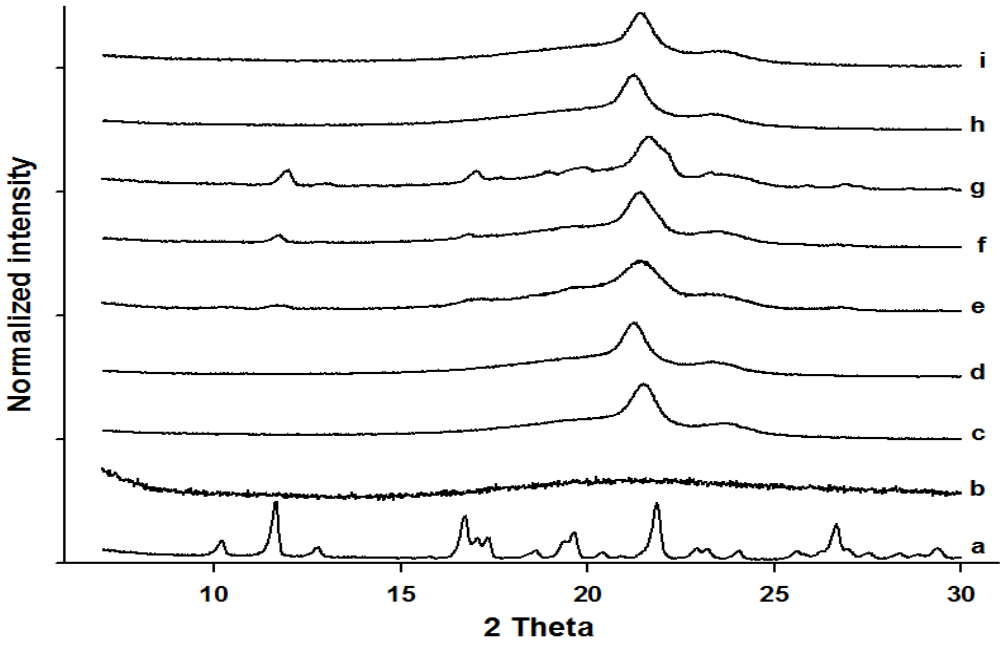


**Figure 42.** XRD diffractograms of (a) raw crystalline indomethacin, (b) quenched-cooled amorphous indomethacin, (c) drug-free EVA 5 filament; (d) drug-free EVA 5 3D prototype; (e) physical mixture of EVA 5 with 15% indomethacin; (f) 5% drug containing EVA 5 filament; (g) 15% drug containing filament; (h) 5% drug containing EVA 5 3D prototype and (i) 15% drug EVA 5 3D prototype.

## 6.3.3 Thermal analysis

DSC analysis was performed to get further inside into solid-state properties of the components of physical mixture, hot-melt extruded filaments and 3D printed prototypes.

### 6.3.3.1 DSC analysis of PCL filaments and printed prototypes

DSC analysis was performed on *ex tempore* prepared, 1 month old hot-melt extruded filaments and 1 week old 3D printed prototypes. The thermograms for the PCL samples are presented in Figure 43. The thermogram of the PCL filament reveals a broad endothermic event with the onset temperature of 54 ºC and the peak maximum of around 60 ºC. The DSC

thermogram of the filament, containing 5% indomethacin was near identical with the DSC trace of pure PCL. For the filament with 15% drug loading, the thermogram exhibits two endothermic events at onset temperatures of 55 ºC and 78 ºC and peak maxima at 60 ºC and 97 ºC. The thermogram of the highest drug-loaded filament show as well two endothermic events with onset temperature of 55 ºC and 101 ºC and peak maxima at 60 ºC and 125 ºC, respectively. The peak with peak maxima at 60 ºC corresponds to the characteristic peak of PCL, and the latter peaks maxima (97 ºC and 125 ºC) should be the melting point of indomethacin. The depression in the melting point of APIs has been previously reported in the literature and is due to the fact that a part of the drug was dissolved in the polymer during hot-melt extrusion (Almeida et al., 2011, Cheng et al., 2010). The proportion of the dissolved drug out of the loaded amount was the lowest for the highest drug-containing filament as the depression in the melting point of the drug was the lowest, whereas enthalpy of fusion was the highest. XRD analysis revealed some degree of crystallinity in the filament, containing 5% indomethacin, whereas DSC analysis did not detect any characteristic peaks. It can be due to the fact that the present crystalline indomethacin started dissolving in the melting PCL during DSC experiments at the elevated temperature as this phenomenon has been seen already by other researchers (Gogos et al., 2012). The thermogram of the physical mixture, containing 5% indomethacin, showed a depressed onset of the melting peak of indomethacin at 152 ºC with a peak maximum at 160 ºC, indicating that drug started dissolving in the melting polymer during DSC experiments. The results from the thermograms of 3D printed samples showed the same trend as XRD analysis. The crystalline indomethacin was well detected in the prototypes, containing the highest amount of API. The melting peak of indomethacin was further depressed to the onset temperature of 99 ºC and 123 ºC in the thermograms of the prototypes with 30% drug loading. It underlines the fact that 3D printing caused further dissolution of crystalline indomethacin in the molten polymer. The tiny trace of the crystalline indomethacin was observed in the prototype, containing 15% of the drug, whereas XRD did not reveal any degree of crystallinity of the drug in this sample. Obviously, the recrystallization of the drug could take place as DSC analysis was performed on the 1 week old sample, whereas XRD analysis was done with 1 day old prototype. Besides the molecularly dispersed and crystalline indomethacin, 15% drug-loaded prototypes could contain the amorphous indomethacin, as the printing temperature (100 ºC) of the corresponding filaments was conducted above the detected melting point of the drug. However, the presence of the amorphous phase was not detected as the melting of PCL hided the possible glass transition of the drug. Due to the evidence of the melting point depression,

it was impossible to conclude in which polymorphic form the crystalline indomethacin was present in the filaments and 3D printed devices.

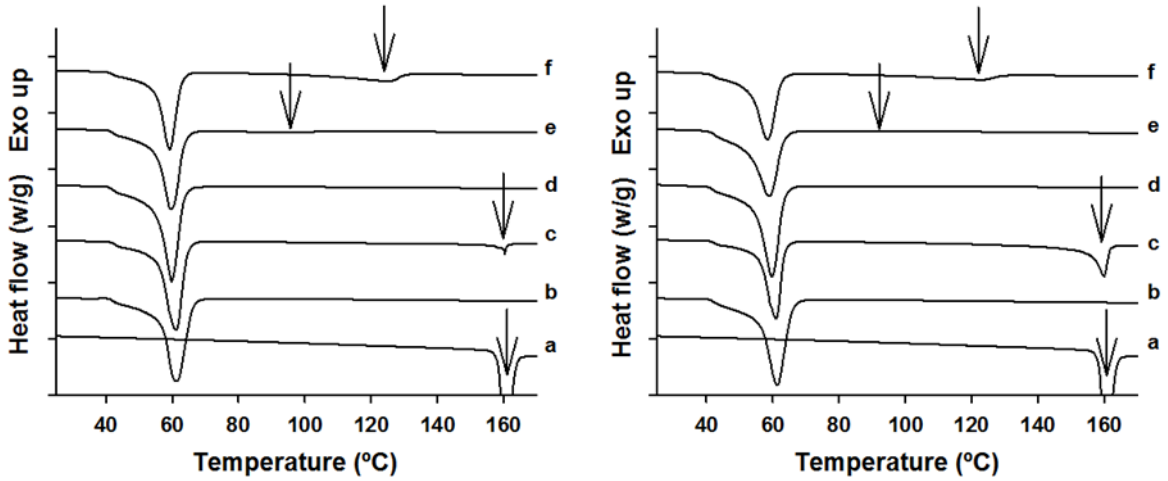


**Figure 43.** DSC thermograms of filaments (left, b, d-f) and 3D printed samples (right, b, d-f): (a) raw γ-indomethacin; (b) drug-free PCL; (c) physical mixture of PCL with 5% (left) and 30 % (right) indomethacin; (d) formulation with 5% indomethacin; (e) 15% indomethacin and (f) 30% indomethacin. The arrows show the detected melting of indomethacin.

### 6.3.3.2 DSC analysis of EVA 5 filaments and printed prototypes

The thermograms for the EVA samples are presented in Figure 44. The thermogram of the EVA filament reveals two endothermic peaks with the onset temperatures of 42 ºC and 73 ºC and the peak maximums of around 46 ºC and 90 ºC. Those peaks indicate that EVA 5 contains two different types of crystals (polymorphs) in its structure (Almeida et al., 2011). The DSC thermogram of the filaments, containing 5% and 15% indomethacin, exhibits the same endothermic events that the drug-free filament, and another endothermic event with an onset at 124 ºC and 158 ºC, respectively. The latter peaks maxima (142 ºC and 160 ºC), should be the melting point of γ-indomethacin. The depression in the melting point of the API in the filament containing 5% drug, was due to the fact that the drug was able to dissolve in the polymer at some extent during DSC analysis (Gogos et al. 2012). Dissolution of the drug in the polymer could not happen during HME, because the prepared filaments did not reveal any indication of yellow color as a characteristic feature of the dissolved or amorphous drug. The differences in the thermograms of the physical mixture and filament

with 15% drug load could be related to the fact that it was possible to obtain a relatively homogeneous solid dispersion during HME, whereas the prepared physical mixture was not homogeneous, and separated regions of both components were present in it.

The thermogram of the drug-free 3D printed EVA prototype reveals the same endothermic peaks that the drug-free filament. 3D printing was conducted at the temperature 165 ºC that is above the melting point of indomethacin. As a result, the presence of the amorphous indomethacin in addition to the crystalline ones was observed in the thermograms of 3D printed prototypes, containing 15% drug. The presence of the peak, corresponding to the melting of the metastable form of indomethacin at onset temperature of 149 ºC, could be a result of recrystallization of the amorphous phase as well as melting of already formed metastable polymorph of indomethacin. The rapid application of high temperature during 3D printing could be the reason for the incomplete conversion of the drug from its crystalline state to amorphous. In addition, molten and cooled down amorphous indomethacin has a tendency to recrystallize to a stable form through the formation of metastable polymorph in a fast pace by storing it in the ambient conditions (Karmwar et al., 2011). Both aspects could contribute to the existence of drug in the crystalline and amorphous state after printing. The exact solid state of the drug in the 3D printed prototype with 5% drug loading was not evident. The further depression in the melting point of drug, in comparison with the corresponding filament, was due to the higher amount of the drug that was dissolved in the polymer. Obviously, 3D printing had assisted in the improvement of solubility of indomethacin in EVA 5 polymer.

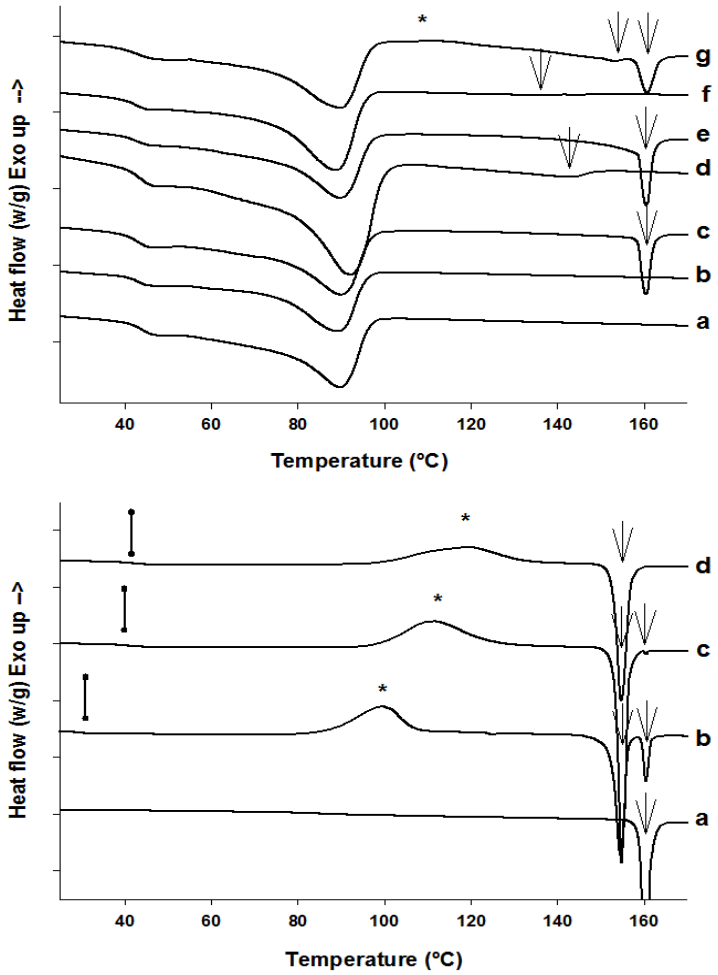


**Figure 44.** DSC thermograms of EVA 5 based samples (top): (a) drug-free filament; (b) drug-free 3D prototype; (c) physical mixture with 15% indomethacin; (d) 5% drug containing filament; (e) 15% drug containing filament; (f) 5% drug containing 3D prototype and (g) 15% drug 3D prototype; and (bottom): (a) raw indomethacin (IND); (b) quenched-cooled (QC) indomethacin after 3 days storage in ambient conditions; (c) QC IND after 1 h of storage and (d) freshly prepared QC IND. The arrows show the detected melting of indomethacin. The star shows the observed recrystallization of amorphous indomethacin. The lines point at the detected glass transition of IND.

## 6.3.4 ATR-IR

ATR-IR analysis was conducted to get further insight in the degree of crystallization of the drug in the filaments and the printed prototypes.

### 6.3.4.1 ATR-IR analysis of PCL filaments and printed prototypes

PCL used in this study had a strong absorption peak at 1722 $cm^{-1}$. According to the literature PCL has a peak at 1717 $cm^{-1}$ that could be due to a carbonyl C=O stretching (Aghdam et al., 2012). The presence of crystalline drug was detected on the surface of all filaments (approx. 1 month old) and cross-sections of formulations with 15% and 30% drug content. In the 3D printed prototype (2 weeks old) some degree of crystallinity was seen on the surface of samples with 15% and 30% API content as well as in the cross-section of 30% indomethacin samples, presented in Figure 45. Only a single peak of crystalline indomethacin at 1691±1 $cm^{-1}$ due to benzoyl C=O vibration (Ewing et al., 2014) was present in all those spectra. Therefore, it was impossible to reveal the exact polymorphic form of the drug in the formulations, as the peak at 1691 $cm^{-1}$ can be related to both γ- and α-forms of indomethacin. It is worth to mention that the window for ATR-IR analysis is very small, therefore, the obtained spectra is not representative for the entire sample as it is taken from a very restricted area. It is known from the content analysis that the samples are not very homogeneous. It could give a rise to the fluctuating results in the spectra of the same sample. In spite of that the obtained results from ATR-IR analysis were generally in accordance with the data received from XRD and DSC experiments.

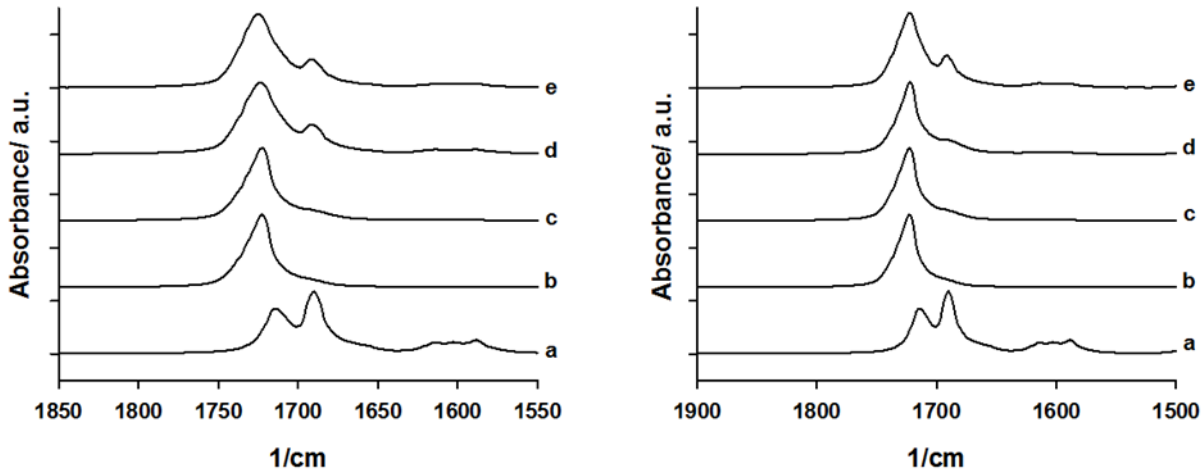


**Figure 45.** ATR spectra of cross-sections of filaments (left, c-e) and 3D printed samples (right, c-e): (a) raw γ-indomethacin; (b) cross-section of drug-free PCL filament; (c) formulation with 5% indomethacin; (d) 15% indomethacin and (e) 30% indomethacin.

### 6.3.4.2 ATR-IR analysis of EVA filaments and printed prototypes

The EVA polymer used in this study had a strong peak at 1738±2 $cm^{-1.}$ According to the literature EVA has a peak at 1739 $cm^{-1}$ due to a carbonyl C=O stretching (Martínez-García et al., 2007). The spectra of surface and cross-sections of the drug loaded filaments, both 5% and 15%, exhibited a peak at 1690±1 $cm^{-1,}$ Figure 46. Crystalline γ-indomethacin has a peak at 1691±1 $cm^{-1}$ due to benzoyl C=O vibration (Ewing et al., 2014) and α-indomethacin has a characteristic peak at 1690 $cm^{-1}$ (Kaneniwa et al., 1985). Both α-indomethacin and amorphous indomethacin have another characteristic peak at 1735 $cm^{-1}$, which is close to the EVA peak 1739 $cm^{-1}$. This made it difficult to conclude in which solid-state form the drug was in the filaments and printed prototypes. There were no further characteristic peaks of indomethacin present in the spectra of the filaments, and therefore, the solid-state form of indomethacin in the formulations was impossible to reveal. In the 3D printed prototype containing 5% indomethacin the peak at 1691±1 was present together with a peak at 1676±1, Figure 46. Those peaks were present on both the spectra of surfaces and cross-sections. The amorphous indomethacin has a peak at 1680-1684 (Ewing et al., 2014). The printing temperature of the prototypes was 165 ºC, that is above the melting point of the drug. It can be concluded that in the printed prototype containing 5% indomethacin the indomethacin

was present as amorphous indomethacin and in some content as crystalline indomethacin. The spectra of the printed prototype containing 15% indomethacin had peaks at 1712±1, 1688±2 and 1588±1 $cm^{-1}$. The peaks at 1712±1 $cm^{-1}$ and 1588±1 $cm^{-1}$ correspond to the characteristic γ-indomethacin peaks. The peak at 1688±2 $cm^{-1}$ can be either the peak of α-indomethacin or amorphous indomethacin, since in the literature the reported respective peaks are 1689±1 and 1682±2 (Ewing et al., 2014). Since the printing temperature was above the melting point of indomethacin, and the printed prototypes were of yellow color, it can be concluded that amorphous indomethacin was present in the printed samples, despite the fact that some characteristic peaks of amorphous indomethacin were the same as the characteristic peaks of the polymer.

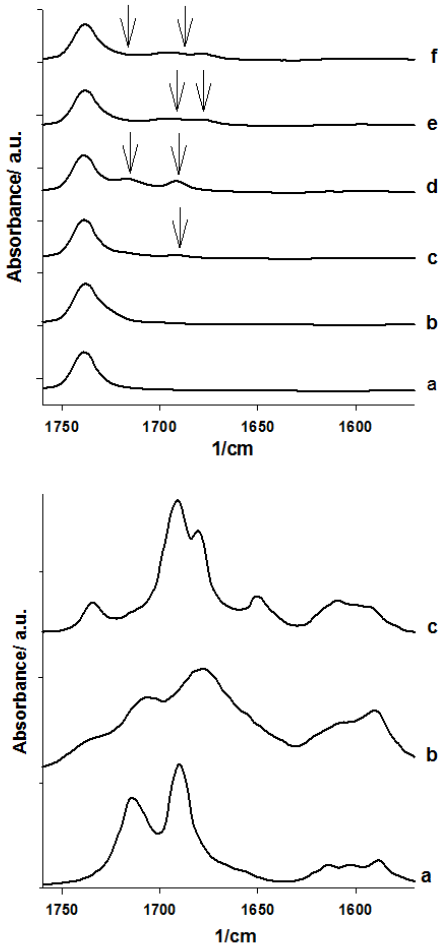


**Figure 46.** ATR-IR spectra of cross-sections of EVA 5-based samples (top): (a) drug-free filament; (b) drug-free 3D prototype; (c) 5% drug containing filament; (d) 15% drug containing filament; (e) 5% drug containing 3D prototype and (f) 15% drug 3D prototype; and (bottom): (a) raw indomethacin (IND); (b) freshly prepared quenched-cooled (QC) indomethacin; and (c) metastable α-form of indomethacin. The arrows show the characteristic peaks of indomethacin in the EVA 5-based samples.

### 6.3.5 Drug content analysis and uniformity of content

Drug content analysis was performed on the PCL filaments to determine the actual amount of indomethacin in the extruded filaments. EVA polymer has a limited number of the relatively toxic solvent in which it could be potentially dissolved. As the manufacturing process of both PCL and EVA filaments was the same, therefore, the obtained values from the content analysis of drug-loaded PCL filaments were used in the calculations of the actual amount drug in filaments made of both polymers. The theoretical drug polymer ratio in the filaments were 5:95, 15:85 and 30:70. The actual drug content was lower than the theoretical, as shown in Table 17.

**Table 17.** Drug content analysis results on the extruded filaments. Data are presented as mean ± standard deviation, n=3.

| Sample | Theory (mg) | Theory (%) | Theory (ratio) | Actual (mg) | Actual (%) | Actual (ratio) |
|---|---|---|---|---|---|---|
| PCL+5% IND | 6.5±0.1 | 100±0.1 | 5.0:95.0 | 4.8±0.1 | 73.6±0.3 | 3.7:96.3 |
| PCL+15% IND | 19.5±0.2 | 100±0.2 | 15.0:85.0 | 15.0±0.2 | 76.8±1.1 | 11.5:88.5 |
| PCL+30% IND | 39±0.1 | 100±0.1 | 30.0:70.0 | 35.3±4.0 | 89.8±10.3 | 27.0:73.0 |

A smaller content of indomethacin than theoretically expected could be explained with the evident drug loss in the beginning of the HME process as micronized indomethacin is a very cohesive and adhesive powder with poor flow properties. The first reason for low drug content is that the drug and the polymer were pre-weighed into plastic bags before the extrusion and some part of the micronized indomethacin was lost due to the difficulty of detaching it from the surfaces of the plastic bag. Secondly, some of the drug was lost when it was fed into the loading hopper due to the strong attachment to the surfaces of the hopper. Thirdly, some of the micronized indomethacin powder got attached to the screws in the barrel, where the loader was located. The drug loss in percentage was highest for the lowest drug polymer ratio (5:95), because the attachment to the container and loading hopper was near the same for all formulations. The loss of material was a problem only with the indomethacin, because the polymers were fed as pre-cut bars (PCL) or pellets (EVA), and they were easier to load into the extruder. If the polymer would have been as a powder with the same particle size and cohesive/adhesive nature as indomethacin, the loss of material would have been closer to that of indomethacin. To prevent the loss of the drug the process should be further optimized. The loss of indomethacin could have been smaller, if the pre-weighing would have been done in a metal container with the reduced adhesion to the

micronized drug particles. In addition, pre-mixing step in a separate mixer at elevated temperature could be included in the HME process to ensure the homogeneous appearance of the load material before its supply to the type of the mini-extruder used in this work. The loss of indomethacin could also have been taken into account already when the materials were weighed, by increasing the indomethacin amount to be expected to be lost during HME process.

Based on the content analysis of the filaments, calculations were done to know the actual amount of drug in the PCL 3D printed samples, EVA 5 filaments and 3D printed samples. The results are presented in Table 18 and 19, respectively.

**Table 18.** Drug content in the 3D printed PCL prototypes.

| 3D printed PCL prototypes | | | | |
|---|---|---|---|---|
| **Sample** | **Theoretical drug content (%)** | **Theoretical drug amount (mg)** | **Actual drug content (%)** | **Actual drug amount (mg)** |
| IUS 1 | 5 | 6.59±0.07 | 3.7 | 4.87±0.05 |
| IUS 2 | 5 | 15.23 | 3.7 | 11.27 |
| IUS1 | 15 | 28.18±0.25 | 11.5 | 16.42±0.19 |
| IUS 1 | 30 | 36.08±0.65 | 27.0 | 32.93±0.59 |

**Table 19.** Drug content in the EVA 5 filaments and 3D printed prototypes.

| EVA 5 filaments and 3D printed prototypes | | | | |
|---|---|---|---|---|
| **Sample** | **Theoretical drug content (%)** | **Theoretical drug amount (mg)** | **Actual drug content (%)** | **Actual drug amount (mg)** |
| Filament | 5 | 2.88±0.04 | 3.7 | 2.13±0.03 |
| Filament | 15 | 8.80±0.08 | 11.5 | 6.74±0.06 |
| IUS 2 | 5 | 12.30±0.30 | 3.7 | 9.10±0.22 |
| IUS 2 | 15 | 39.89±0.20 | 11.5 | 30.57±0.16 |
| 3D printed rod | 5 | 2.85±0.02 | 3.7 | 2.11±0.02 |
| 3D printed rod | 15 | 9.98±0.07 | 11.5 | 7.65±0.05 |

The uniformity of content is important in pharmaceutical applications. In the HME process the type of extruder and the residence time in the extruder are factors that affect the homogeneity of the formulations (Leister et al., 2012). Co-rotating twin-screw extruders has better mixing capabilities than single-screw extruders. Although, the HME was performed with a twin-screw extruder, there were poor homogeneity of the extruded filament with the highest drug loading (SD 4.0), Table 17. The extruder was a small-scale extruder with two screws consisting of only one single screw element. The HME set-up could have been a reason for the poor homogeneity of the formulation, with the highest drug content as the machine could not produce efficient mixing of the highly cohesive indomethacin with the molten polymer. Another factor that affects the homogeneity is the residence time. It is

important, because it has to be long enough to sufficiently melt and mix the materials in the barrel. With heat or shear sensitive materials it is important to optimize the residence time in the process, to know the required time to get a homogenous product, since longer times can cause decomposition of the materials (Leister et al., 2012). The determination of appropriate residence time was based on the torque during the extrusion process. In the beginning of the process the torque was high. It decreased and stabilized with the time when a certain degree of homogeneity was reached. According to the literature the residence time in larger twin-screw extruders are about 2 minutes (Breitenbach, 2002), and therefore the used residence time should have been long enough. The needed mixing time depends on the extruder type, and can therefore not be directly compared, but should give some indications about the needed time to give a homogenous melt. In conclusion, the HME process must be optimized to get the drug homogenously dispersed in the polymer. A different model of extruder with more powerful mixing capacity or a longer residence time could be tested.

## 6.4 *In vitro* drug release

### 6.4.1 Solubility determination of indomethacin in the release media

The solubility of indomethacin was determined in three different media: pure water, 0.9 % NaCl and 1 % (2-Hydroxypropyl)-ß-cyclodextrin. The results are presented in Table 20. Solubility was highest in 1 % (2-Hydroxypropyl)-ß-cyclodextrin with water as solvent at 37 ºC. The solubility of indomethacin in water and 0. 9 % NaCl was near the same. The drug release studies were conducted at 37 ºC, however the UV measurements were analyzed immediately in ambient conditions. Despite the good solubility of indomethacin in 1 % (2-Hydroxypropyl)-ß-cyclodextrin, 0.9 % NaCl was chosen as the release media as 0.9 % NaCl is used a lot as a physiological release, and it is a cheap medium to be used in a long run.

**Table 20.** The solubility of indomethacin in different release media.

| **Media** | **RT (mikrog/ml±SD)** | **37ºC (mikrog/ml±SD)** |
|---|---|---|
| Water | 5.82±0.15 | 6.59±0.09 |
| 0.9% NaCl | 6.77±0.07 | 7.48±0.07 |
| 1% (2-Hydroxypropyl)-ß-cyclodextrin | 22.50±0.05 | 25.57±0.57 |

## 6.4.2 Drug release from PCL and EVA filaments and the 3D printed prototypes

### 6.4.2.1 Drug release from the PCL filaments and 3D printed prototypes

In Tables 21 and 22 and Figure 47 (left) the cumulative percentage and the daily mean release data of IND from PCL filaments (1-3 weeks old) over a period of 30 days *in vitro* release test under sink conditions are presented. The filament containing 5% indomethacin showed an initial burst release phase. After the initial fast release the drug release rate gradually slowed down followed by a sustained release phase. The filaments containing 15% and 30% showed a lower initial burst release. The initial fast release was due to immediate dissolution of the drug located on or near the surface of the filament (Cheng et al., 2009). After the initial phase, the drug was released slowly by diffusion of drug molecules from the interior of the polymer matrix. The overall drug release percentage was highest for the filament containing 5% indomethacin and lowest for the filament with 30% indomethacin after 30 day release. In the literature it has been previous reported that the drug release from higher drug-loaded PCL implants was faster than from a lower drug-loaded PCL implants (Li et al., 2010). However, the drug was present mostly in its crystalline state in those studies. In this work, based on XRD, DSC and ATR-IR analysis the drug had completely or almost completely dissolved under extrusion only in the filament containing 5 %. In both the filaments containing 15 % and 30 % indomethacin, the drug was at least partially in its crystalline state. The dissolution rate of amorphous indomethacin or dissolved indomethacin is faster than the crystalline counterpart, and therefore, the release percentage of the drug is higher from the filaments containing almost or near almost dissolved indomethacin (5%).

As expected, the overall daily release amount of the drug decreased faster for the filament containing 5% indomethacin than for the two other filaments. The filament containing 15% indomethacin released higher amount of the drug during the first days than the filament containing 30%. Evidently, the highest amount of the molecularly dispersed drug was present on the surface of the filament containing 15% indomethacin. After a few days, the slowest decrease in the drug amount was observed for the filament with highest drug loading as the slow diffusion from the interior to the exterior of all filaments became the predominant release mechanism.

**Table 21.** Cumulative percentage release of drug from PCL filaments with different drug loading content (n=3).

| Sample | Cumulative release %[1] (%±SD) | | | | |
|---|---|---|---|---|---|
| | **0.25d** | **1d** | **2d** | **15d** | **30d** |
| Filament 5% | 13.48±1.23 | 28.04±3.15 | 40.78±4.70 | 90.35±10.19 | 104.13±10.52 |
| Filament 15% | 3.63±0.54 | 9.78±1.33 | 15.88±1.67 | 49.32±2.20 | 64.39±1.53 |
| Filament 30% | 1.33±0.07 | 3.75±0.35 | 6.32±0.19 | 23.66±0.89 | 34.87±0.86 |

[1]Calculated from the actual indomethacin amount

**Table 22.** Daily release of indomethacin from PCL filaments.

| Sample | Daily release from PCL filaments (mikrog±SD) | | | | |
|---|---|---|---|---|---|
| | **0.25d** | **1d** | **2d** | **15d** | **30d** |
| Filament 5% | 645.0±0.04 | 1341.1±0.07 | 609.3±0.17 | 126.9±0.37 | 24.9±0.37 |
| Filament 15% | 580.6±0.07 | 1562.3±0.17 | 974.9±0.22 | 265.1±0.30 | 104.6±0.21 |
| Filament 30% | 442.0±0.02 | 1250.4±0.09 | 853.4±0.05 | 351.7±0.25 | 190.5±0.25 |

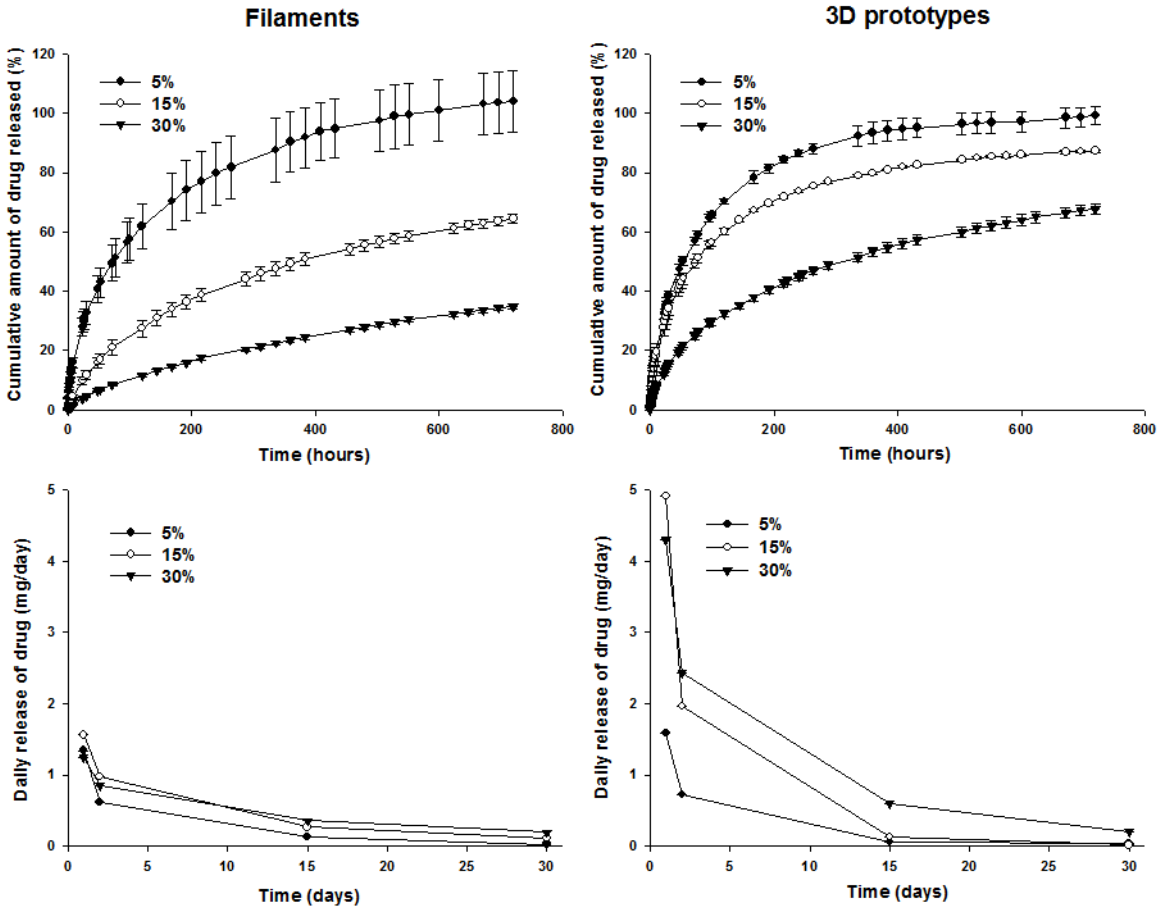


**Figure 47.** Cumulative percentage release (top) and daily release (bottom) of indomethacin from PCL filaments and 3D prototypes.

**Table 23.** Cumulative percentage indomethacin release from PCL IUS 1 prototypes (n=3).

| Sample | Cumulative release %[1] (% ± SD) | | | | |
|---|---|---|---|---|---|
| | **0.25d** | **1 d** | **2 d** | **15 d** | **30 d** |
| IUS 1 5% | 16.12±0.86 | 32.54±1.49 | 47.34±1.65 | 93.58±3.61 | 99.38±2.96 |
| IUS 1 15% | 13.69±2.30 | 29.95±2.77 | 41.91±2.06 | 79.85±0.36 | 87.30±0.49 |
| IUS 1 30% | 5.75±0.43 | 13.26±0.47 | 20.17±0.89 | 53.34±1.65 | 67.89±1.82 |

[1] Calculated from the actual IND amount

**Table 24.** Daily drug release from the PCL IUS 1 prototypes (n=3).

| Sample | Daily release from IUS 1 prototypes (mikrog. ± SD) | | | | |
|---|---|---|---|---|---|
| | **0.25d** | **1d** | **2d** | **15d** | **30d** |
| IUS 1 5% | 785.9±0.04 | 1586.5±0.07 | 721.7±0.08 | 53.9±0.12 | 31.4±0.11 |
| IUS 1 15% | 2245.8 ±0.36 | 4914.8±0.41 | 1965.1±0.28 | 124.7±0.19 | 11.1±0.24 |
| IUS 1 30% | 1864.7±0.11 | 4303.0±0.09 | 2434.9±0.18 | 600.8±0.47 | 205.3±0.57 |

In Tables 23 and 24 and Figure 47 (right) the cumulative release and the daily release data of IND from the 3D printed PCL IUS 1 implants (1-2 weeks old) over a period of 30 days is presented. All three prototypes showed an initial burst release phase. The first burst release phase was followed by slow diffusion of the drug from interior to exterior through the voids, remained after already released drug molecules/crystals (Figure 48). The initial burst release was lower for the prototypes with the highest drug loading. After the initial fast release a sustained drug release phase was monitored. The drug release was fastest for the prototype containing 5% indomethacin, and slowest for the prototype with 30% indomethacin. The release profiles from the prototypes with 5 % and 15 % indomethacin were closer to each other than in the case of the corresponding filaments. It can be explained with the fact that the drug in those prototypes was mainly present in the molecularly dispersed state, whereas in the 15% drug-loaded filament contained the drug mostly in the crystalline form. The geometry of the extruded filaments and the printed prototypes differ, and therefore, the release rate cannot be compared directly. In Figure 49 pictures of all drug-loaded IUS 1 after drug release is presented.

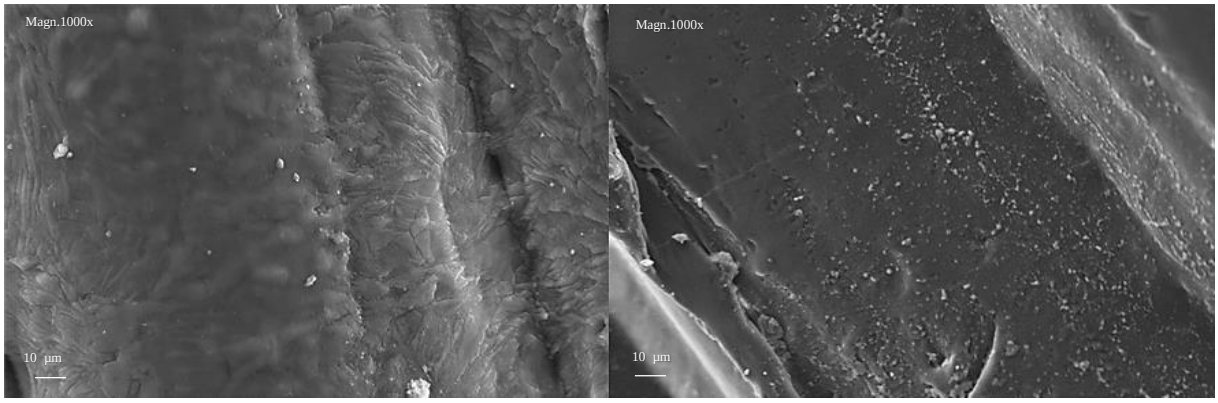


**Figure 48.** SEM images of the surface of 15% drug-loaded IUS 1 prototype before (left) and after (right) release tests.

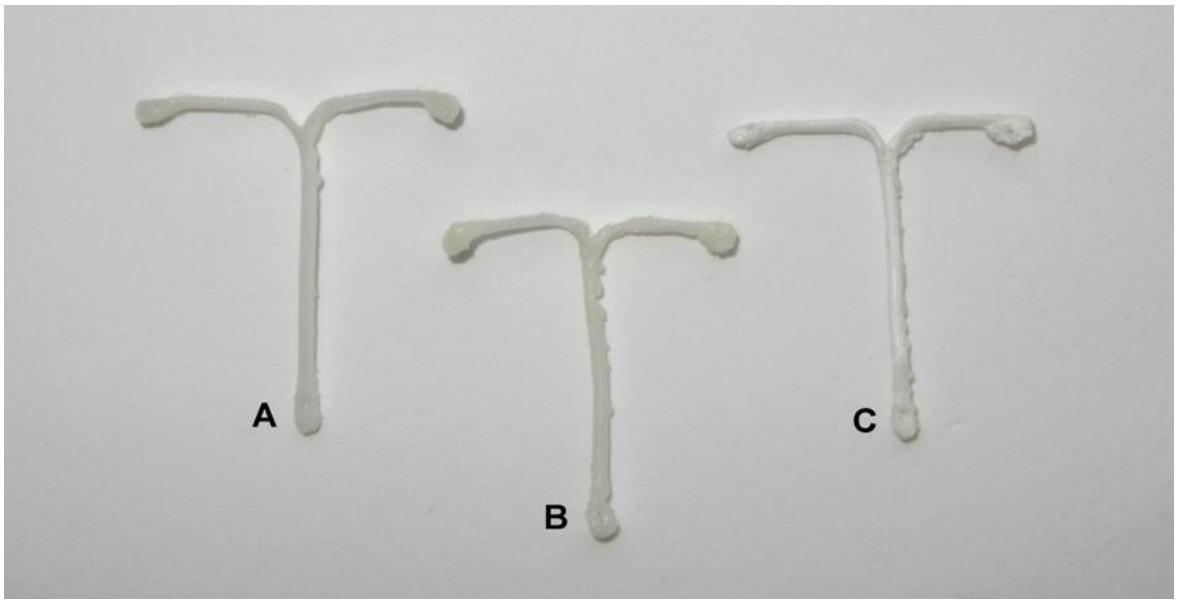


**Figure 49.** 3D printed IUS1 prototypes with: (A) 5%, (B) 15% and (C) 30% indomethacin loading after release tests.

In Figure 50 the geometry of IUS 1 and IUS 2 (left) and the release profiles for IUS 1 5% and IUS 2 5% (right) are presented. The diameter of the IUS 1 is smaller than the one for the IUS 2. In addition, the infill printing parameters were 10% and 100% for IUS 1 and IUS 2, respectively, meaning that IUS 2 had more solid structure and less porous structure than IUS 1. As can be seen in the percentage release (Figure 50, right) the release rate from IUS 1 is faster. This is in accordance with earlier studies on PCL implants (Li et al., 2010). This is due to the fact that an increase in the implant diameter results in a longer diffusion path for drug diffusion from the PCL matrix. In Table 25 the cumulative percentage and daily drug release is presented.

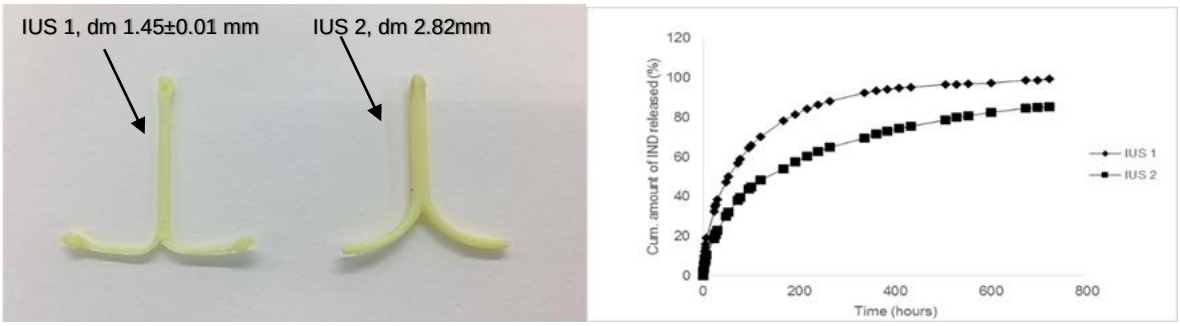


**Figure 50.** The geometry and the diameter of IUS 1 (infill 10%) and IUS 2 (infill 100%) (left) and the cumulative percentage drug release from IUS 1 and IUS 2 prototypes (right).

**Table 25.** Cumulative percentage release and daily release from IUS 2 prototypes (n=1)

| **Sample** | **Cumulative release %[1]** | | | | |
|---|---|---|---|---|---|
| | **0.25d** | **1d** | **2d** | **15d** | **30d** |
| IUS 2 5% | 9.06 | 18.82 | 30.02 | 71.44 | 85.32 |

[1] Calculated from the actual IND amount

| **Sample** | **Daily release from IUS 2 prototypes (mikrog)** | | | | |
|---|---|---|---|---|---|
| | **0.25d** | **1d** | **2d** | **15d** | **30d** |
| IUS 2 5% | 1020.9 | 2121.4 | 1261.6 | 238.1 | 43.8 |

### 6.4.2.2 Drug release from the EVA 5 filaments and 3D printed prototypes

The cumulative and daily release of indomethacin from the EVA 5 filaments is presented in Tables 26 and 27 and in Figure 51A. The cumulative percentage drug release after 30 days was higher from the filament containing 5% than from the one containing 15%. This is in accordance with previous results presented in literature (Andersson et al., 2011), with an EVA grade of VA-content of 18% with etonogestrel as a model drug. In a study with an EVA containing 40% VA with a crystalline freely water soluble drug, the release rate was faster from devices with higher drug loadings (Almeida et al., 2011). Almeida et al. (2011) reported that the release rate from EVA is a combination of different parameters, such as drug crystallinity, polymer crystallinity, drug loading and extrusion temperature. In addition, drug solubility in the release medium plays an important role and affects the release rate of the drug from the polymer at some extent. SEM images of the surfaces of 5 % drug-loaded filaments before and after dissolution test is presented in Figure 52. After drug release the surface is more porous because of disappearance of drug particles.

**Table 26.** Cumulative percentage release from EVA 5 filaments (n=3).

| Sample | Cumulative release %[1] | | | | |
|---|---|---|---|---|---|
| | **0.25d** | **1d** | **2d** | **15d** | **30d** |
| Filament 5% | 2.30±0.09 | 5.48±0.15 | 7.30±0.15 | 21.19±0.29 | 29.26±0.40 |
| Filament 15% | 1.72±0.04 | 2.74±0.05 | 3.68±0.04 | 10.68±0.15 | 15.00±0.20 |

[1] Calculated from the actual IND amount

**Table 27.** Daily release from EVA 5 filaments (n=3).

| Sample | Daily release from EVA 5 filaments (mikrog±SD) | | | | |
|---|---|---|---|---|---|
| | **0.25d** | **1d** | **2d** | **15d** | **30d** |
| Filament 5% | 49.02±0.01 | 116.62±0.02 | 38.63±0.01 | 15.56±0.01 | 9.62±0.01 |
| Filament 15% | 79.23±0.01 | 184.96±0.01 | 64.80±0.01 | 26.49±0.01 | 13.72±0.01 |

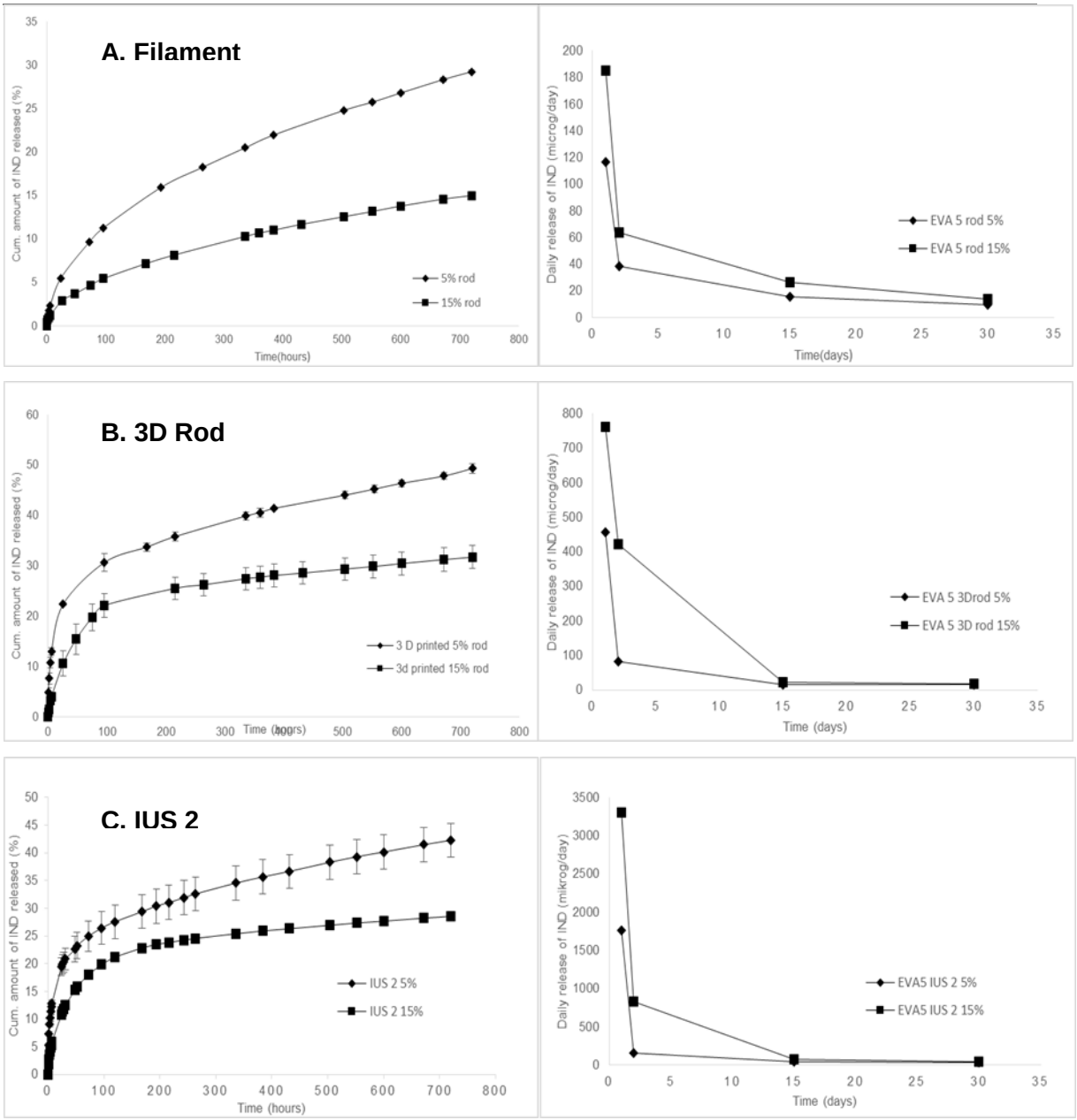


**Figure 51.** The cumulative and daily release from (A) EVA 5 filaments, (B) EVA 5 3D printed rods and (C) EVA 5 3D printed IUS 2 prototypes.

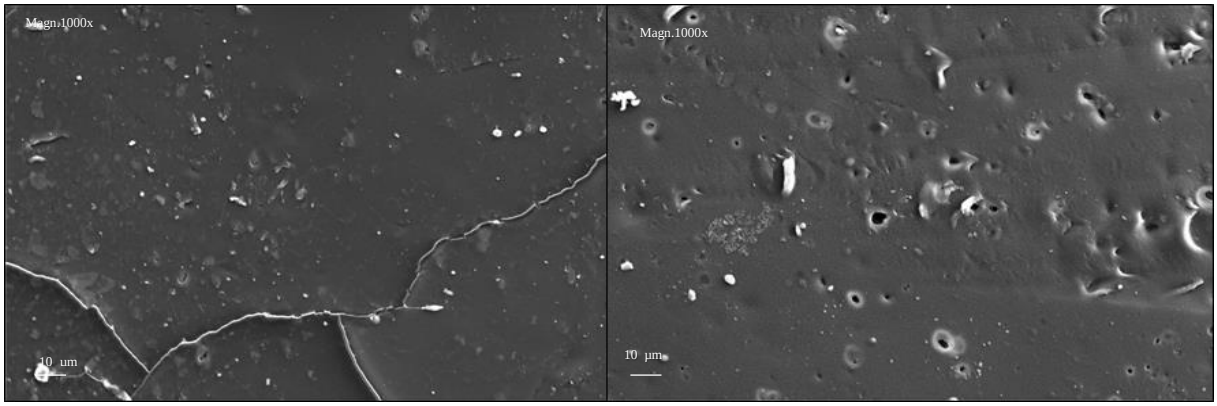


**Figure 52.** SEM images of the surfaces of EVA 5% drug-loaded filaments before (left) and after (right) drug release tests.

The drug release from the 3D printed rods and IUS 2 prototypes containing 5% indomethacin was faster than the drug release from the counterparts containing 15% indomethacin (Figure 51B-C and Tables 28-31). Both exhibits a burst release during the first days. The release rates are higher than those for the extruded filaments, which is due to the fact that the printing temperature was above the melting point of the drug. According to the XRD, DSC and ATR-IR analysis most of the drug had melted and/or dissolved during the printing, which made the drug release from the printed rods faster than from the extruded counterparts. In Figure 53 SEM images of the IUS 2 prototypes before and after drug release tests is presented.

**Table 28.** Cumulative percentage release from 3D printed EVA 5 rods (n=3).

| **Sample** | **Cumulative release % from 3D printed rod[1]** | | | | |
|---|---|---|---|---|---|
| | **0.25d** | **1d** | **2d** | **15d** | **30d** |
| 3D Rod 5% | 13.02±0.73 | 21.59±0.28 | 25.38±0.64 | 40.58±0.88 | 49.33±0.95 |
| 3D Rod 15% | 4.03±0.92 | 9.94±2.50 | 15.45±3.04 | 27.74±2.20 | 31.71±2.27 |

[1] Calculated from the actual IND amount

**Table 29.** Daily release from 3D printed EVA 5 rods (n=3).

| **Sample** | **Daily release from EVA 5 3D printed rod (mikrog±SD)** | | | | |
|---|---|---|---|---|---|
| | **0.25d** | **1d** | **2d** | **15d** | **30d** |
| 3D Rod 5% | 276.44±0.02 | 455.60±0.01 | 83.30±0.01 | 14.73±0.02 | 15.81±0.01 |
| 3D Rod 15% | 308.13±0.07 | 760.04±0.23 | 421.36±0.23 | 23.15±0.16 | 17.75±0.16 |

**Table 30.** Cumulative percentage release from EVA IUS 2 prototypes (n=3).

| Sample | Cumulative release %[1] | | | | |
|---|---|---|---|---|---|
| | **0.25d** | **1d** | **2d** | **15d** | **30d** |
| IUS 2 5% | 12.28±0.56 | 19.41±1.59 | 22.56±2.30 | 35.13±3.08 | 42.27±3.05 |
| IUS 2 15% | 5.33±0.30 | 10.79±0.35 | 15.19±0.29 | 25.65±0.43 | 28.33±0.51 |

[1] Calculated from the actual IND amount

**Table 31.** Daily release from EVA 5 IUS 2 prototypes (n=3).

| Sample | Daily release from EVA 5 IUS 2 prototypes (mikrog±SD) | | | | |
|---|---|---|---|---|---|
| | **0.25d** | **1d** | **2d** | **15d** | **30d** |
| IUS 2 5% | 1108.98±0.02 | 1766.85±0.13 | 157.22±0.19 | 50.79±0.27 | 36.49±0.27 |
| IUS 2 15% | 1629.31±0.08 | 3299.47±0.10 | 826.85±0.01 | 76.71±0.14 | 48.98±0.16 |

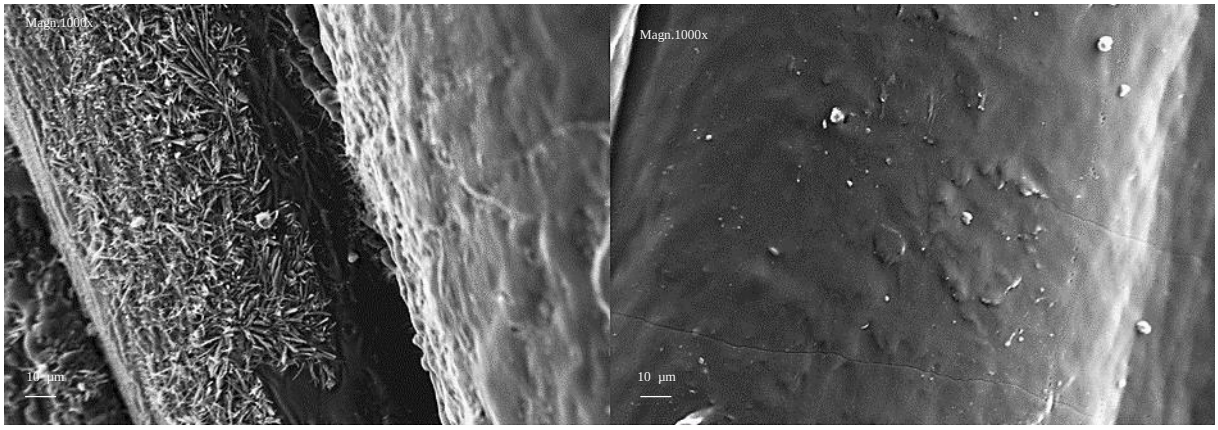


**Figure 53.** The surfaces of EVA IUS 2 5% drug-loaded prototypes before (left) and after (right) release tests.

In conclusion, the drug release from the printed devices depended on the geometry of the devices, the matrix polymer and the degree of the crystallinity of the incorporated drug. The drug release rate was slower for the devices with a bigger device diameter. The drug release rate from the EVA polymer was slower than for the PCL polymer. The cumulative percentage drug release was slower from the devices with higher drug loading than from those with lower drug loading, this was due to the fact that in the devices with higher drug loading there were more crystalline drug that in those with lower drug loading.

## 6.4.3 Drug release mechanism

### 6.4.3.1 Release mechanisms for the PCL samples

The *in vitro* drug release data for the PCL samples were fitted by zero-order, first-order, Higuchi and Korsmeyer-Peppas models (Dash et al., 2010). The data of all models are presented in Table 32. It was shown that the best fit was obtained by the Higuchi square root model, $R^2$ value for all samples was >0.992, indicating that the drug diffusion is the predominant release mechanism of the drug from PCL polymer, regardless of the geometry of the samples and the amount of drug loading. The change in the value of the release constant $k_H$ was in accordance with the observed release profile data (Figure 47), i.e. the closer the release profiles of the different formulations, the more similar value of the their constant is.

**Table 32**. Data of drug release profiles fitted by mathematical kinetic models. First 60% of drug release data were used in the models to obtain the correlation coefficient $R^2$.

| | **Zero-order** $M_t/M_\infty=Q_0+k_0t$ | **First-order** $logC=logC_0-kt/2.303$ | **Higuchi** $M_t/M_\infty=k_Ht^{1/2}$ | | **Korsmeyer-Peppas** $M_t/M_\infty=kt^n$ | |
|---|---|---|---|---|---|---|
| | **$R^2$** | **$R^2$** | **$k_H$** | **$R^2$** | **n** | **$R^2$** |
| Filament 5% | 0.9391 | 0.9351 | 6.01 | 0.9986 | 0.57 | 0.9952 |
| Filament 15% | 0.9620 | 0.9741 | 2.67 | 0.9980 | 0.68 | 0.9952 |
| Filament 30% | 0.9323 | 0.9795 | 1.37 | 0.9974 | 0.73 | 0.9955 |
| IUS 1 5% | 0.9380 | 0.9801 | 7.05 | 0.9978 | 0.58 | 0.9909 |
| IUS 1 15% | 0.9031 | 0.9567 | 6.10 | 0.9926 | 0.65 | 0.9697 |
| IUS 1 30% | 0.9072 | 0.9608 | 2.87 | 0.9961 | 0.60 | 0.9878 |
| IUS 2 5% | 0.9071 | 0.9494 | 6.6 | 0.9958 | 0.70 | 0.9737 |

### 6.4.3.2 Release mechanisms for the EVA 5 samples

The *in vitro* drug release data for the EVA samples was fitted by zero-order, first-order, Higuchi and Korsmeyer-Peppas models. The correlation coefficient ($R^2$) of all models and the n value for the Korsmeyer-Peppas model are listed in Table 33. It was shown that for the 3D printed samples the best fit was obtained by the Korsmeyer-Peppas model, $R^2$ value for all samples was >0.94. In the Korsmeyer-Peppas model the *n* value characterize the release mechanism of drug from a device. For the case of a cylinder the *n* value of $0.45\leq$ corresponds to a Fickian diffusion mechanism, whereas $0.45\leq n=0.89$ to non-Fickian transport (Dash, 2010). For all 3D printed samples the *n* value was $\leq 0.45$, except for the 3D printed Rod

15%, which was 0.5113. The fact that the prototype IUS 2 is not a cylinder and the surface is of a layered structure may also lead to variations in the kinetics of the drug release.

For the extruded filaments the best fit was obtained by the Higuchi model, $R^2 \geq 0.9989$, indicating that the drug diffusion is the predominant release mechanism for the filament.

**Table 33.** Data of drug release profiles fitted by mathematical kinetic models.

| | **Zero-order** $M_t/M_\infty=Q_0+k_0t$ | **First-order** $logC=logC_0-Kt/2.303$ | **Higuchi** $M_t/M_\infty=k_Ht^{1/2}$ | | **Korsmeyer-Peppas** $Mt/M\infty=kt^n$ | |
|---|---|---|---|---|---|---|
| | **$R^2$** | **$R^2$** | **$k_H$** | **$R^2$** | **n** | **$R^2$** |
| Filament 5% | 0,9178 | 0.9351 | 0.8180 | 0.9989 | 0.5469 | 0.9958 |
| Filament 15 % | 0.9389 | 0.9476 | 0.4350 | 0.9998 | 0.5347 | 0.9984 |
| IUS 2 5% | 0.7568 | 0.7978 | 0.9916 | 0.9218 | 0.2824 | 0.9762 |
| IUS 2 15% | 0.6905 | 0.7134 | 0.8131 | 0.8912 | 0.4020 | 0.9564 |
| 3D Rod 5% | 0.7807 | 0.8260 | 1.2087 | 0.9365 | 0.3146 | 0.9744 |
| 3D Rod 15% | 0.7230 | 0.7476 | 0.9192 | 0.9069 | 0.5113 | 0.9432 |

## 6.4.4 Degradation of PCL under *in vitro* release

The degradation of PCL was done by evaluation of the *in vitro* mass loss of the polymer. The change in the molecular weight of the polymer during release studies was not analyzed. EVA is a non-degradable polymer, and therefore, the mass loss was not studied.

For the PCL samples with the lowest drug loading, 5%, the mass loss of the polymer was lowest for both the filament and the IUS1 sample compared to those with higher drug loading, as presented in Table 34. The highest polymer mass loss was in the samples with the highest drug loading. According to Cheng et al. (2010) the higher PCL mass loss percentage for samples with higher drug loading, can be due to the fact that higher drug loading generates more pores after drug release and the release media can penetrate into the PCL matrix and facilitate the degradation process. In addition, the presence of weakly acidic indomethacin (pKa 4.5) might speed up the formation of acidic degradation products and by that decrease the degradation half-life of PCL (Cheng et al., 2009). The mass loss for the printed samples, with different drug loading were higher than for the respective hot melt extruded filaments, except for the 5% samples. However, in 5 % samples the difference was insignificant, ($p>0.05$, Students unpaired *t*-test). The higher mass loss of the prototypes

could be explained with their less compact structure of them, compared to the corresponding filaments. IUS 1 prototypes were printed with 10% infill parameter that made the internal structure partly hollow, whereas the filaments were extruded to be homogeneously solid inside.

The results showed a low degradation rate of PCL (≤3.12 %) over the 30 days release test, which is in accordance with earlier studies (Cheng et al., 2010, Fialho et al., 2008). The degradation of PCL is a two phase process with an initial molecular weight loss due to chain scission, without a significant weight loss. When the loss of molecular weight is up to 5000, the mass loss begins due to the diffusion of small polymeric fragments out of the matrix (Sinha et al., 2004, Merkli et al., 1998). The surface has more voids after release tests than before, which is due to the disappearance of drug particles from the polymer (Figure 48, under *in vitro* release tests).

**Table 34.** Mass loss of PCL for the samples after 30-day release.

| **Sample** | **Mass loss of PCL(%)[1]** |
|---|---|
| Filament 5% | 1.34±0.19 |
| Filament 15% | 1.53±0.07 |
| Filament 30% | 2.14±0.02 |
| IUS 1 5% | 0.96±0.39 |
| IUS 1 15% | 2.40±0.21 |
| IUS 1 30% | 3.12±0.79 |
| IU2 2 5% | 0.81 |

[1] (the initial weight of sample-the final weight of sample-the weight of drug released)/total weight of PCL (actual)*100

# 7. Further investigations

In order to succeed with the successful printing using the FDM™ technique, several aspects must be taken into account, which include the printers hard- and software, printing material properties and the geometry of the prototype. To obtain 3D printed PBDS with high quality that complies with the pharmaceutical standards, further investigations and improvements in the material selection and the manufacturing process must be done. The appropriate material must be selected based on the existing printing equipment boundaries, or vice versa, the printer must be selected based on the desired properties of the pharmaceutical formulations.

The material properties that must be taken into account includes materials column strength, viscosity and MI, stiffness and thermal conductivity. In order to determine the printability of a pharmaceutical formulation, e.g. the melt flow behavior, finite element analysis (FEA) can be used. FEA models for simulation of the melt flow in the liquefier for different materials has been reported by Ramanath et al. (2008) and Nikzad et al. (2009). Not only the melt flow behavior is crucial, but the formulations capability to be loaded in the liquefier is important. Mathematical models have been introduced to be able to calculate the buckling tendency of a material (Venkataraman et al., 2000). The impact on the loading process of nozzle angle and pressure drop estimation models have been reported (Turner et al., 2014). In order to be able to use these models the printers hardware properties must be determined. In Table 35 a summary of important printer properties to be taken into account in the FDM™ process.

**Table 35.** Important printer properties in a FDM™ process.

| **Printer properties** | |
|---|---|
| ***Hardware:*** | |
| **Closed build chamber** | Possible to adjust the envelope temperature, artifacts |
| **Adjustable loading temperature** | Increases the amount of possible materials |
| **Heated or vacuum build plate** | Better adhesion to build plate |
| **Changeable extruder and nozzle size** | Different melt flow behavior of different materials, residues from other materials, resolution |
| **Adjustable filament loading rates and mechanism** | Needed motor torque and pinch roller size and surface is different for the materials |
| **Big filament diameter** | Bigger diameters decreases the buckling tendency |
| **Dual- or several extruder system** | Different material for support structures, possible to print with several materials at the same time |
| ***Software:*** | |
| **Adjustable slice thickness and road width** | Printing resolution affects the quality |
| **Several patterns of building the infill** | Quality and device strength issues |
| **Adjustable envelope temperature** | Bonding between layers and adjacent roads, build plate adhesion |
| **Adjustable printing temperature and speed** | Increases the amount of possible materials and prototype geometries |

Further investigations of the printed prototypes regarding mechanical strength, the stability of the drug in the polymer and the effect on different drug loadings and additives, such as barium sulfate (for a diagnostical aid in medical imaging of IUS), must be conducted in order to produce market-appropriate products.

Since there have not been reported about any FDA approved 3D printed PBDS in the literature, the regulatory aspects of 3D printed PBDS must be determined. In October 8-9, 2014 FDA had a workshop where medical device manufacturers, additive manufacturing companies and academia were invited to discuss technical challenges and solutions for 3D printing in the medical field (FDA, 2014). There have been FDA approved medical devices implanted in patients, but they have all received a 510(k) clearance through the existing regulatory pathway. To get a 510(k) clearance the medical device must be "substantially" equivalent to a device that is already marketed for the same use. However, the FDA are

considering whether they will continue to give 510(k) clearance or if the 3D printed devices need premarket approval in the future (Stuver, 2014). The use of pharmaceutics in 3D printed devices has not been widely discussed. Visiongain has published a report "3D Printing for Healthcare: R&D, Industry and Market 2014-2024" where 3D printing of pharmaceuticals is discussed, unfortunately the report does not have open access, and therefore, the summarized data could not be used in this work (Visiongain, 2014).

The suitability of the new variants of the FDM™ technique, especially the AKF technique, in printing of pharmaceuticals should to be determined, since that technique may offer the use of the wider diversity of suitable feedstock material than the FDM™ process does. Many of the difficulties in the FDM™ technique were filament- and liquefier-specific, which should not be an issue in the AKF technique

# 8. Swedish summary

**3-D utskrifter av polymerbaserade läkemedelsfrisättande prototyper**

## 8.1 Inledning

Läkemedelsföretagen behöver hitta nya innovativa produkter i sin produktportfolie i och med att det introduceras årligen färre nya läkemedelsmolekyler på marknaden, på grund av ökad konkurrens från generiska marknader och för att förlänga livscykeln på redan existerande produkter. Även behovet av personifierad medicinering ökar intresset för nya tillverkningsmetoder.

Många nya framställningstekniker har introducerats inom läkemedelsindustrin de senaste åren, däribland strängsprutning, även kallat för smältextrudering, och olika utskriftstekniker, bland annat tredimensionella (3D) utskriftsteknologier. Både strängsprutning och den i den här studien använda 3D utskriftsteknologin FDM™, baserar sig på att polymeren smälts, varefter smältan matas ut genom ett munstycke i en förutbestämd form.

I den här studien tillverkades det med hjälp av 3D utskriftsteknologin FDM™ polymerbaserade läkemedelsfrisättande system.

## 8.2 Målsättningar

Målsättningen med studien var att utforska potentialen av 3D utskriftsteknologin i tillverkningen av läkemedelsfrisättande prototyper. Målsättningen var att tillverka prototyper av både ett original skrivarråmaterial, polykaprolakton (PCL), och av ett nytt råmaterial för skrivaren, etylenvinylacetat (EVA). Utskrivbarheten av formuleringar med olika mängd av läkemedlet indometacin studerades. Dessutom studerades det i vilken polymorfisk form läkemedlet befann sig både i de strängsprutade rundtrådarna och i de utskrivna prototyperna och frisättningen av läkemedlet från bådadera.

Målsättningarna var att studera:

- utskrivbarheten av läkemedelsfrisättande prototyper med hjälp av FDM™ tekniken

- utskrivbarheten av ett nytt råmaterial för skrivaren
- karakterisering av läkemedlets polymorfa form i de utskrivna prototyperna
- morfologin och läkemedelsfrisättningen från de utskrivna prototyperna

## 8.3 Material och metoder

Två olika polymerer användes som råmaterial för de utskrivna prototyperna, PCL och EVA, inkorporerade med läkemedlet indometacin (IND). PCL är en långsamt nedbrytbar polymer, medan EVA är en stabil polymer. IND som användes som ett modelläkemedel, är ett anti-inflammatoriskt läkemedel som har använts i kopparspiraler för att minska biverkningar under användningen av spiralen. Utskriftsexperiment gjordes med enbart polymererna och med polymererna inkorporerade med olika mängd läkemedel.

Processen började med att tillverka rundtråd genom strängsprutning av polymer pelletsen utan eller med läkemedel. Geometrin för prototyperna ritades med hjälp av ett tredimensionellt datorprogram, *Rhinoceros*, varefter de exporterades till skrivarens mjukvara. Skrivaren som användes i studien var MakerBot Replicator 2 (USA). De olika prototyperna som slutligen användes i studien namngavs till IUS 1, IUS 2 och Ring. Rundtråden matades sedan in i 3D-skrivaren och skrevs ut enligt den förutbestämda geometrin. För att utskrivandet av prototyperna skulle vara möjligt behövde viskositeten för smältan vara den rätta, detta undersöktes med hjälp av ett reologiskt experiment.

Då de olika prototyperna var framställda utfördes olika experiment för att granska morfologin och för att karakterisera i vilken polymorfisk form läkemedlet existerade i de utskrivna prototyperna. Detta utfördes även på rundtråden. Metoder som användes för att granska morfologin var både visuell och mikroskopisk (SEM) karakterisering. XRD, DSC och ATR-IR metoderna användes för att karakterisera läkemedlet i rundtråden och de utskrivna prototyperna. Rundtråden granskades också med avseende på mängden läkemedel genom att lösa upp läkemedlet och polymeren i ett lösningsmedel.

Frisättningen av läkemedlet från rundtråden och prototyperna studerades i 30 dagar i en fysiologisk saltlösning som media. Prototyperna var placerade i en flaska med saltlösning vid en temperatur på 37 ± 0.02 ºC i ett skakande vattenbad. Prover togs under bestämda tidpunkter och media byttes vid behov för att hålla lösningens IND koncentration under 20

% av en mättad lösning. Eftersom PCL är en nedbrytbar polymer granskades även graden av nedbrytningen av polymeren under frisättningen.

## 8.4 Resultat

Rundtrådar tillverkades av de båda polymererna med hjälp av strängsprutning. Både rundtrådar utan och med läkemedel var möjliga att tillverka. Tillverkningstemperaturen var i båda fallen under läkemedlets smältpunkt, men naturligtvis över polymerens smältpunkt. Största problemet vid tillverkningen var att få den rätta dimensionen på rundtråden så att det var möjligt att använda den vid utskrivandet av prototyper, eftersom skrivaren endast godkände material med diametern 1.75±0.05 mm. Faktorer som påverkade kvaliteten på rundtrådarna var (i) skruvens hastighet i apparaturen, (ii) viskositeten, som påverkar storleken på munstyckets diameter vid utmatningen, (iii) mängden smälta inne i apparaturen och (iv) materialets värmeledningsförmåga.

Utskrivandet av prototyper var möjligt både med skrivarens original råmaterial PCL och det nya råmaterialet, EVA. Av tolv olika kvaliteter av EVA polymeren var det endast möjligt att skriva ut prototyper med sex, av vilka endast två av dem var av god kvalitet. En av dem, EVA 5, valdes ut för vidare studier. PCL polymeren skrevs ut under läkemedlets smältpunkt, medan EVA 5 polymeren behövde en högre temperatur för att vara utskrivbar. Faktorer som påverkar utskrivandet är (i) rundtrådens diameter och jämnhet, (ii) materialets böjningsstyvhet och -styrka och (iii) materialets flytbarhet som smälta. Förutom att dessa egenskaper påverkar skilt för sig, visade det sig också att förhållandet mellan böjningsstyvheten och viskositeten är avgörande för att materialet skall vara möjligt att använda i skrivaren. Även egenskaper hos skrivarens hård- och mjukvara och prototypens geometri påverkar utskrivbarheten av ett material och kvaliteten på prototypen. Den typ av skrivare som användes i den här studien är optimerad för endast ett eller några få material, vilket begränsar möjligheterna till att använda i forsknings- och läkemedelsutvecklingssyften. Materialen som är möjliga att skriva ut behöver ha egenskaper, som exempelvis böjningsstyvhet och viskositet, som är liknande original skrivarråmaterialets egenskaper.

Det var inte stora skillnader i utskrivbarheten av prototyper utan eller med läkemedel. Utskrivbarheten av EVA 5 polymeren med 15 % läkemedel var den formuleringen som gav den bästa kvaliteten vid utskrivandet. Detta var troligtvis på grund av en lägre viskositet av smältan, som en större mängd smält läkemedel gav upphov till, då utskrivningstemperaturen var över läkemedlets smältpunkt. Processparametrarna i vilken experimenten utförs har även stor betydelse på utskrivbarheten och den slutliga kvaliteten. Varje material har en övre och en undre gräns för både utskriftstemperaturen och temperaturen för utskriftsförhållandena för att få en produkt med god kvalitet.

Karakteriseringen av rundtråden och prototyperna gjordes med flera olika metoder. Det var omöjligt att med säkerhet säga i vilken polymorfisk form indometacin var i rundtrådarna eller i de utskrivna prototyperna. Detta berodde på att många av de karakteristiska pikarna för polymererna i de olika metoderna var nära de karakteristiska pikarna för indometacinets olika polymorfiska former. De utskrivna prototypernas yta hade en ojämnare struktur än rundtrådens, detta beror på att utskrivandet sker lager på lager och man kunde tydligt se strukturen av de olika lagren.

Läkemedelsfrisättningen var snabbare från PCL än från EVA 5 polymeren. Frisättningen från båda polymererna var snabbare från proven innehållande mindre mängd läkemedel än från de med högre läkemedelskoncentration. Detta på grund av att i proven med mera indometacin var en del i kristallin form, medan det till största delen var upplöst eller smält i proven med mindre mängd läkemedel.

## 8.5 Slutsatser och framtidsutsikter

Studien visade att det var möjligt att skriva ut prototyper innehållande läkemedel med hjälp av FDM™ tekniken. Det var även möjligt att introducera ett nytt råmaterial för skrivaren som användes i den här studien och att skriva ut prototyper med detta. Det är dock en stor mängd processparametrar och processvariabler som måste tas i beaktande för att erhålla prototyper av god kvalitet. De regulatoriska aspekterna av 3D utskrivna läkemedelsfrisättande produkter måste även undersökas eftersom det inte tidigare har introducerats dylika på marknaden. Även läkemedlets stabilitet och prototypernas mekaniska hållfasthet måste undersökas.

3D teknologin är en innovativ framställningsmetod som består av många olika utskriftstekniker, många av dem med stor potential att användas vid tillverkningen av läkemedelsfrisättande produkter. Nya 3D utskriftstekniker introduceras årligen på marknaden med vilka valmöjligheten av råmaterialet och kvaliteten på utskrifterna troligtvis förbättras.

# 9. Conclusions

Experimental work was done with the original printer feedstock polymer to print drug-loaded prototypes by using the MakerBot Replicator 2. It was possible to print drug-loaded prototypes of PCL with the 3D printing technique used in this study. This was done without any modifications of the printer.

A new feedstock material was tested, the EVA copolymer, to evaluate the printability of drug-free and drug-loaded filaments. Out of twelve tested grades of the EVA copolymer it was possible to print DDS prototypes with six different EVA copolymers, but only two with sufficient print quality, EVA 5 and EVA 7. Of the two successfully printed copolymers, EVA 5 was further investigated regarding the printability of drug-loaded filaments. The printing process, though, is a complex interplay between many variables and parameters, and the process needs optimization for each new feedstock.

The drug release from the printed devices depended on the degree of crystallinity of the incorporated drug. The drug release from the PCL prototypes was faster than the drug release from the EVA prototypes. The drug was dissolved in the PCL at least in some extent under the extruding process, while in EVA, the drug melted under the printing process due to higher printing temperatures. The stability of the amorphous drug in the prototypes under storage was not determined.

The 3D printing field is an innovative field and many new 3D technologies have entered and are entering the market the last years. Besides the FDM™ technique there is the AKF 3D printing technique, which could be more versatile for printing of PBDS. The regulatory aspects and landscape of this new manufacturing technology of PBDS have to be clarified in order to get an understanding of the potential of its use in future fabrication of drug delivery systems and medical devices.

# 10. References


3D printing Industry, 2014. URL: http://www.3dprintingindustry.com. Accessed 28.10.2014.

AGARWALA, M., JAMALABAD, V., LANGRANA, N., SAFARI, A., WHALEN, P. and DANFORTH, S., 1996. Structural quality of parts processed by fused deposition. *Rapid Prototyping Journal,* **2**(4), pp. 4-19.

AGHDAM, R., NAJARIAN, S., SHAKHESI, S., KHANLARI, S., SHAABANI, K. and SHARIFI, S., 2012. Investigating the effect of PGA on physical and mechanical properties of electrospun PCL/PGA blend nanofibers. *Journal of Applied Polymer Science,* **124**(1), pp. 123-131.

ALMEIDA, A., POSSEMIERS, S., BOONE, M.N., DE BEER, T., QUINTEN, T., VAN HOOREBEKE, L., REMON, J.P., VERVAET, C., 2011. Ethylene vinyl acetate as matrix for oral sustained release dosage forms produced via hot-melt extrusion. *European Journal of Pharmaceutics and Biopharmaceutics,* **77**(2), pp. 297-305.

ALMEIDA, A., BRABANT, L., SIEPMANN, F., DE BEER, T., BOUQUET, W., VAN HOOREBEKE, L., SIEPMANN, J., REMON, J.P. and VERVAET, C., 2012. Sustained release from hot-melt extruded matrices based on ethylene vinyl acetate and polyethylene oxide. *European Journal of Pharmaceutics and Biopharmaceutics,* **82**(3), pp. 526-533.

ANDERSON, K., et al. Controlled release of Active Pharmaceutical Ingredients from Ethylene Vinyl Acetate Copolymers, Celanese White Paper, 2011.

Arcam, 2014. URL:http://www.arcam.com/technology/electron-beam-melting/.

ARBURG, 2014.
URL:http://www.arburg.com/fileadmin/redaktion/Mediathek/Prospekte/ARBURG.

BASAK, P., ADHIKARI, B., BANERJEE, I. and MAITI, T.K., 2009. Sustained release of antibiotic from polyurethane coated implant materials. *Journal of Materials Science,* **20**(1), pp. 213-221.

BAUM,M.M., BUTKYAVICHENE, I., GILMAN, J., KENNEDY, S., KOPIN, E., MALONE, A.M., NGUYEN, C., SMITH, T.J., FRIEND, D.R., CLARK,M.R. and MOSS, J.A., 2012. An intra vaginal ring for the simultaneous delivery of multiple drugs. *Journal of Pharmaceutical Science*, **101**, pp. 2833-2843.

BELLINI, A., SHOR, L. and GÜCERI, S., 2005. New developments in fused deposition modeling of ceramics. *Rapid prototyping Journal,* **11**(4), pp. 214-220.

BERMAN, B., 2012. 3-D printing: The new industrial revolution. *Business Horizons,* **55,** pp. 155-162.

Bilby3D, 2014. URL: https://bilbycnc.freshdesk.com/support/articles/59269-makerbot-replicator-2-cleaning-the-drive-grear, Accessed 25.6.2014.

BODMEIER, R., CHEN, H., 1988. Preparation and characterization of microspheres containing the anti-inflammatory agents, indomethacin, ibuprofen and ketoprofen. *Journal of Controlled Release,* **10**, pp 167-175.

BORDES, C., FRÉVILLE, V., RUFFIN, E., MAROTE, P., GAUVRIT, J.Y., BRIANÇON, S. and LANTÉRI, P., 2010. Determination of poly(ε-caprolactone) solubility parameters: Application to solvent substitution in a microencapsulation process. *International journal of pharmaceutics*, **383**(1–2), pp. 236-243.

BOSE, S., VAHABZADEH, S. and BANDYOPADHYAY, A., 2013. Bone tissue engineering using 3D printing. *Materials Today*, (12), pp. 496-504.

BOSWORTH, L.A. and DOWNES, S., 2010. Physicochemical characterisation of degrading polycaprolactone scaffolds. *Polymer Degradation and Stability*, **95**(12), pp. 2269-2276.

BRACHE, V., PAYA'N, L.J., FAUNDES, A., 2013. Current status of contraceptive vaginal rings. *Contraception*, **87**(3), pp. 264-272.

BREITENBACH, J., 2002. Melt extrusion: from process to drug delivery technology. *European Journal of Pharmaceutics and Biopharmaceutics*, **54**, pp. 107-117.

Business Insider, 2014. :http://www.businessinsider.com/3d-printed-houses-are-here-2014-9, Accessed 28.10.2014.

Celanese, 2014. URL: http://www.celanese.com/.

Celanese, 2014 a, URL: http://www.vitaldose.com/resource/files/EVA_DrugDelivery_Applications_Overview.pdf.

CHENG, L., GUO, S. and WU, W., 2009. Characterization and in vitro release of praziquantel from poly(ε-caprolactone) implants. *International journal of pharmaceutics*, **377**(1–2), pp. 112-119.

CHENG, L., LEI, L. and GUO, S., 2010. In vitro and in vivo evaluation of praziquantel loaded implants based on PEG/PCL blends. *International journal of pharmaceutics*, **387**(1–2), pp. 129-138.

CHIENG, Y.W., 1987. ImplanTable Therapeutic systems. In Robinson, J.R. and LEE, V.H.L., Contolled drug delivery, Fundamentals and Applications, 2nd ed. Marcel Dekker Inc., 1987.

Clinical trials, 2014. URL:https://clinicaltrials.gov/.

COLEMAN, M.M., SERMAN, C.J., BHAGWAGAR, D.E. and PAINTER, P.C., 1990. A practical guide to polymer miscibility. *Polymer*, **31**(7), pp. 1187-1203.

COMB, J.W. and PRIEDEMAN, W.R., 1993. Control parameters and material selection criteria for rapid prototyping systems, in Marcus, H.L, BEAMAN, J.J., BARLOW, J.W., BOURELL, D.L. and CRAWFORD, R.H. (Eds), Proceedings of the Solid Freeform Fabrication Symposium, Vol.4, 1993, The University of Texas at Austin, Austin TX, pp. 86-91.

COMB, J.W., PRIEDEMAN, W.R. and TURLEY, P.W., 1994. FDM technology process improvements. in Marcus, H.L, BEAMAN, J.J., BARLOW, J.W., BOURELL, D.L. and CRAWFORD, R.H. (Eds), Proceedings of the Solid Freeform Fabrication Symposium, Vol.5, 1994, The University of Texas at Austin, Austin TX, pp. 42-49 .

Conrad, 2014. Multipurpose prevention technologies. URL:http://www.conrad.org/prevention.html, Accessed 11.11.2014.

CT, 2014. URL: http://www.creativetools.se/3d-skrivare-info, Accessed 30.11.2014.

Custompart, 2014. URL: http://www.custompartnet.com/wu/direct-metal-laser-sintering.

DASH, S., MURTHY, P.N., NATH, L. and CHOWDHURY, P., 2010. Kinetic modeling on drug release from controlled drug delivery systems. *Acta Polonia Pharmaceutica,* **67**(3), pp. 217-223.

DIEZ, E., CAMACHO, J., DIAZ, I. and OVEJERO, G., 2014. Turbidimetric and intrinsic viscosity study of EVA copolymer-solvent systems. *Polymer bulletin,* **71**(1), pp. 193-206.

ELOMAA, L., TEIXEIRA, S., HAKALA, R., KORHONEN, H., GRIJPMA, D.W. and SEPPÄLÄ, J.V., 2011. Preparation of poly(Ɛ-caprolactone)-based tissue engineering scaffolds by stereolithography. *Acta biomaterialia,* **7**, pp. 3850-3856.

ESPALIN, D., ARCAUTE, K., RODRIGUEZ, D., MEDINA, F., POSNER, M. and WICKER, R., 2010. *Rapid Prototyping Journal*, **16**(3), pp. 164-173.

EWING, A.V., CLARKE, G.S. and KAZARIAN, S.G., 2014. Stability of indomethacin with relevance to the release from amorphous solid dispersions studied with ATR-FTIR spectroscopic imaging. *European Journal of Pharmaceutical Sciences,* **60**(0), pp. 64-71.

FDA, 2014. URL: http://www.fda.gov/MedicalDevices/NewsEvents/WorkshopsConferences/ucm397324.htm, Accessed 01.11.2014.

FIALHO, S.L., BEHAR-COHEN, F. and SILVA-CUNHA, A., 2008. Dexamethasone-loaded poly(ε-caprolactone) intravitreal implants: A pilot study. *European Journal of Pharmaceutics and Biopharmaceutics,* **68**(3), pp. 637-646.

FORSTER, A., HEMPENSTALL, J., TUCKER, I. and RADES, T., 2001. Selection of excipients for melt extrusion with two poorly water-soluble drugs by solubility parameter calculation and thermal analysis. *International journal of pharmaceutics,* **226**(1–2), pp. 147-161.

FU, Y. and KAO, W.J., 2010. Drug release kinetics and transport mechanisms of non-degradable and degradable polymeric delivery systems. *Expert Opinion Drug delivery*, **7**(4), pp. 429-444. doi:10:1517/17425241003602259.

GOGOS, C.G., LIU, H., WANG, P., 2012. Laminar dispersive and distributive mixing with dissolution and applications to Hot-melt Ectrusion. In: Douroumis, D. (Ed.), Hot-melt extrusion: pharmaceutical applications. A John Wiley & Sons, Ltd., Publications, 261-284.

GOYANES, A., BUANZ, A.B.M., BASIT, A.W and GAISFORD, S., 2014. Fused-filament 3D printing (3DP) for fabrication of Tablets. *International Journal of Pharmacutics,***476**(9), pp. 88-92.

GREENHALGH, D., WILLIAMS, A., TIMMINS, P. and YORK, P., 1999. Solubility parameters as predictors of miscibility in solid dispersions. *Journal of pharmaceutical sciences,* **88**(11), pp. 1182-1190.

GUO, Q., GUO, S. and WANG, Z., 2007. A type of esophageal stent coatimg composed of 5-fluorouracil-containing EVA layer and one drug-free protective layer: in vitro release, permeation and mechanical properties. *Journal of Controlled Release,* **118**, pp. 318-324.

HAN, Y.A., SINGH, M. and SAXENA, B.B., 2007. Development of vaginal rings for sustained release of nonhormonal contraceptives and anti-HIV agents. *Contraception,* **76**, pp. 132-138.

HAUSMAN, K., 2014. 3D printing for Dummies. John Wiley & Sons, Inc.

HOFFMAN, A.S., 2008, The origins and evolution of "contolled2 drug delivery systems. *Journal of Controlled Release,* **132**, pp. 153-163.

HUANG, X., BRAZEL, C.S., 2001. On the importance and mechanisms of burst release in matrix-controlled drug delivery systems. *Journal of Controlled Release,* **73**(2), pp. 121-136.

HUTMACHER, D.W., SCHANTZ, J.T., LAM, C.X.F., TAN, K.C. and LIM, T.C., 2007.State of the art and future directions of scaffold-based bone engineering from a biomaterials perspective. *Journal of Tissue Engineering and Regenerative medicine,* 2007(1), pp. 245-260.

Intechopen, 2014. URL:http://www.intechopen.com/source/html/18160/media/image23.png

JENKINS, R., SNYDER, R. L., 1996. Introduction to X-ray powder diffractometry, Wiley, New York.

JENSEN, J.T., 2013. Vaginal ring delivery of selective progesterone receptor modulators for contraception, *Contraception,* **87**(3), pp. 314-318.

KANENIWA, N., OTSUKA, M. and HAYASHI, T., 1985. Physicochemical characterization of indomethacin polymorphs and the transformation kinetics in ethanol. *Chemical & pharmaceutical bulletin,* **33**(8), pp. 3447-55.

KARMWAR, P., GRAESER, K., GORDON, K.C., STRACHAN, C.J. and RADES, T., 2011. Investigation of properties and recrystallisation behaviour of amorphous indomethacin samples prepared by different methods. *International journal of pharmaceutics,* **417**(1–2), pp. 94-100.

KATSTRA, W.E., PALAZZOLO, R.D., ROWE, C.W., GIRITLIOGLU, B., TEUNG, P and CIMA, M.J., 2000. Oral dosage forms fabricated by Three Dimensional Printing™. *Journal of Controlled Release,* **66**, pp. 1-9.

KHALED, S.A., BURLEY, J.C., ALEXANDER, M.R. and ROBERTS, C.J., 2014. Desktop 3D printing of controlled release pharmaceutical bilayer Tablets. *International Journal of Pharmaceutics,* **461**(11), pp. 105-111.

LABARRE, D.J-.P., PONCHEL, G. and VAUTHIER, C., 2011. Biomedical and pharmaceutical polymers, Pharmaceutical Press, USA.

LEISTER, D., GEILEN, T., GEISSLER, T., 2012. Twin-screw Extruders for Pharmaceutical Hot-Melt Extrusion: Technology, Tecniques and Practises In: Douroumis, D. (Ed.), Hot-melt extrusion: pharmaceutical applications. A John Wiley & Sons, Ltd., Publications, 23-42.

LI, C., CHENG, L., ZHANG, Y., GUO, S. and WU, W., 2010. Effects of implant diameter, drug loading and end-capping on praziquantel release from PCL implants. *International journal of pharmaceutics,* **386**(1–2), pp. 23-29.

LI, Z. and TAN, B.H., 2014, Towards the development of polycaprolactone based amphiphilic block copolymers: molecular design, self-assembly and biomedical applications. *Materials Science and Engineering C,* 2014, http://dx.doi.org/ 10.1016/j.msec.2014.06.003.

LIANG, J., LI, Y., GU, X., GAO, Y. and LIU, J., 2008. Investigation of the release behaviour of cupric ion for three types of Cu-IUDs and indomethacin for medicated Cu-IUD in simulated uterine fluid. *Contraceptive,* **77**(4), pp. 299-302.

LIU, H., WANG, P., ZHANG, X., SHEN, F. and GOGOS, C.G., 2010. Effects of extrusion process parameters on the dissolution behavior of indomethacin in Eudragit® E PO solid dispersions. *International Journal of Pharmaceutics,* **383**(1–2), pp. 161-169.

LIU, P., RONG, X., LARU, J., VAN VEEN, B., KIESVAARA, J., HIRVONEN, J., LAAKSONEN, T. and PELTONEN, L., 2011. Nanosuspensions of poorly soluble drugs: Preparation and development by wet milling. *International Journal of Pharmaceutics,* **411**(1–2), pp. 215-222.

MALCOLM, R.K., FETHERSTON, S.M., McCOY, C.F., BOYD, P. and MAJOR, I., 2012. Vaginal rings for delivery of HIV microbicides. *International Journal of Women`s health,* **4,** pp. 595-605.

MARIN, E., BRICENO, M.I., and CABALLERO-GEORGE, C., 2013. Critical evaluation of biodegradable polymers used in nanodrugs. *International Journal of Nanomedicine,* **8,** pp. 3071-3091.

Martello, 2014a. URL:http://www.martello.co.uk/assets/images/gifs/sla_diagram.gif, Accessed 11.11.2014.

Martello, 2014b. URL:http://www.martello.co.uk/assets/images/gifs/sls_diagram.gif, Accessed 11.11.2014.

Martindale 32th Edition, pp. 45-48.

MARTÍNEZ-GARCÍA, A., SÁNCHEZ-RECHE, A., GISBERT-SOLER, S., CEPEDA-JIMÉNEZ, C.M., TORREGROSA-MACIÁ, R. and MARTÍN-MARTÍNEZ, J.M., 2007. Corona discharge treatment of EVAs with different vinyl acetate contents. *Journal of Adhesion Science & Technology,* **21**(5), pp. 441-463.

MDT, 2014. URL: http://www.mdtmag.com/articles/2013/11/first-510k-clearance-customized-3d-printed-polymeric-cranial-implants, Accessed 29.11.2014.

MELCHELS, F.P.W., FEIJEN, J. and GRIJPMA, D.W., 2009. A poly(D,L-lactide) resin for the preparation of tissue engineering scaffolds by stereolithography. *Biomaterials,* **30**, pp. 3801-3809.

MELCHELS, F.P.W., FEIJEN, J. and GRIJPMA, D.W., 2010. A review on stereolithography and its applications in biomedical engineering. *Biomaterials,* **31**, pp. 6121-6130.

MERKLI, A., TABATABAY, C., GURNY, R. and HELLER, J., 1998. Biodegradable polymers for the controlled release of ocular drugs. *Progress in polymer science,* **23**(3), pp. 563-580.

MOSTAFA, N., SYED, H., IGOR, S. and ANDREW, G., 2009. A Study of Melt Flow Analysis of an ABS-Iron Composite in Fused Deposition Modelling Process. *Tsinghua Science and Technology,* **14**, pp. 29-37.

NICHOLSON, J.W., 1997. The chemistry of polymers, Second edition. The Royal Society of Chemistry, 1997.

NIKZAD, M., MASOOD, S.H., SBARSKI, I. and GROTH, A., 2009. A study of melt flow analysis of an ABS-Iron composite in Fused Deposition Modelling Process. *Tsinghua Science and Technology,* **5**(38), pp. 29-37.

Perstorp, 2014, Properties and processing of Capa™ thermoplastics, Technical information Leaflet TI 1639, Perstorp. Accessed 04.07.2014.

Polysciences, 2014. URL: http://www.polysciences.com/Catalog/Department/Product/98/categoryid--286/pageindex---1/productid--1138/, Accessed 28.10.2014.

POMPCI, S., ARELLI, F., LABARDI, L., MARCASCIANO, F., CARAVELLI, G., CESARINI, C. and ABATE, O., 2012). Breast reconstruction with polyurethane implants: preliminary report. *European Journal of Plastic Surgery,* **35**(6), pp. 441-447.

Population Council, 2014, Project: The investigational Nestorone®/Ethinyl estradiol one-year contraceptive vaginal ring. http://www.popcouncil.org/research/one-year-contraceptive-vaginal-ring, accessed 11.11.2014.

Popular3Dprinters, 2014. URL:http://www.popular3dprinters.com/electron-beam-melting-ebm/, Accessed 12.11.2014.

Pubmed, 2014. URL:https://pubchem.ncbi.nlm.nih.gov/compound/indomethacin

RAMANATH H.S., CHUA C.K., LEONG K.F, SHAH K.D., 2008. Melt flow behaviour of poly-Ɛ-caprolactone in fused deposition modelling. *Journal of material science. Materials in medicine,* **19**(7) pp. 2541-2550.

RENGIER, F., MEHNDIRATTA, A., von TENGG-KOBLIGK, H., ZECHMANN, C.M., UNTERHINNINGHOFEN, R., KAUCZOR, H.U. and GIESEL, F.L., 2010. 3D printing based on imaging data: review of medical applications. *International Journal of computer assisted radiology and surgery,* **5**, pp. 335-341.

REYES, J., EVA foamed excipient: Novel way to deliver stem cells, growth factors and biologics for controlled releas applications, Celanes Irving, TX, 75039 USA. http://www.celanese.com/-/media/EVA%20Polymers/Files/Whitepapers/EVA-Foamed-Excipient-whitepaper.pdf, Accessed 12.11.2014.

REYES, J.D. Innovative use of ethylene vinyl acetate polymers for advancing healthcare. Celanese Corporation, Irving, TX, USA http://www.celanese.com/-/media/EVA%20Polymers/Files/Whitepapers/Celanese-Innovative-Uses-of-Ethylene-Vinyl-Acetate-Polymers-for-Advancing-Healthcare.pdf, Accessed 12.11.2014.

RONG H-J., CHEN W-L., GUO, S-R., LEI, L., SHEN, Y-Y., 2012. PCL films incorporated with paclitaxel/5-fluorouracil: Effects of formulation and spacial architecture on drug release. *International Journal of Pharmaceutics,* (2), pp. 242-251.

ROWE, C.W., KATSTRA, W.E., PALAZZOLO, R.D., GIRITLIOGLU, B., TEUNG, P. and CIMA, M.J., 2000. Multimechanism oral dosage forms fabricated by three dimensional printing™. *Journal of Controlled Release,* **66,** pp. 11-17.

SACHS, E., CIMA, M., WILLIAMS, P., BRANCAZIO, D. and CORNIE, J., 1992. 3-Dimensional printing- rapid prototyping tooling and prototypes directly from a CAD model. *Journal of Engineering for Industry-transactions of the ASME,* **114**(4), pp. 481-488.

SANDLER, N., SALMELA, I., FALLARERO, A., ROSLING, A., KHAJEHEIAN, M., KOLAKOVIC, R., GENINA, N., NYMAN, J. and VUORELA, P., 2014. Towards fabrication of 3D printed medical devices to prevent biofilm formation. *International Journal of Pharmaceutics,* 459(1-2), pp. 62-64.

SAVOLAINEN, M., HEINZ, A., STRACHAN, C., GORDON, K.C., YLIRUUSI, J., RADES, T. and SANDLER, N., 2007. Screening for differences in the amorphous state of indomethacin using multivariate visualization. *European Journal of Pharmaceutical Sciences,* **30**(2), pp. 113-123.

SCHIERHOLZ, J.M., STEINHAUSER, H., RUMP, A.F.E, BERKELS, R and PULVERER, G., 1997. Controlled release of antibiotics from biomedical polyurethanes: morphological and structural features. *Biomaterials,* **18**(12), pp. 839-844.

SCHÜLLER-RAVOO, S., TEIXEIRA, S.M., FEIJEN, J., GRIJPMA, D.W. and POOT, A.A., 2013. *Macromolecular Bioscience,* **13**, pp. 1711-1719.

Sculptify, 2014. URL: http://sculptify.com/.

SHASTRI, P.V., 2002. Toxicology of polymers for implant contraceptives for women. *Contraception,* **65**, pp. 9-13.

SHOR, L., GORDON, J., AN, Y., GÜCERI, S. and SUN, W., 2009. Precision extruding deposition of polycaprolactone and composite polycaprolactone/hydroxyapatite scaffolds for tissue engineering. *Journal of Manufacturing Science and Engineering,* **130**(2), pp. 73-74.

SIEPMANN, J., GÖPFERICH, A., 2001. Mathematical modeling of bioerodible, polymeric drug delivery systems. *Advanced Drug delivery Systems,* **48,** pp. 229-247.

SIMMONS, A., PADSALGIKAR, A.D., FERRIS, L.M and POOLE-WARREN, L.A., 2008. Biostability and biological performance of a PDMS-based polyurethane for controlled drug release. *Biomaterials,* **29**(20), pp. 2987-2995.

SINHA, V.R., BANSAL, K., KAUSHIK, R., KUMRIA, R. and TREHAN, A., 2004. Poly-ε-caprolactone microspheres and nanospheres: an overview. *International journal of pharmaceutics,* **278**(1), pp. 1-23.

SINKO, P. J. 2011. Drug release and dissolution in Martin´s physical pharmacy and pharmaceutical sciences, 6th edition, Wolters Kluwer, Lippincott Williams & Wilkins, 2011.

SITRUK-WARE, R., NATH, A., MISHELL Jr, D.R., 2013. Contraception technology: past, present and future. *Contraception,* **87**(3), pp. 319-330.

SOLORIO, L., CARLSON, A., ZHOU, H. and EXNER, A.A., 2014. ImplanTable drug delivery systems in Bader, A.R. and Putnam D.A. (ED); Engineering polymer systems for drug delivery, John Wiley & sons, Inc., 2014.

STUVER, N., 2014. http://www.healthreformwatch.com/2014/11/06/16132/comment-page-1/, Accessed 15.11.2014.

Stratasys, 2014. URL: http://www.stratasys.com/.

SUN, Q., RIZVI, G.M., BELLEHUMEUR, C.T. and GU, P., 2008. Effect of processing conditions on the bonding quality of FDM polymer filaments. *Rapid prototyping Journal*, **14**(2), pp 72-80.

SURWASE, S.A., BOETKER, J.P., SAVILLE, D., BOYD, B.J., GORDON, K.C., PELTONEN, L. and STRACHAN, C.J., 2013. Indomethacin: New polymorphs of an old drug. *Molecular Pharmaceutics*, **10**(12), pp. 4472-4480.

SYMES, M.D., KITSON, P.J., YAN, J., RICHMOND, C.J., COOPER, G.J.T, BOWMAN, R.W., VILBRANDT, T. and CRONI, L., 2012. Integrated 3D-printed reactionware for chemical synthesis and analysis. *Nature Chemistry*, **4**, pp. 349-354. DOI:10.1038/NCHEM.1313.

Technical data sheet, ATEVA® 1070, Celanese. URL: http://www.celanese.com/cn-cn/-/media/EVA%20Polymers/Files/Technical%20Data%20Sheets/Ateva_EVA_1070.pdf, Accessed 11.4.2014.

Technical data sheet, ATEVA® 1081, Celanese. URL: http://www.celanese.com/cn-cn/-/media/EVA%20Polymers/Files/Technical%20Data%20Sheets/Ateva_EVA_1081.pdf, Accessed 11.4.2014.

Technical data sheet, ATEVA® 1075A, Celanese. URL: http://www.celanese.com/cn-cn/-/media/EVA%20Polymers/Files/Technical%20Data%20Sheets/Ateva_EVA_1075A.pdf, Accessed 15.08.2014.

Technical data sheet, ATEVA® 1241, Celanese. URL: http://www.celanese.com/cn-cn/-/media/EVA%20Polymers/Files/Technical%20Data%20Sheets/Ateva_EVA_1241.pdf, Accessed 15.08.2014.

Technical data sheet, ATEVA® 1641, Celanese. URL: http://www.celanese.com/cn-cn/-/media/EVA%20Polymers/Files/Technical%20Data%20Sheets/Ateva_EVA_1070.pdf, Accessed 15.08.2014.

Technical data sheet, ATEVA® 1821A, Celanese. URL: http://www.celanese.com/cn-cn/-/media/EVA%20Polymers/Files/Technical%20Data%20Sheets/Ateva_EVA_1821A.pdf,Accessed 11.04.2014.

Technical data sheet, ATEVA® 1850A, Celanese. URL: http://www.celanese.com/cn-cn/-/media/EVA%20Polymers/Files/Technical%20Data%20Sheets/Ateva_EVA_1850.pdf, Accessed 15.08.2014.

Technical data sheet, ATEVA® 1880A, Celanese. URL: http://www.celanese.com/cn-cn/-/media/EVA%20Polymers/Files/Technical%20Data%20Sheets/Ateva_EVA_1880A.pdf, Accessed 11.04.2014.

Technical data sheet, ATEVA® 2821A, Celanese. URL: http://www.celanese.com/cn-cn/-/media/EVA%20Polymers/Files/Technical%20Data%20Sheets/Ateva_EVA_2821A.pd Accessed 11.04.2014.

Technical data sheet, ATEVA® 3325A, Celanese. URL: http://www.celanese.com/cn-cn/-/media/EVA%20Polymers/Files/Technical%20Data%20Sheets/Ateva_EVA_3325A.pdf, Accessed 11.04.2014.

The Economist, 2014. URL: http://www.economist.com/node/21553017/print, Accessed 28.10.2014.

Thre3D, 2014.: URL:https://thre3d.com/how-it-works/3d-printing-process.

THURMAN, A.R., CLARK, M.R., HURLBURT, J.A and DONCEL, G.F., 2013. Intravaginal rings as delivery systems for microbicides and multipurpose prevention technologies. *International Journal of Women´s health,* **5**, pp. 695-708.

TURNER, B., STRONG, R. and GOLD, S.A., 2014. A review of melt extrusion additive manufacturing processes: I. Process design and modeling. *Rapid Prototyping Journal, 2014,* **20**(3), pp. 192-204.

van LAARHOVEN, J.A.H., KRUFT, M.A.B., VROMANS,H., 2002. effect on supersaturation and crystallization phenomena on the release properties of a contolled release device based on EVA copolymer. *Journal of Controlled release,* 2002, **82**(2-3), pp. 309-317.

VALIGRA, L., 2012. Excipient excitement, new formulations, delivery methods extend product life and improve pharma´s profitability, *Pharmaceutical Formulation and Quality,*October 2012, pp. 19-22.

VENKATARAMAN, N., RANGARAJAN, S., MATTHEWSSON, M.J., HARPER, B., SAFARI, A., DANFORTH, S.C., WU, G., LANGRANA, N., GUCERI, S. and YARDIMCI, A., 2000. Loadstock material property-process relationships in fused deposition of ceramics (FDC). *Rapid prototyping journal,* 2000, **6**(4), pp. 244-252.

Visiongain, 2014. 3D Printing for Healthcare: R&D, Industry and market 2014-2024. https://www.visiongain.com/Report/1184/3D-Printing-for-Healthcare-R-D-Industry-and-Market-2014-2024, accessed 07.08.2014.

WOODRUFF, M., MARIA, A. and HUTMACHER, D., 2010. The return of a forgotten polymer -- Polycaprolactone in the 21st century. *Progress in polymer science,* **35**(10), pp. 1217-1256.

WU, G., WU, W., ZHENG, Q., LI, J. ZHOU, J. and HU, Z., 2014. Experimental study of PLLA/INH slow release implant fabricated by three dimensional printing technique and drug release characteristics in vitro. *BioMedical Engineering Online*, **13**(97), pp 1-11. Accessed 31.10.2014.

YU, D.G., BRANFORD-WHITE, C., MA, Z.-H., ZHU, L.-M., LI, X.-Y. and YANG, X.-L., 2009. Novel drug delivery devices for providing linear release profiles fabricated by 3DP. *International Journal of Pharmaceutics,* **370**(1-2), pp160-166.

YU, D.G., ZHU, L.-M., BRANFORD-WHITE, C.J. and YANG, X.L., 2007. Three-dimensional Printing in Pharmaceutics: Promises and Problems. *Journal of pharmaceutical sciences,* **97**(9), pp. 3666-3690.

ZEIN, I., HUTMACHER, D.W., TAN, K.C. and TEOH, S.H., 2002. Fused deposition modeling of novel scaffold architectures for tissue engineering applications. *Biomaterials,* 2002, **23**(4), pp 1169-1185.

ZHOU, J and LU, L. 2011. Biomimetic structured porogen freeform fabrication system for tissue engineering, in Pramatarova,L. (ed): On Biomimetics, Intech, August 29.2011, pp. 53-90. Available from: http://www.intechopen.com./books/on-biomimetics/biomimetic-structured-porogen-freeform-fabrication-systen-for-tissue-engineering.

URL: https://www.merck.com/product/usa/pi_circulars/n/nuvaring/nuvaring_ppi.pdf

URL: http://www.mirena-us.com/

URL: http://www.path.org/publications/files/RHSC_progesterone_br.pdf